OPTICAL PROPERTIES OF PORCINE DERMIS IN THE NEAR INFRARED REGION BETWEEN 900NM AND 1500NM

A Thesis

Presented to

the Faculty of the Department of Physics

East Carolina University

In Partial Fulfillment

of the Requirements for the Degree

Master of Science in Applied Physics

by

Yong Du

July 2000

Abstract

Yong Du OPTICAL PROPERTIES OF PORCINE DERMIS IN THE NEAR INFRARED REGION BETWEEN 900nm AND 1500nm. (Under the direction of Dr. Xin-Hua Hu) Department of Physics, July 2000.

The purpose of this thesis is to study the optical properties of porcine dermis in the shortwave infrared region between 900nm and 1500nm. The collimated and diffuse transmittance and diffuse reflectance of porcine skin dermis samples within 30 hours postmortem have been measured. Monte Carlo simulations have been performed to inversely determine the absorption coefficient, scattering coefficient and asymmetry factor of the dermis samples in the spectral range from 900 to 1500nm. We further analyzed the sensitivity of the parameter values on the experimental errors and inverse calculation procedures. The state of cellular integrity of the skin samples following optical measurements was verified using transmission electron microscopy (TEM). These results were correlated to study postmortem effects on the *in vitro* optical properties of the porcine dermis. We concluded that the wavelength dependence of optical properties of the dermis remains unchanged for samples stored within crushed ice for up to 30 hours postmortem while the values of the parameters vary due to the modification in the water content of the tissue. Preliminary investigations were performed on the optical properties of normal human breast tissues in the same near infrared region and the scattering of a laser beam by cultured cells at 1064nm.

OPTICAL PROPERTIES OF PORCINE SKIN DERMIS IN THE NEAR INFRARED REGION BETWEEN 900NM AND 1500 NM

by

Yong Du

APPROVED BY:
DIRECTOR OF THESIS_____
XIN-HUA HU, Ph.D.

COMMITTEE MEMBER_____
MUMTAZ A. DINNO, Ph.D.

COMMITTEE MEMBER_____
JAMES M. JOYCE, Ph.D.

COMMITTEE MEMBER_____
MARGIT SCHMIDT, Ph.D.

CHAIR OF THE DEPARTMENT OF PHYSICS_____
CHARLES E. BLAND, Ph.D.

DEAN OF THE GRADUATE SCHOOL_____
THOMAS L. FELDBUSH, Ph.D.

Acknowledgements

First and foremost, I would like to take this opportunity to thank the physics department for their help and support throughout my study and research here.

I would like to thanks Dr. Xin-Hua Hu and Dr. Jun Qing Lu, for the guidance and support they have provided since I started to work in the Biomedical Laser Laboratory, for their constant encouragement and helps without which I would not have all these works presented here.

I would like to thank Dr. M. Schmidt for her teaching me the cell culture techniques and providing the cell culture lab. Her patience on my acquiring the delicate skills needed for growing cells is deeply appreciated. Additional thanks go to Dr. G. Kalmus and Michael Cariveau, for their helps in the tissue and providing the TEM analysis. I am also grateful to Dr. Mumtaz Dinno for sharing with me his wealth of knowledge in the area of biomedical physics, and to Dr. Yongqing Li for loaning his inverted microscopy setup to me for imaging cell culture. Many thanks to Dr. Joyce, and Dr. Schmidt for their serving on my thesis committee, reviewing the manuscript, and for making sure I met all the graduation requirements set by the department and the university.

My acknowledgment is extended to my friends Dr. Xiao-Ning Pan, Qiyin (Chevy) Fang, Ke Dong and Di Wu. Dr. Pan and Chevy's helps in my experiments, Ke and Di's helps in programming, and all of their helps in personal life were priceless.

I would also like to give my appreciates to Kenneth Jacobs, Jim Gilbert, Carl Hartsfield and Raymond Mills, for they help in making experimental apparatus, without them my experiments would never be able to finished.

Finally, I owe my gratitude to my parents and my sisters for their endless support of my education and to my wife Yuehong Wang, for her understanding and encouragement through all these years.

The research assistantship of my work is supported by the grant from National Institute of Health (R15GM/OD55940-01).

Table of Contents

List of Tables

List of Figures

List of Symbols and Abbreviations

δ^2……Square Root Error

g…….Asymmetry Factor

mm…….Millimeter

μm……..Micrometer

μ_a……Absorption Coefficient

μ_s……Scattering Coefficient

μ_t……Attenuation Coefficient

n…….Refractive Index

R_d……...Diffuse Reflectance

T_d……Diffuse Transmittance

T_c……Collimated Transmittance

T…….Postmortem Time

Φ…….Scattering Phase Function

p……..Normalized Phase Function

γ.…….Spherical Albedo

1. Introduction

Understanding the optical properties of biological tissues have become increasingly important over the past decades due to the growing applications of laser radiation in medicine and surgery. Unlike visible light, short-wave infrared (SWIR) light between 700 and 1500nm can penetrate deeply into the skin tissues and therefore offers potential spectral windows for functional imaging and medical monitoring without ionizing radiation hazards. A fundamental challenge in achieving medical application of the SWIR light is to understand the relation between the optical response of the skin and its structures. The light propagation in a strong turbid system such as the skin can be analyzed by a differential-integral equation of radiation transfer based on energy conservation law [Chandrasekhar 1950]. While the radiative transfer equation may be analytically solved for a few cases with simple boundary conditions, various approximations have to be resorted to obtain light distributions in problems with realistic boundary conditions. The radiative transfer modeling of light propagation can be statistically realized through Monte Carlo simulations in investigating light interaction with a turbid system [Wilson and Adams 1983; Keihzer *et al* 1989]. Within the framework of radiative transfer, the bulk response to the radiation by the system, assuming macroscopic homogeneity, can be characterized mainly with three parameters: the absorption coefficient μ_a, the scattering coefficient μ_s and an asymmetry factor $g=\langle\cos\theta\rangle$, where θ is the scattering angle and the sharp brackets represent ensemble

averaging using a scattering phase function p(θ). However, these parameters cannot be directly measured. Therefore, inverse methods have to be employed to calculate the parameters from experimentally observable quantities. Various numerical methods based on the radiative transfer theory have been used for the inverse calculation. Among these the Monte Carlo simulations provide a versatile tool to accurately model the light propagation in a turbid medium.

Extensive measurements have been carried out on skin tissues in the visible and some portions of the SWIR regions to study optical properties of the skin tissues [Anderson and Parrish 1981, van Gemert *et al* 1989]. Nevertheless, the strong scattering of light in the spectral regions in the skin tissue and lack of efficient mathematical tools has prevented accurate analysis of the light propagation to determine their optical parameters until recently. The rapid progress in computer technology has enabled wide acceptance of computing intensive modeling tools such as the Monte Carlo techniques. Recent studies with inverse calculations based on the Monte Carlo and adding-doubling methods, however, only provided skin tissues' optical properties from the visible to SWIR regions up to 1000nm in wavelength [Graaf *et al* 1993, Prahl *et al* 1993, Beek *et al* 1997, Simpson *et al* 1998]. As a result, a significant gap exists in the database of the skin optics in the SWIR region in which a weak water absorption band is known to exist at 1450nm, and the tissue scattering is expected to decrease as the light wavelength increases. Therefore, the SWIR region provides an interesting window to understand the interplay between the water and cellular components in the optical response by the skin tissues and may present significant opportunities for imaging the scattering-dominated skin tissues

with various techniques such as the optical coherent tomography [Tearney *et al* 1995]. The lack of accurate optical parameters between 1000 and 1500nm for the skin tissue, however, has prevented the investigations of imaging possibility. This study was initiated to obtain these parameters in the porcine skin dermis which has been widely used as a model of the human skin dermis [Lavker *et al* 1991].

In this thesis project, we have investigated the light-tissue and light-cell interaction with emphasis on the *in vitro* measurements of reflectance and transmittances of porcine dermis and the inverse calculations of the three optical parameters by a Monte Carlo method. The approach here is similar to those first reported by Peters *et al.* on determining optical parameters of human breast tissues [Peters *et al* 1990]. The effects of postmortem times and different tissue storage conditions on the optical properties of the dermis have been examined through study of μ_a, μ_s and g. Transmission electron microscopy (TEM) was employed to examine possible relations between the change in optical properties and the ultrastructure of the dermis. Furthermore, we analyze the sensitivity of the calculated values of the optical parameters on the experimental errors and inverse calculation procedures and discuss ways to improve the accuracy of the results.

Chapter 2 provides the background information on the radiometry and radiative transfer theory and the Monte Carlo simulation algorithms and codes. Chapter 3 describes the experimental methods to measure diffuse reflectance, diffuse transmittance and collimated transmittance with the details of optical setup. Tissue preparation and data

processing are described in Chapter 4. We present and discuss the results in Chapter 5 and conclude the thesis with Chapter 6.

2. Theoretical Background

The strong elastic scattering of visible and SWIR light by biological tissues, such as the skin, makes it very difficult to study light propagation inside the tissues. Elastic scattering of visible and near-infrared light is a result of the microscopic inhomogenuity in the refractive index associated with the cellular structure of the tissue on the scales of micrometer, or the scales of the wavelength. In any realistic model of light propagation in the turbid media of tissues, the substantial scattering needs to be accounted for. Two theoretical approaches can be adopted in modeling light propagation: the wave approach based on the Maxwell equation and energy approach based on the radiative transfer theory. The wave approach encounters profound difficulties in obtaining solutions when applied to biological tissue whose responses are of random nature in both space and time. In these cases, the radiative transfer theory often serves as a feasible framework to understand and model the light propagation in biological tissue. In this chapter, we will introduce first the basic concepts and terms of radiometry and the radiative transfer theory and then the treatment of light scattering. The modeling of light propagation by a Monte Carlo method will be discussed together with the simulation codes in FORTRAN.

2.1. Basic Radiometry Concepts

Radiometry deals with the problems of measuring the energy content of optical radiation fields and determining how this energy propagates through an optical system.

To do this, certain radiometric concepts and definitions are required which are listed in Table 1 [Boyd 1983, O'Shea 1985].

Table 1 Radiometric quantities and units

Quantity	Symbol	Definition	Unit
Radiant Energy	Q_e	$\int \Phi_e dt$	Joule
Radiant energy density	μ	dQ_e/dV	Joule/m^3
Radiant power, flux	Φ_e, P	dQ_e/dt	Watts
Radiant exitance	M	$d\Phi_e/dA$	Watts/m^2
Radiant intensity	I_e	$d\Phi_e/d\Omega$	Watts/sr
Irradiance	E_e, I	$d\Phi_e/dA$	Watts/m^2
Radiance	L_e	$d^2\Phi_e/dA_{proj}d\Omega$	Watts/m^2-sr

An ideal point source is a small source of light that radiates equally in all directions with in a zero volume. Real light sources with dimensions small compared to the observation distance are treated as point sources, such as the stars. To measure the portion of space into which a point source is radiating, we use the concept of a solid angle $\Omega=A/R^2$ where A is the area intercepted by the cone on the surface of a sphere of radius R centered on the

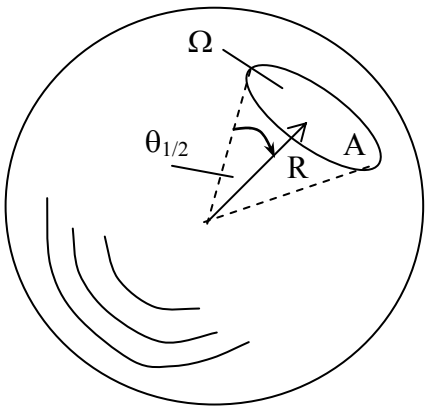

Fig. 1 The definition of the solid angle

cone vertex (Fig. 1). In 3-d space, the solid angle subtended by a sphere is 4π (sr) while the solid angle subtended by a right circular cone of half vertex angle $\theta_{1/2}$, shown in Fig. 2, is $4\pi\sin^2(\frac{\theta_{1/2}}{2})$.

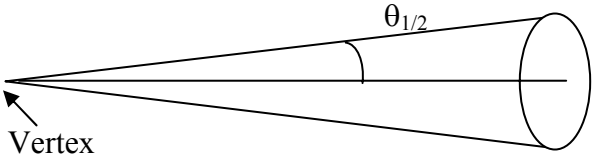

Fig. 2 Right circular cone

The following parameters are defined to characterize the properties of point sources. The radiant energy Q_e(J) is the total radiation energy leaving a source or delivered by the source. The total energy contained in a radiation field could be expressed in energy density $\mu = dQ_e/dV$, where dV is the volume element of the radiation field. The amount of radiative energy leaving the source per unit time is the radiation flux or power $\Phi_e = dQ_e/dt$. Flux emitted per unit area of source surface is called exitance $M = d\Phi_e/dA$. The "brightness" of a source is measured by its radiance L_e which is defined as flux per unit of source area dA_S per unit solid angle leaving a source:

$$L_e = \frac{d^2\Phi_e}{dA_S d\Omega}. \qquad (2.1)$$

An extended source may be thought of as a large collection of point sources distributed uniformly across a source area. If one observes the source at some angle θ to the surface normal, the source area should be substituted by the projected area

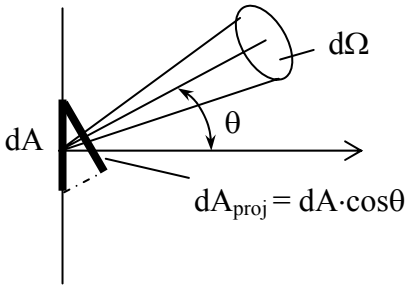

Fig. 3 Geometrical quantities appearing in the definition of radiance

along the direction as $dA_{proj} = dA_S\cos\theta$ (Fig. 3), and the radiance becomes:

$$L_e = \frac{d^2\Phi_e}{dA_S \cos\theta d\Omega}. \tag{2.2}$$

The quantity that describes the radiant output of a source is intensity I_e which is the flux (power) per unit solid angle emitted by an entire source in a given direction. Intensity is most useful for describing point sources:

$$I_e = \frac{d\Phi_e}{d\Omega} = \int_{source} L_e \cdot dA_{proj}. \tag{2.3}$$

Considering the detection of light, we define an irradiance as the the flux per unit area received by a real or imaginary surface element dA of a target $E_e = \frac{d\Phi_e}{dA} = \frac{I_e d\Omega}{dA}$ (W/m^2), where $d\Omega$ is the solid angle element subtended by dA at the source. For a point source of intensity I_e, it is easy to find the irradiance on dA as the following:

$$E_e = \frac{d\Phi_e}{dA} = \frac{I_e d\Omega}{dA} = \frac{I_e \cos\theta dA/r^2}{dA} = \frac{I_e \cos\theta}{r^2}, \tag{2.4}$$

where θ is the angle between r and the normal of target surface. The power received by the target is given by

$$\Phi_e = \frac{dQ_e}{dt} = \int E_e dA. \tag{2.5}$$

A light source with radiance L_e completely independent of viewing angle, or satisfying the Lambert's law, is defined as a Lambertian source. This applies to most

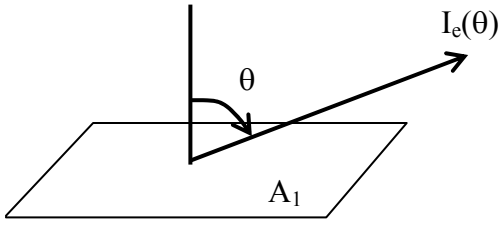

Fig. 4 The Lambertian source

incoherent radiation sources such as emitters, scatters and diffuse reflection surfaces. For Lambertian sources (Fig. 4), the radiant intensity in the θ direction is

$$I_e(\theta) = \int_{source} L_e \cdot dA_{proj} = \int_{source} L_e \cdot \cos\theta \cdot dA = L_e \cdot \cos\theta \cdot A_1 = I_0 \cos\theta \,. \qquad (2.6)$$

Here we used the fact that $I_0=L_eA_1=\Phi_e/\Omega$ since L_e is assumed to be independent of θ, where Φ is the total flux of the light generated from the source and Ω is the solid angle into which Φ is emitted, as shown in the Fig. 4.

Based on Eq. (2.6), the differential intensity from an element of source dA_1 becomes:

$$dI_e(\theta) = L_e \cdot \cos\theta \cdot dA_1 \,. \qquad (2.7)$$

Now considering another surface dA_2 at a distance D from dA_1, the solid angle subtended by dA_2 at the center of dA_1 is given by $d\Omega_{A2} = \frac{\cos\theta_2 dA_2}{D^2}$ (Fig. 5). From the above analysis for the Lambertian sources we could obtain for the flux arriving at the surface dA_2 from the source dA_1 as the following:

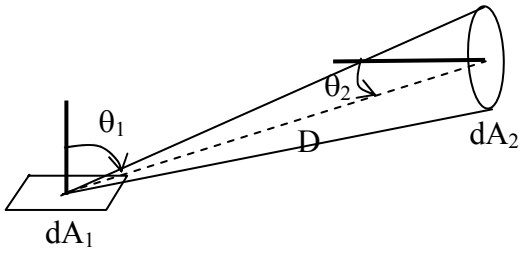

Fig. 5 Target in the radiation field of a Lambertian source

$$d^2\Phi_2 = dI_e(\theta_1)d\Omega_{A2} = L_e \cos\theta_1 dA_1 \frac{\cos\theta_2 dA_2}{D^2} \,. \qquad (2.8)$$

2.2. Single-Scattering vs Multiple-Scattering

As discussed previously, light scattering shares the same physical origin of microscopic inhomogeneity in the dielectric properties of medium with light reflection,

refraction and diffraction [Kortum 1969]. The angular distribution of scattered light intensity from a scattering center of single particle is generally far from isotropic, depending on the size, state, and polarizability of the particle and on the direction of observation. Rigorous treatments based on the Maxwell's equations exist only in the forms of the Rayleigh scattering [Ishimaru, 1978] for single-scattering by molecules of low density, whose linear dimension is much smaller than the visible light wavelength, and the Mie theory for scattering by a spherical particle of any size [Bohren and Huffman 1983]. As an example of the wave approach, we will discuss the Rayleigh scattering in the following.

Rayleigh first developed the theory about the light scattering by the molecules of gas [Rayleigh 1881 and 1899]. He assumed that the electric field of the incident light wave excites the electrons of a molecule into forced oscillations of the same frequency, the frequency of the radiation being supposed to be very much smaller than the natural frequency of the electrons. If the dimensions of the molecules considered are small compared with the wavelength, it can be assumed that all the electrons oscillate in

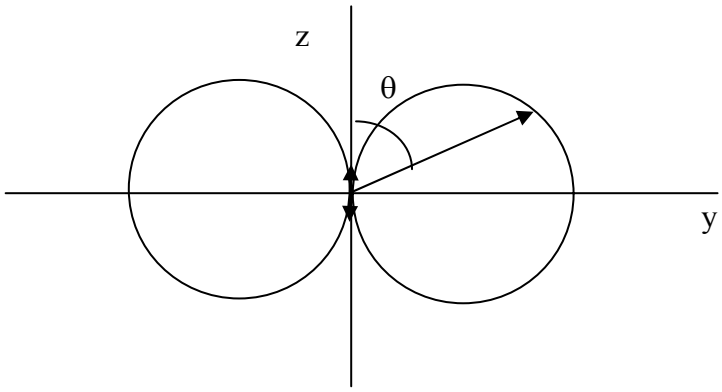

Fig. 6 The Radiation characteristic of a dipole oscillating induced by vertically polarized light incident in x-axis direction (vertical to the paper).

phase so that the molecule forms an oscillating dipole and radiates secondary waves of the same frequency in all direction, which can be defined as the scattered wave of the primary. The electrical dipole moment $\vec{\mu}_i$ induced in the molecule depends upon the primary field strength $\vec{E}$ as $\mu_i = \alpha\vec{E}$. The amplitude of the wave emitted from the oscillating dipole induced from vertically polarized light is described as:

$$A = \frac{4\pi^2\nu^2}{c^2 R}\mu_i \sin\theta . \tag{2.9}$$

Here ν is the frequency of incident light, R the distance from dipole, θ the angle from the direction of dipole (Fig. 6). For a monochromatic incident wave with an electric field given by $\vec{E} = \vec{E}_0 e^{i2\pi\nu(t-\frac{R}{c})}$, the light intensity is related to the field as $I_0 = \frac{c}{8\pi}\vec{E}_0^{\,2}$ and the intensity of scattering light as $I = \frac{c}{4\pi}A^2$. This leads us to the intensity ratio of scattered to the incident light:

$$\frac{I_\theta}{I_0} = \frac{1}{R^2}\left(\frac{2\pi}{\lambda_0}\right)^4 \alpha^2 \sin^2\theta , \tag{2.10}$$

where λ_0 is the wavelength in vacuum. If the input light is unpolarized, Eq. (2.10) could be modified to the Rayleigh scattering formula for dilute gas:

$$\frac{I_\theta}{I_0} = \frac{4\pi^2(n-1)}{N^2\lambda_0^{\,4}R^2}\left(\frac{1+\cos^2\theta}{2}\right), \tag{2.11}$$

where N is the density of the molecular in a gas and n is the refractive index. From Eq. (2.11) we can see the scattered intensity is inversely proportional to the fourth power of the wavelength λ_0 and depends on the angle of scattering. It must be emphasized again

the Rayleigh scattering only suitable for the isotropic molecules which are very small compared with the wavelength. If the molecule is in same dimension as the wavelength, the interference and the size of dipoles need to be considered. It has been shown that with increasing scattering angle and diameter of molecules, the scattered intensity decreases as a result of interference and scattered radiation becomes unsymmetrical [Kortum 1969].

When considering turbid media with high density of particles or scattering centers, the photons will undergo multiple scatterings. In these cases, one should take into account the interference of the scattered wave fields by multiple scattering centers in the wave approach, which makes the analytical solution nearly impossible for tissue optics because of the complexity of the problem. Instead, the energy approach has to be resorted without direct consideration of light interference. As we will discuss later, the energy approach characterizes the medium's response to the incident light by optical parameters of the medium: the absorption and scattering coefficients and scattering phase function. These parameters, however, can be defined on the basis of wave approach treatment of light scattering by a single microscopic particle.

To illustrate the relationship between the two approaches, we discuss this problem in two steps [Ishimaru, 1978]. First, we consider light scattering and absorption by a single particle and then derive a general formulation for multiple scattering. Let us begin from a linearly polarized light propagating in a medium with dielectric constant ε_0 and permeability μ_0, with the electric field of the incident light wave given by:

$$\vec{E}_i(r) = \vec{E}e^{ik\hat{i}\cdot r}, \tag{2.12}$$

where $\vec{E}$ is the field magnitude, $\hat{i}$ a unit vector in the direction of wave propagation, λ the wavelength in the medium and $k = \omega\sqrt{\mu_0\varepsilon_0} = 2\pi/\lambda$ the wave number. The scattering center, or the particle (Fig. 7), has a relative dielectric constant given by

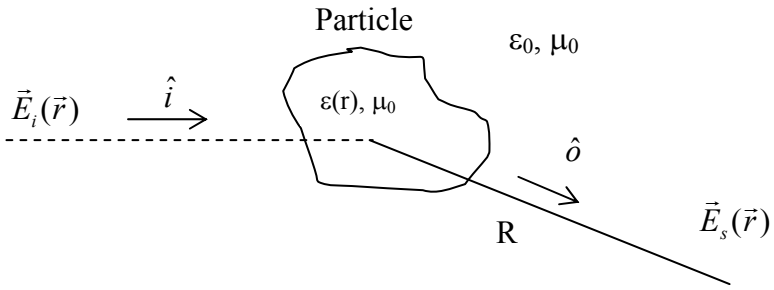

Fig. 7 A plane wave incident upon a particle

$$\varepsilon_r(r) = \frac{\varepsilon(r)}{\varepsilon_0} = \varepsilon_r'(r) + i\varepsilon_r''(r)\,. \tag{2.13}$$

which is in general complex and a function of position. The field at a distance R from a reference point in the particle, in the direction of a unit vector $\hat{o}$, can be found by adding the incident field $\vec{E}_i$ and scattered field $\vec{E}_s$. For near field within a distance $R<D^2/\lambda$ (where D is the dimension of the particle), the scattered field $\vec{E}_s$ is very complicated because of the interference between contributions from different parts of the particle. For far field at $R>D^2/\lambda$, however, the scattered field $\vec{E}_s$ behaves as a spherical wave and can be written as

$$\vec{E}_s(r) = \vec{E}\, f(\hat{o},\hat{i})\frac{e^{ikR}}{R}, \tag{2.14}$$

where $\vec{E}f(\hat{o},\hat{i})$ represents the amplitude, phase and polarization of the scattered wave and is called the scattering amplitude. The scattered wave is in general elliptically polarized even for an incident wave with linear polarization.

Considering the scattered power flux density S_s at a distance R from the particle in the direction $\hat{o}$ caused by an incident power flux density S_i, we can define the differential scattering cross section as:

$$\sigma_d(\hat{o},\hat{i}) = \lim \frac{R^2 S_s}{S_i}|_{R\to\infty} = | f(\hat{o},\hat{i}) |^2 = \frac{\sigma_t}{4\pi} p(\hat{o},\hat{i}), \tag{2.15}$$

where $\eta_0 = \sqrt{\mu_0 \varepsilon_0}$ is the impedance of the medium surrounding the particle and S_i and S_s are the magnitudes of the incident and the scattering power flux density vectors given by

$$\vec{S}_i = \frac{1}{2}(\vec{E}_i \times \vec{H}_i^{\,*}) = \frac{|E_i|^2}{2\eta_0}\hat{i}, \qquad \vec{S}_s = \frac{1}{2}(\vec{E}_s \times \vec{H}_s^{\,*}) = \frac{|E_s|^2}{2\eta_0}\hat{o}, \tag{2.16}$$

The function $p(\hat{o},\hat{i})$ is a dimensionless quantity called scattering phase function and σ_t is the total cross section to be defines next. We can see that σ_d has the unit of area per solid angle and relates to the cross section of the particle causing uniformly distributed scattered wave $\vec{E}_s(r)$ over one steradian solid angle about direction $\hat{o}$ and varying with $\hat{o}$. Integrating the differential scattering cross section σ_d over the full solid angle surrounding the particle, we find the scattering cross section σ_s of a particle leading to the scattered wave $\vec{E}_s$

$$\sigma_s = \int_{4\pi} \sigma_d d\omega = \int_{4\pi} | f(\hat{o},\hat{i}) |^2 d\omega = \frac{\sigma_t}{4\pi} \int_{4\pi} p(\hat{o},\hat{i})\, d\omega, \tag{2.17}$$

where dω is the differential solid angle. The ratio of the scattering cross section to the total cross section is called the albedo of a single particle, given by

$$\alpha = \frac{\sigma_s}{\sigma_t} = \frac{1}{\sigma_t}\int_{4\pi} |f(\hat{o},\hat{i})|^2 d\omega = \frac{1}{4\pi}\int_{4\pi} p(\hat{o},\hat{i})\, d\omega \,. \tag{2.18}$$

Similarly, we can define a cross section associated with a particle which corresponds to the absorbed ratio of the incident radiation power as the absorption cross section σ_a. The sum of the scattering and absorption cross sections provide the total cross section σ_t

$$\sigma_t = \sigma_s + \sigma_a \,. \tag{2.19}$$

Now we turn to the multiple scattering of light in a turbid medium with randomly distributed scattering centers with a density ρ. Because of the randomness of particle distribution, we can neglect the interference between waves scattered by different particles. Accounting for the power scattered or absorbed from all particles, we find the incident power density S_i at d from the incident point as

$$S_i(d) = S_{i0} e^{-\int_0^d \rho\sigma_t ds}, \tag{2.20}$$

where the integration is over the path of the light traveling and $\tau = \int_0^d \rho\sigma_t ds$ is named as the optical pathlength or depth. The quantity

$$\mu_t = \rho\sigma_t \,, \tag{2.21}$$

is defined as attenuation coefficient. Combining Eq. (2.20) with (2.18), we obtain the absorption coefficient and scattering coefficient as

$$\mu_a = \rho\sigma_a \qquad \text{and} \qquad \mu_s = \rho\sigma_s \,, \tag{2.22}$$

respectively. We note that the above derivations may fail if the density of the scattering and absorption centers in the turbid medium is very high. Detailed discussion, however, is beyond the scope of this thesis [Ishimaru, 1978].

2.3. Radiative Transfer Theory

The radiative transfer theory [Sobolev 1963] deals only with transport of radiative energy through a medium containing scattering and absorbing centers. The basic equation in radiative transfer theory can be obtained from the principle of energy conservation in the following form: [Chandrasekhar, 1960]

$$\frac{dL(\vec{r},\vec{s})}{ds} = -\mu_t L(\vec{r},\vec{s}) + \mu_t \Im, \tag{2.23}$$

where $L(\vec{r},\vec{s})$ is the light radiance at position $\vec{r}$ in a direction defined by unit vector $\vec{s}$ and the unit of radiance is given by $\frac{W}{m^2 \cdot steradian}$. The left side of Eq. (2.23) is the projection of the radiance gradient along the direction $\vec{s}$ and the first term on the right side represents the loss rate of the radiance due to both scattering and absorption. The attenuation coefficient μ_t is defined as the sum of the absorption coefficient μ_a and scattering coefficient μ_s. The second term on the right side, $\mu_t \Im$, is a "source" function symbolizing the radiance gain rate due to scattered light from other directions back into $\vec{s}$ and other light sources in the medium. In a turbid and source-free medium, such as the skin tissues, the source function $\Im$ can be written as:

$$\Im(\vec{r},\vec{s}) = \frac{1}{4\pi}\int_{4\pi}\Phi(\vec{s},\vec{s}')L(\vec{r},\vec{s}')d\Omega', \tag{2.24}$$

where the phase function $\Phi(\vec{s},\vec{s}')$ describes the probability of light energy $L(\vec{r},\vec{s}')d\Omega'$ being scattered from the $\vec{s}'$ into the $\vec{s}$ direction and $d\Omega'$ denotes the element of solid angle in the $\vec{s}'$ direction. Thus the equation of transfer becomes:

$$\vec{s}\cdot\vec{\nabla}L(\vec{r},\vec{s}) = -\mu_t L(\vec{r},\vec{s}) + \frac{\mu_t}{4\pi}\int_{4\pi}\Phi(\vec{s},\vec{s}')L(\vec{r},\vec{s}')d\Omega'. \tag{2.25}$$

If the scattering is symmetric about the direction of the incoming light, the phase function will only be a function of the angle θ between $\vec{s}'$ and $\vec{s}$, i.e., $\Phi(\vec{s},\vec{s}') = \Phi(\theta)$. A widely used form of the phase function was proposed by Henyey and Greenstein as [Henyey *et al* 1941, van Gemert *et al* 1989],

$$\Phi(\theta) = \frac{\gamma(1-g^2)}{(1+g^2-2g\cos\theta)^{\frac{3}{2}}}, \tag{2.26}$$

where γ is the spherical albedo and g is the asymmetry factor as defined in the following:

$$g = \frac{1}{4\pi\gamma}\int_{4\pi}\Phi(\theta)\cos\theta d\Omega', \tag{2.27}$$

$$\gamma = \frac{1}{4\pi}\int_{4\pi}\Phi(\vec{s},\vec{s}')d\Omega', \tag{2.28}$$

$$= \frac{\mu_s}{\mu_t} = \frac{\mu_s}{\mu_s+\mu_a}. \tag{2.29}$$

A normalized phase function is denoted as $p(\vec{s},\vec{s}')$, representing the angular distribution of scattering probability:

$$\int_{4\pi} p(\vec{s},\vec{s}')d\Omega' = 1, \tag{2.30}$$

which leads to

$$p(\theta) = \frac{\Phi(\theta)}{4\pi\gamma} = \frac{(1-g^2)}{4\pi(1+g^2-2g\cos\theta)^{\frac{3}{2}}}. \tag{2.31}$$

Assuming that the scattering and absorbing centers are uniformly distributed in a turbid medium, the radiance may be further divided into two parts: the scattered radiance L_s and the coherent radiance L_c [Lu *et al*, 1999, Yoon *et al* 1987],

$$L(\vec{r},\vec{s}) = L_c(\vec{r},\vec{s}) + L_s(\vec{r},\vec{s}). \tag{2.32}$$

The reduction in the coherent radiance, i.e., the portion of the incident radiation which has neither been scattered nor absorbed, is described by:

$$\frac{dL_c(\vec{r},\vec{s})}{ds} = -\mu_t L_c(\vec{r},\vec{s}). \tag{2.33}$$

which is often called the Lambert-Beer's law. Therefore, the scattered radiance L_s must satisfy

$$\vec{s}\cdot\nabla L_s(\vec{r},\vec{s}) = -\mu_t L_s(\vec{r},\vec{s}) + \mu_s \int_{4\pi} p(\vec{s},\vec{s}')[L_s(\vec{r},\vec{s}') + L_c(\vec{r},\vec{s}')]d\Omega'. \tag{2.34}$$

Most biological soft tissues, including the skin tissue, are highly turbid media with various chromophore and the water component in the tissue absorbing light. In this thesis study, we intend to investigate the response of porcine skin to SWIR light by measuring the various experimental observables on tissue samples in a slab form. In these cases, light scattering by a tissue sample can be divided into two types: bulk scattering and deflection due to surface roughness and index mismatch. The radiative transfer theory has

been proved to be an excellent model to describe light propagation in the tissue bulk without considering coherence and polarization. The rough surface effect, however, has not been studied because of the lack of appropriate analytical tools and surface characterization data. As a result, we will assume that the two surfaces of tissue samples are optically flat and smooth in our modeling and keep the experimental conditions as close as possible by sandwiching the sample between two optical windows and moistening with 0.9% saline to reduce index mismatch.

2.4. Inverse Calculation with the Monte Carlo Simulations

The radiative transfer equation could only be solved analytically in a few cases with very simple boundary conditions. Numerical methods are generally resorted to solve radiative transfer problems. Among these, the Monte Carlo simulation provides a simple, widely applicable and yet accurate method. Using a random walk model [Wilson et al, 1983]. the Monte Carlo simulation offers nearly exact solution to 3-D problems of radiative transport of arbitrary boundary conditions [Song, 1999 and Dong 1999].

In a typical Monte Carlo calculation, one starts with a given set of optical parameters of the medium in which light propagate, such as μ_a, μ_s and g, and proceeds to obtain various quantities such as diffuse reflectance, diffuse transmittance and collimate transmittance that are experimental observable. In our investigations, however, this process has to be inverted because the optical parameters are not known *ab initio*. In fact, these parameters are the results to be obtained from the experimental data of transmittance and reflectance. Therefore, this type of calculations is named as inverse

problem. A simple way to do this is to build a table of diffuse reflectance and transmittance versus μ_a, μ_s and g which can be used later to look up the values of the parameters from experimental data [Firbank 1993]. For samples of variable thickness, which are the cases in our studies, this method would require a lot of calculations to ensure the accuracy of the result. Instead, we modified an existing Monte Carlo simulation program that has been recently developed at Biomedical Laser Laboratory at East Carolina University [Song, 1999 and Dong 1999] to calculate diffuse reflectance and transmittance of light from a skin sample in a slab form with thickness D. We briefly describe the major features of the Monte Carlo codes in this section before providing details on the inverse determination of optical parameters in the next section.

To simulate light distribution at the two sides of a slab skin tissue sample, we inject N photons into the sample in a direction perpendicular to the sample surface and track their 3-D trajectories inside the sample until they exit. The scattering and absorption of a tracked photon are described as random events with probability distribution dictated by scattering and absorption coefficients, respectively. The probability distribution function for the free path length of scattering L_s for a photon between two scattering events is assumed as [Keijzer, 1989]

$$P(L_s) = \mu_s e^{-\mu_s L_s}. \tag{2.35}$$

The parameter L_s is sampled from a uniformly distribution of random numbers (RND) between 0 and 1 to satisfy the above equation through the following transformation:

$$L_s = -\ln(1 - RND)/\mu_s. \tag{2.36}$$

Similarly, the total path length of a photon traveled before being absorbed, L_a, is obtained from

$$L_a = -\ln(1 - RND)/\mu_a . \tag{2.37}$$

Before a photon is injected at the tissue surface, its total path length L_a is first determined from Eq.(2.36). Then the parameter L_s is determined from Eq.(2.35) each time before the tracked photon is allowed to travel before next scattering. Using the a Heyey-Greenstein distribution Eq. (2.25) as the phase function, the distribution functions of azimuthal ($0 \le \phi \le 2\pi$) and polar scattering angles ($0 \le \theta \le \pi$) for a photon are given by:

$$p(\cos\theta) = \frac{(1-g^2)}{2(1+g^2-2g\cos\theta)^{3/2}}, \tag{2.38}$$

$$p(\phi) = \frac{1}{2\pi}, \tag{2.39}$$

where g is the asymmetry factor defined as the ensemble average of $\cos\theta$, i.e., $g = \langle\cos\theta\rangle$. Once the tracked photon exit from the tissue sample, the position and the direction of the photon at the exit point will be used to determine if the photon contributes to collimated reflectance or diffused reflectance or collimated transmittance or diffuse transmittance. After injection and tracking of all the incident photons, N, the total number of the outgoing photons are tallied to calculate diffuse reflectance R_d, diffuse transmittance T_d, and collimated transmittance T_c by dividing the number of each type of photons by N.

2.5. Algorithms and The Codes

The Monte Carlo simulation codes were developed for a tissue phantom based on the experiments configuration. In the program the slab sample is hold in two sapphire windows as show in Fig. 8. The light scattering and absorption in the windows are negligible. There are four parallel interfaces, two tissue-sapphire interfaces and two sapphire-air interfaces. Refraction and reflection at these interfaces are considered. The Monte Carlo codes can be divided into four major modules with a flow chart included in Appendix C. The initial module deals with initial photon injection, which decides the distribution of the photon density and the specular reflection on the input surface. The photon tracking module follows the trajectory of a photon propagating inside media simulating a skin sample sandwiched between two sapphire widows. When the tracked photon enters the neighborhood of an interface, another module was used to determine if the photon reflects from or transmits through the interface. The last module tracks the path of these photons enter the sapphire windows, and decides if they could be counted as diffuse transmission, reflection or collimated transmission and reflection. Detail discussions about each module are given in this section with major module codes listed in Appendix C.

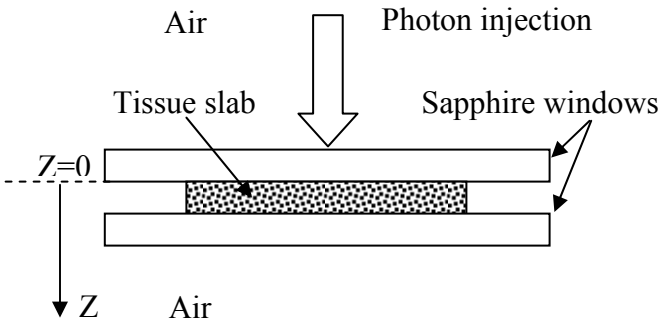

Fig. 8 Phantom for Monte Carlo simulation.

2.5.1.The Initial Calculation

The first 200 lines of the main program and the subroutine "Initl_sys" start the inverse calculation by initializing parameters about tissue size, attenuation coefficient amuT (μ_t), absorption coefficient amuA (μ_a) and asymmetry factor g, etc. Using a Cartesian coordinate system (x, y, z), a tissue slab with thickness z0 (mm) is placed in the x-y plane at z = 0 with the light beam on the sapphire-tissue interface incident from the sapphire side: $z = 0^-$. The incident point of the beam is visualized as a sieve with circular meshes of area $\pi(NR0)^2$, where the parameter NR0 is used to control the total number of injected photons. Each photon will be injected through one of these meshes with the x, y coordinates of the mesh stored in the arrays Xinc() and Yinc(), respectively. The following codes provide the coordinate of each mesh:

```
DO 1440 Iyinc=1,2*NR0+1
        Yinc_nn=NR0-(Iyinc-1)
        NNx=0
        DO 2440 Ixinc=1,2*NR0+1
                Xinc_nn=NR0-(Ixinc-1)
                rsq=Xinc_nn*Xinc_nn+Yinc_nn*Yinc_nn
                if ( rsq.LE.(NR0**2) ) then
                  NNx=NNx+1
                  Xinc(NNx)=fr0*Xinc_nn
                  Yinc(NNx)=fr0*Yinc_nn
                end if
2440    end do
```

where $fr0=R_{tissue}/NR0$ stands for the length of each mesh. The distribution of the photons injected at each mesh will be varied according to the profile of the input beam. For a "top-hat" beam assumed in this study, in which the photon density is a constant over the beam area, the number of the meshes inside the beam area is same as the number injected

photons. The following subroutine decides the reflection of the injected photon at the sapphire-tissue interface

```
Subroutine Tophat_beam(idum,x1,y1,Ir,aIr)
        Implicit real(a-h, o-z)
        external Ran2
common/medium/Aindex,g,winDEX
common/beam/R0,aI0,tows,ovf,fr0,Zpls_w,xpls_w
         r1s=x1*x1+y1*y1
         aIr=aI0
         phii=atan(sqrt(r1s)*ovf)
         call Refrct(phii,winDEX,aindex,Rphii)
         Rans=Ran2(idum)
         ref_int=Rphii-Rans
         if(ref_int.ge.0)then
                Ir=0
         end if
         return
         end
```

The reflection coefficient is calculated from the Fresnel formula [Jackson 1976] and compared to a random number draw from a uniform distribution between 0 and 1 to determine the fate of a tracked photon when it travels upon an interface. If the reflection coefficient is smaller than the random number, the photon is reflected. Otherwise, the photon transmits through the interface with a refraction angle given by the Snell's law. The photon will be tracked until it is absorbed inside the tissue or escape into air. The following codes provide an example of treating photons at a sapphire-air interface from the sapphire side:

```
Do while(JFK.eq.0)
        CALL refrct(0.0,winDEX,1.0,Rphii)
        temp_ran=Ran2(idum)
        ref_res=Rphii-temp_ran

        if( ref_res.ge.0.0) then
          Ir=1
          CALL Tophat_beam(idum,x1,y1,Ir,aIr
          JFK=Ir
        else
```

```
            Ir=0
            JFK=1
          end if
end do
```

If the tracked photon escapes from the sapphire-air interface, the tracking stops and next photon will be injected as indicated by setting the parameter Ir=0. If the photon is reflected back into the sapphire side, the subroutine "Tophat_beam" will be called to continue photon tracking until the photon exit from the sapphire layer (JFK=1). The attenuation coefficient of the window holding the tissue sample is set to zero in the SWIR region. Once a tracked photon enters the tissue layer, the refraction angle is calculated in the subroutine "Initl_coord1" as the variable phi1:

```
subroutine Initl_coord1(idum,Ibeam,F,x1,y1,z1,phi1,psi1)
        Implicit real(a-h, o-z)
        external Ran2
        common/beam/R0,aI0,tows,ovf,fr0,Zpls_w,xpls_w
        common/const/Pi,zero_p,one_m
        common/medium/Aindex,g,winDEX

        Z1=zpls_w*Ran2(idum)
        if (x1.eq.0.) then
                thta1=pi/2.
                if(y1.lt.0.) thta1=-pi/2.
                if(y1.eq.0.) thta1=0.
        else
                thta1=ATAN(y1/x1)
        end if
        if( x1.lt.0.) thta1=PI+thta1
        if(thta1.lt.0.) thta1=2.*PI+thta1
        PSI1=THTA1+PI

        R1=sqrt(x1*x1+y1*y1)

        phi1=(Ibeam-1)*asin(winDEX*R1/sqrt(R1*R1+(F-Z1)*(F-Z1))/aindex)
        return
        end
```

In our case of collimated and normal incident beam, the incidence angle of photon is 0° degree so both reflection and refraction angle are 0° degree unless the photon re-enters the tissue layer due to backscattering.

2.5.2.Photon Tracking Inside Tissue

After injected into the tissue, the trajectory of the photon is determined by a series of change in its position and direction as a result of scattering before it is absorbed or escaped. The free path length DL traversed by a photon before being absorbed is random chose with a mean value of by $1/\mu_a$, see Eq. (2.31), in the following codes before tracking the photon inside the tissue:

```
TEMP=Ran2(idum)
DL=-ALOG(1.-TEMP)/amuA
maxshot=Int(DL/deltad)
```

The distance D between two consecutive scattering events is random chose with a mean value of $1/\mu_s$:

```
TEMP=ran2(idum)
D=-ALOG(1.-TEMP)/amuS
DT = DT + D.
```

DT here records the actual photon travel distance in tissue and is compared to the free path length DL to determine if the photon is absorbed. The scattering angle is calculated using subroutine "scatt_dir":

```
subroutine scatt_dir(idum, Phii, Psii)
    Implicit real(a-h, o-z)
    external Ran2
    common/const/Pi,zero_p,one_m
```

```
common/medium/ainDex,g,winDEX
common/cphs/phs1,phs2,phs3,phs4
common/dir/phi_im1,psi_im1,sinphi,cosphi,sinpsi,cospsi
common/coord/X_im1,Y_im1,Z_im1

cosgt1=0.
TT=ran2(idum)

cosphis=phs1+phs2/(phs3+phs4*TT)**2.

if(g.eq.0.) cosphis=2.*TT-1.

phis=acos(cosphis)
sinphis=sin(phis)
PSIS=2.*PI*ran2(idum)

ALPHA=COSPHIS*SINPHI + SINPHIS*COS(PSIS)*COSPHI
TT=COSPHIS*COSPHI-SINPHIS*COS(PSIS)*SINPHI
if(abs(TT).gt.1.)then
         cosgt1=TT
         TT=nint(TT/abs(TT))
end if
PHIi=ACOS(TT)
PSIi=PSI_im1+ATAN(SINPHIS*SIN(PSIS)/ALPHA)
IF(ALPHA.LT.0.0) PSIi=PSIi+PI

if(abs(cosgt1).gt.1.00000001) write(*,*)'cos(phi)>1 ',cosgt1
        return
        end
```

Here the polar angle Psii and azimuthal angle Phii are calculated according to the Eq. (2.32) and (2.33).

2.5.3.Photon Refraction and Reflection at An Interface

Each time after a scattering, the position of the next scattering center (Xi, Yi, Zi) will be determined to see if the photon may travel out of the tissue before reaching the position. A condition of Zi larger than z0 or smaller than 0 means the tracked photon will hit the tissue-sapphire interface. Based on the coordinate of the previous scattering center (X_im1, Y_im1, Z_im1) and the scattering angle it is fairly straightforward to calculate

the probability for photon to be either reflected or refracted as described previously. Two subroutines, "refrct" and "reflct", are written for this purpose:

```
subroutine Refrct(phii,ani,anr,Rphii)
        Implicit real(a-h, o-z)
        common/const/Pi,zero_p,one_m

        sinphir=ani*sin(phii)/anr

        Rphii=1.
        if(abs(sinphir).le.zero_p) then
                Rphii=(anr-ani)/(anr+ani)
                Rphii=Rphii*Rphii
        else if (abs(sinphir).lt.one_m)then
                phir=asin(sinphir)
                sinphip2=sin(phii+phir)
                sinphip2=sinphip2*sinphip2
                sinphim2=sin(phii-phir)
                sinphim2=sinphim2*sinphim2

        Rphii=0.5*sinphim2/sinphip2*(1.+(1-sinphip2)/(1.-sinphim2))
        endif
        return
        end



Subroutine reflct(Rans,Zout,Zi,ref_int)
        mplicit real(a-h, o-z)

        common/const/Pi,zero_p,one_m
        common/medium/ainDex,g,winDEX
        common/snap/DTp,deltaD,Lshot,nshot,nishot
        common/ref/ref_norm,Iout,intref
        common/dir/phi_im1,psi_im1,sinphi,cosphi,sinpsi,cospsi

        sign_zi=sign(1.,zi)
        PHI1=sign_zi*phi_im1+int(1.-sign_zi)*0.5*Pi

        CALL Refrct(phi1,aindex,winDEX,Ref)

        ref_int=Ref-Rans
        if(ref_int.lt.0.) then
                Iout=Iout+1
                nshot=nishot
                ref_int=ref_int*zi
        else
                intref=intref +1
                phi_im1=pi-phi_im1
                Zi=Zi-2.*Zout*sign_zi
```

```
            ref_int=0.
end if
return
end
```

The "refrct" calculates the refraction angle and the value of reflection coefficient Rphii at the interface and "reflct" calls subroutine "refrct" and compares the reflection coefficient to a random number Rans to determine if the photon will be reflected or refracted.

2.5.4.Effect of Sapphire Windows

Even without considering absorption and scattering inside the sapphire windows as the sample holder, the windows have significant influence on the simulation results for the tissue configurations we considered here. Four interfaces, two sapphire-tissue and two sapphire-air, have to be taken into account. The refractive index of sapphire used in experiment is around 1.75 in the SWIR region. Because the relative large index mismatch at all the four interfaces, even the photons with large incident angle at tissue-sapphire interface could escape from the tissue. Thus the total number of photons being absorbed by tissue is reduced from the cases without considering the windows or increased reflectance and transmittance in the simulation. In other words, the inversely determined absorption coefficient is larger than that without considering the windows.

The photons escaped into the air will be divided into four groups corresponding to their relation to the integrating sphere. Those photons hitting the inside surface of the sphere are counted as either diffusely reflected, Ird, or diffusely transmitted, Itd,

depending on which side of tissue the photon escaped from. The other two groups of escaped photons are counted towards the collimated transmission and specular reflection. The ratios of Ird and Itd to the total photon number N, converted from the number of the photons injected at the window-tissue interface at z = 0 to the air side of the air-window interface, are obtained to find the diffuse reflectance R_d and diffuse transmittance T_d.

3. Experimental Techniques I

Integrating spheres can be used for scattered light signal measurements or as sources of illumination. The reflectance of human skin has been measured *in vivo* in as early as 1950's with an integrating sphere [Jacquez and Kuppenheim 1955]. During the last two decades, the integrating sphere technique has been widely used to measure the reflection and transmission of various soft tissues in the visible and near-infrared regions [Simpson C R *et al* 1998, Peters V G *et al* 1990, Yoon G *et al* 1987, Beek J F *et al* 1997, Pickering J W *et al* 1993, Pickering J W *et al* 1992]. In this chapter we will provide a detailed derivation of the integrating sphere theory for measuring diffuse reflectance and diffuse transmittance and illustrate the spatial filtering technique for measuring the collimated transmittance. In addition, we will discuss the mechanism of CCD camera for measuring 2-D distribution of scattered light in the studies of scattering of a laser beam at 1064nm by cultured cells.

3.1. Integrating Sphere Technique

The technique of using integrating spheres to measure scattered light signals appeared as early as 1920s' [Karrer 1921, Rosa and Taylor 1922, Hardy and Pineo 1931]. The inner surface of a sphere is typically made of or coated by high reflectivity materials in the form of rough surface to homogenize the light distribution inside the sphere.

Ideally, the inner surface of the integrating sphere should reflect light uniformly according to Lambert's law without absorption.

Different theories of integrating sphere appeared from 1920s' to 1950s' [Rosa and Taylor 1922, Hardy and Pineo 1931, Moon 1940, Walsh 1953]. It was only until 1960's that complete theories in forms easily understood by experimenters were widely accepted [Jacquez and Kuppenheim 1955, Miller and Sant 1958, Goebel 1967]. Since then the integrating sphere technique has become an established method to measure the diffuse reflectance and/or diffuse transmittance of turbid sample. An integrating sphere works as a radiation collector to spatially integrates incident radiant flux, therefore, the theory of the integrating sphere is based on the analysis of multiple reflections in a cavity.

3.1.1.An Ideal Integrating Sphere.

An ideal integrating sphere is a sphere with inner surface of 100% reflection and obeying the Lambert's law and negligible port sizes for the illumination and detection. Considering a sphere shown in Fig. 9 with radius R and two surface elements, dA_1 and dA_2, we find the following relations: $\theta_1=\theta_2=\theta$ and $D=2R\cos\theta$, where D is the distance between the two elements. Assuming that dA_1 functions as a light source with a radiance L and dA_2 as a target, from the Lambert's law and the Eq. (2.8) the flux radiating from dA_1 and arrival at dA_2 is given by

$$d^2\Phi = L\frac{dA_1 dA_2}{4R^2}. \qquad (3.1)$$

From the above equation, we find that the flux is independent of angle as it travels from one location of the inner surface to another. Therefore, the irradiance on dA_2 of the inner surface can be found as: $E=I_0/4R^2$, where $I_0=LdA_1$ is the intensity of the source element dA_1 in the perpendicular direction and total flux on the entire inner surface is

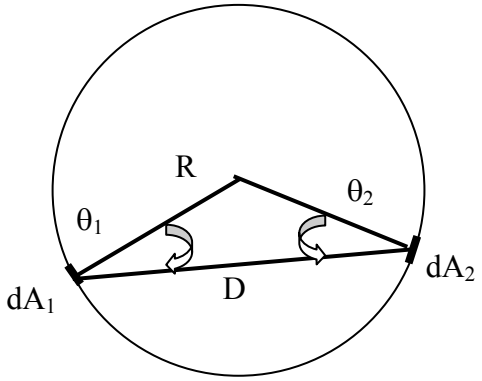

Fig. 9 An ideal integrating sphere

$$\Phi = \int_{entire\,surface} EdA_2 = \pi I_0. \qquad (3.2)$$

Consequently, the fraction of flux on a finite area A_2 to the total flux received by the entire inner surface is simply given by the area ratio, i.e.,

$$F = \frac{\Phi_{A_2}}{\Phi} = \frac{A_2}{4\pi R^2}. \qquad (3.3)$$

3.1.2.The Effect of Port Area with No Reflection

In real integrating sphere with ports for light entry and the detection, the effect of port area on the light distribution has to be considered. We discuss this effect in following two steps.

3.1.2.1.Transient Light Input

Assume that an impulse of radiation of flux or power Φ_0 enters into a sphere as shown in Fig. 10. If ρ is the diffuse reflectance of the wall, the total flux being reflected back to the inner sphere surface is given by $\rho\Phi_0$ and the reflecting area can be treated as an extended source. Since the entry port has no reflection, the ratio of the flux received by the total inner surface of the sphere due to the first reflection to the total reflected power $\rho\Phi_0$ is given by the area ratio:

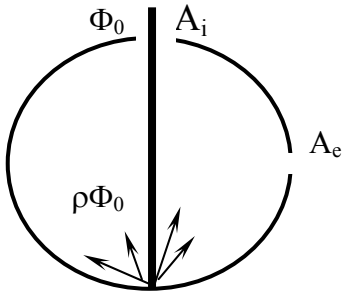

Fig.10 Real integrating sphere

$$F_1 = \frac{\Phi_1}{\Phi_0 \rho} = (\frac{A_s - A_i - A_e}{A_s}) = (1 - f), \tag{3.4}$$

where $f = \frac{A_i + A_e}{A_s}$ is the fraction of the opening area of the ports without reflection (e.g., entry port A_i and detector port A_e) to the total area of the sphere A_s. In the following round of reflection, the flux Φ_1 will be reflected by the inner surface to emit $\rho\Phi_1$ instead of $\rho\Phi_0$, the fraction of this flux arriving at the reflecting part becomes:

$$F_2 = \frac{\Phi_2}{\Phi_1 \rho} = (1 - f). \tag{3.5}$$

Repeating this procedure, we have after the n'th reflection,

$$F_n = \frac{\Phi_n}{\Phi_{n-1} \rho} = (1 - f). \tag{3.6}$$

Inverting the above equation, we find that the flux arriving at the reflecting part of the inner surface after n reflections is given by:

$$\Phi_n = \Phi_{n-1} \rho F_n = \Phi_0 \rho^n (1 - f)^n. \tag{3.7}$$

3.1.2.2. Continuous-wave (cw) Light Input

If we have cw input instead of one impulse, the steady-state flux on the reflecting part of the inner wall of the sphere can be obtained by summing all reflecting fluxes:

$$\begin{aligned}\Phi &= \sum_{i=1}^{n\to\infty}\Phi_i, \\ &= \Phi_0\rho(1-f)[1+\rho(1-f)+\rho^2(1-f)^2+...], \\ &= \Phi_0\frac{\rho(1-f)}{1-\rho(1-f)}, \\ &= \Phi_0 M,\end{aligned} \tag{3.8}$$

where we define a sphere multiplier with $M = \frac{\rho(1-f)}{1-\rho(1-f)}$ which depends on the reflectance of wall and the geometry of the integrating sphere. Two cases of M(ρ,f) are shown in the Fig. 11 with different values of ρ and f. From Fig. 11, one can see clearly that the light signal available for detection becomes very small as the sphere coating reflectivity decreases from 100%. Therefore, an integrating sphere is typically required to have an inner surface of at least 90% reflectivity for measurement of weak light signals.

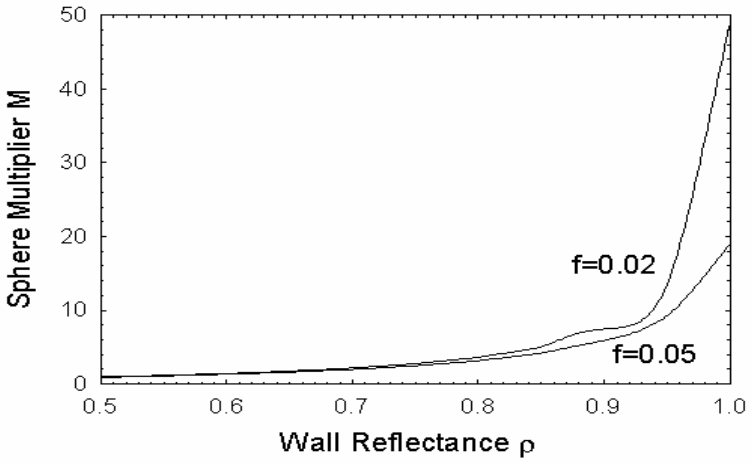

Fig. 11 The dependence of the integrating sphere multiplier on the wall reflectance with different port areas.

3.1.3.Light Detection and the Effect of Reflecting Ports

Now we consider light detected within the integrating sphere with reflecting ports.

3.1.3.1.Port Reflection

If the area of ports can also reflect the light, we will denote ρ_w as the diffuse reflectance of the wall and ρ_i the diffuse reflectance of the port A_i with f_i as the ratio of the A_i to the total area of sphere (Fig. 12). The first reflection provides an initial flux to the inner surface of the sphere:

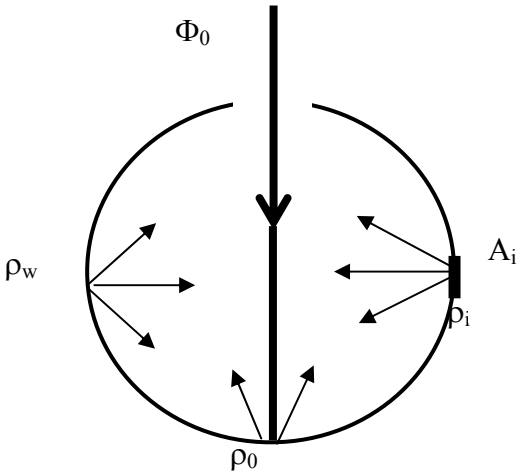

Fig.12 Sphere with reflecting port opening

$$\Phi'_1 = \Phi_0 \rho_0 , \tag{3.9}$$

where ρ_0 is the first reflectance from a sample or the wall. The second reflection includes the contribution from the wall Φ_{w2} and the ports Φ_{i2}, i=1…, whose ratios to the total flux Φ_1 equal to the ratios of their area to the total area of sphere. For multiple ports we get the radiating flux after the second reflection as

$$\Phi'_2 = \Phi'_{w2} + \sum_i \Phi'_{i2} = [\rho_w (1 - \sum f_i) + \sum \rho_i f_i] \Phi'_1 , \tag{3.10}$$

where f_i is the area ratio of the port i to the sphere. After n reflections, we find

$$\Phi'_n = [\rho_w (1 - \sum f_i) + \sum \rho_i f_i]^{n-1} \Phi'_1 . \tag{3.11}$$

Again if we have a cw input, the steady-state radiating flux insider the sphere is obtained by summing all reflected flux given above:

$$\Phi' = \sum_{n=1}^{n\to\infty} \Phi'_n = \Phi_0\rho_0\{1 + [\rho_w(1-\sum f_i) + \sum \rho_i f_i] + [\rho_w(1-\sum f_i) + \sum \rho_i f_i]^2 + ...\},$$
$$= \frac{\rho_0\Phi_0}{1-[\rho_w(1-\sum f_i) + \sum \rho_i f_i]}. \qquad (3.12)$$

3.1.3.2. Light Detected in the Integrating Sphere

The steady-state radiating flux is equally distributed over the inner surface of the sphere. The fraction of the received flux on any finite area A_1, Φ_A, to the total radiating flux Φ' inside sphere will be $\frac{\Phi_{A_1}}{\Phi'} = \frac{A_1}{A}$, here A is the total area of the sphere. So if we have a detector with area A_d installed on the sphere, the flux received by the detector will be $\Phi_d = \frac{A_d}{A}\Phi'$. Combining these results, we have

$$\Phi_d = \frac{A_d}{A}\frac{\rho_0\Phi_0}{1-[\rho_w(1-\sum f_i) + \sum \rho_i f_i]} = M'\frac{A_d}{A}\rho_0\Phi_0, \qquad (3.13)$$

where M' is the sphere multiplier defined by $M' = \frac{1}{1-[\rho_w(1-\sum f_i) + \sum \rho_i f_i]}$ and $\rho_0\Phi_0$ is the flux radiating in the sphere after first reflection from a sample or sphere inner surface, ρ_w is the reflectance of the sphere wall, ρ_i and f_i are the reflectance and area ratio of the i^{th} reflecting port, respectively.

3.2. Measurement of the Diffuse Reflectance and Transmittance

A baffle with identical diffuse reflectance as the sphere inner surface is typically used between the sample and detector to prevent light directly reflected into the detector from the sample. This can minimizes the difference between the results derived above and the actual measurement of diffuse reflectance or transmittance by a photodetector of incomplete absorption (see below). We will first discuss sphere measurement without baffle.

3.2.1.Sphere Measurements without a Baffle

3.2.1.1.Two Sphere Parameters

The general setup of the integrating sphere for optical measurements is shown in the Fig. 13. If A is the total area of sphere, A_d is the area of the detector, A_s is the sample exposed area and A_α is the area of the entrance and/or exit port(s), the fraction of total area of the ports to that of the sphere is given by $f = \frac{A_\alpha + A_d + A_s}{A}$. Among these ports, only the one with sample reflects light,

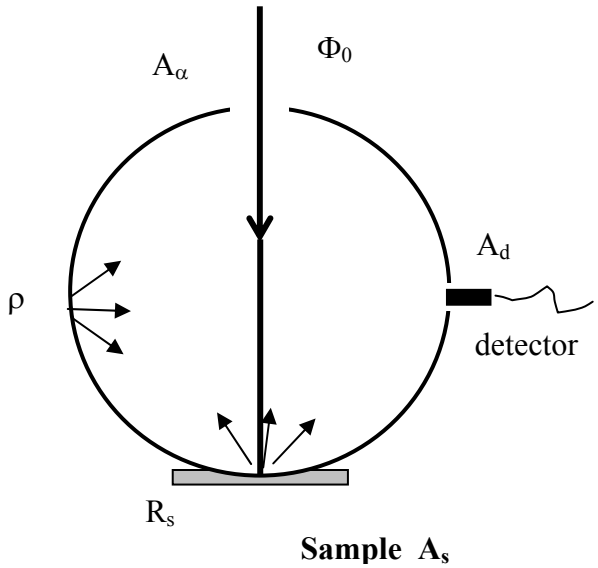

Fig. 13 Measurement for diffuse reflectance

so the sphere multiplier becomes: $M' = \frac{1}{1-\rho(1-f)-R_s\frac{A_s}{A}}$. The flux incident on the detector is given by:

$$\Phi_d = \frac{\frac{A_d}{A}\rho_0\Phi_0}{1-\rho(1-f)\{1-(\frac{1}{1-\rho(1-f)})\frac{R_sA_s}{A}\}} = \frac{\frac{1}{1-\rho(1-f)}\frac{A_d}{A}\rho_0\Phi_0}{1-(\frac{1}{1-\rho(1-f)})\frac{A_s}{A}R_s}. \qquad (3.14)$$

If we define two sphere parameters as:

$$b_1 = \frac{1}{1-\rho(1-f)}\frac{A_d}{A} \qquad \text{and} \qquad b_2 = \frac{1}{1-\rho(1-f)}\frac{A_s}{A}, \qquad (3.15)$$

then above equation can be rewritten as:

$$\Phi_d = \frac{b_1}{1-b_2R_s}\rho_0\Phi_0. \qquad (3.16)$$

It's easy to see that b_1 and b_2 are the parameters determined by the sphere's properties.

3.2.1.2.The Diffuse Reflectance Measurement

To measure the diffuse reflectance of the sample, one installs the sample as show in Fig. 13. For a collimated input beam irradiating a sample, the initial radiating flux $\rho_0\phi_0$ can be written as:

$$\rho_0\Phi_0 = (R_S + R_C)\Phi_0, \qquad (3.17)$$

where the second term represents the contribution of the specular reflection of the collimated input Φ_0 from the sample. Since $R_C\Phi_0$ leaves the sphere through the entrance port, so the second term can be neglected which leads to the flux received by the detector as:

$$\Phi_{ds} = \frac{b_1}{1 - b_2 R_S} R_S \Phi_0 . \tag{3.18}$$

3.1.2.3.The Comparison Measurement

The two sphere parameters b_1 and b_2 are related to the reflectance of the wall, which is a function of the wavelength, temperature and humidity of the air and difficult to determine directly. One can use the following comparison measurement to eliminate the b's to obtain R_s. In this procedure, an additional measurement is made in which the collimated incident beam is aligned in such as angle so it enters the sphere and reflects off the inner surface instead of the sample port (Fig. 14). The diffuse reflection leads to the initial flux as

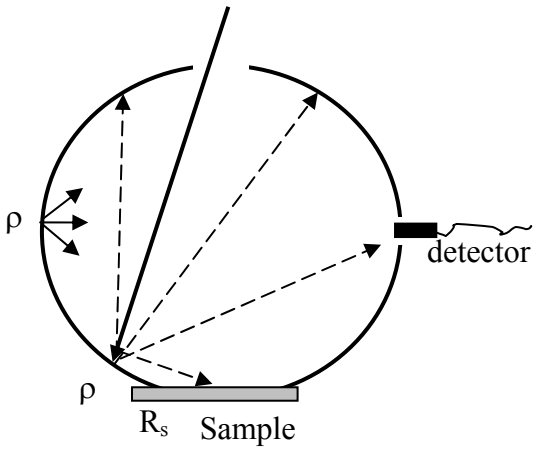

Fig. 14 The calibrate measurement to cancel the sphere parameters.

$$(\rho_0 \Phi_0)' = \rho \Phi_0 , \tag{3.19}$$

where ρ is the reflectance of the sphere wall. And rotating sphere changes Φ_0 by a factor of cosθ if the beam diameter is larger than the entry port. The corresponding flux received by the detector will be

$$\Phi_{dc} = \frac{b_1}{1 - b_2 R_S} \rho \Phi_0 . \tag{3.20}$$

Canceling the sphere parameters b_1 and b_2 by dividing the Eq. (3.18) by (3.20), we obtain the diffuse reflectance of the sample as

$$R_S = \rho \frac{\Phi_{ds}}{\Phi_{dc}}. \tag{3.21}$$

3.1.2.4.The Diffuse Transmittance Measurement

In the diffuse transmittance measurement, the sample is placed at the entrance port of the sphere (Fig 15). The initial flux becomes $\rho_0\Phi_0=(T_S+T_C)\Phi_0$. Here T_C is the collimated transmittance of the sample, and T_S is the diffuse transmittance of the sample. Because the collimated transmission leaves from the exit port as show in the Fig. 15, so $T_C = 0$. Again the flux incident on the detector is: $\Phi_{dT} = \frac{b_1}{1 - b_2 R_S} T_S \Phi_0$. Combine with the result from the Eq. (1.18) diffuse reflectance measurement above to cancel b_1 and b_2 we can get diffuse transmittance of the sample as:

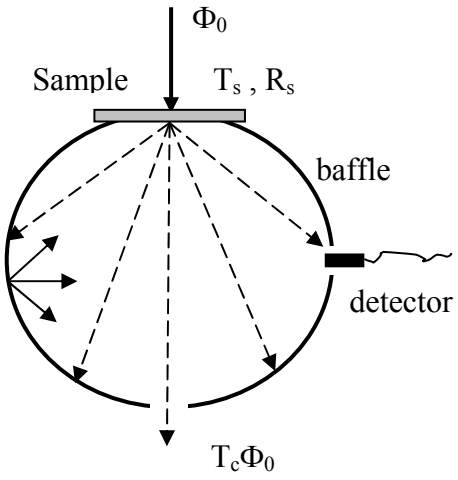

Fig. 15 Measurement of the diffuse transmittance

$$T_S = \frac{R_S \quad \Phi_{dT}}{\Phi_{dS}}. \tag{3.22}$$

3.2.2.Sphere Measurements with a Baffle

3.2.2.1.The Reflectance Measurement

Since the baffle merely redirect the light from a sample, we may assume the baffle as a part of the sphere surface blocking the detector port only to the first flux from the sample. In this case we have to re-analyze the multiple reflections from the inner sphere surface. As shown in the Fig. 16, after the first reflection, the initial radiating power inside the sphere is given by

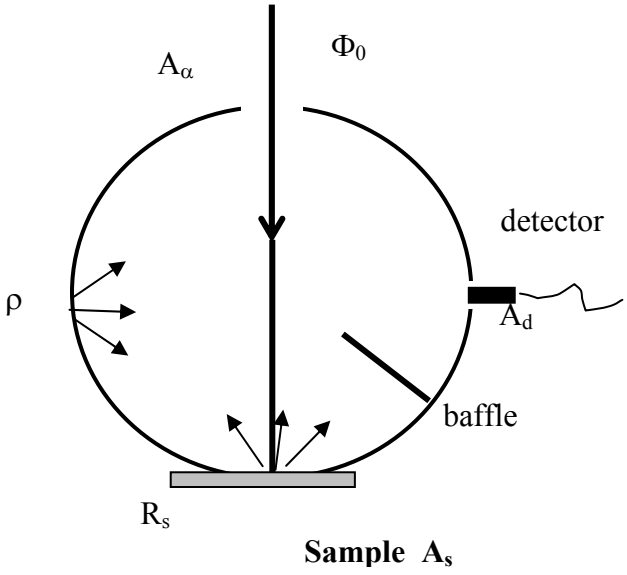

Fig. 16 Diffuse reflectance measurement with baffle

$$\Phi_1' = \rho_0 \Phi_0 = R_S \Phi_0 . \tag{3.23}$$

No flux is received by the detector because of the baffle, so we have $\Phi_{ds1}=0$. After the second reflection, the radiating flux results from two parts due to Φ'_1:

$$\Phi_2' = [\rho(1-f) + \frac{R_S A_S}{A}] \cdot \Phi_1' = [\rho(1-f) + \frac{R_S A_S}{A}] \cdot R_S \Phi_0 . \tag{3.24}$$

The first term is due to the reflection of the wall while the second is due to the diffuse reflection from the sample. But only the first term contributes to the detected flux because of the baffle:

$$\Phi_{ds2} = (\frac{A_d}{A})\rho(1-f)\cdot\Phi'_1 = (\frac{A_d}{A})\rho(1-f)\cdot R_S\Phi_0 . \tag{3.25}$$

Similarly, the third reflection gives rise to a radiating flux:

$$\begin{aligned}\Phi'_3 &= [\rho(1-f)+\frac{R_S A_S}{A}]\cdot\Phi'_2,\\ &= [\rho(1-f)+\frac{R_S A_S}{A}]\cdot[\rho(1-f)+\frac{R_S A_S}{A}]\cdot R_S\Phi_0,\\ &= [\rho(1-f)+\frac{R_S A_S}{A}]^2\cdot R_S\Phi_0.\end{aligned} \tag{3.26}$$

Again the second term in the bracket does not contribute to detected flux, so:

$$\begin{aligned}\Phi_{ds3} &= (\frac{A_d}{A})\rho(1-f)\cdot\Phi'_2,\\ &= (\frac{A_d}{A})\rho(1-f)\cdot[\rho(1-f)+\frac{R_S A_S}{A}]\cdot R_S\Phi_0.\end{aligned} \tag{3.27}$$

In turn we have

$$\begin{aligned}\Phi'_4 &= [\rho(1-f)+\frac{R_S A_S}{A}]\cdot\Phi'_3,\\ &= [\rho(1-f)+\frac{R_S A_S}{A}]^3\cdot R_S\Phi_0,\end{aligned} \tag{3.28}$$

and

$$\begin{aligned}\Phi_{ds4} &= (\frac{A_d}{A})\rho(1-f)\cdot\Phi'_3,\\ &= (\frac{A_d}{A})\rho(1-f)\cdot[\rho(1-f)+\frac{R_S A_S}{A}]^2\cdot R_S\Phi_0,\end{aligned} \tag{3.29}$$

$$\Phi_{dsn} = (\frac{A_d}{A})\rho(1-f)\cdot[\rho(1-f)+\frac{R_S A_S}{A}]^{n-2}\cdot R_S\Phi_0. \tag{3.30}$$

Adding all contributions to the light detector, we find the power received by the detector as

$$\Phi_{ds} = 0 + \sum_{n=2}^{n\to\infty} \Phi_{dsn} = \frac{A_d}{A} R_s \Phi_0 \rho(1-f)\{1 + [\rho(1-f) + \frac{A_s R_s}{A}] + [\rho(1-f) + \frac{A_s R_s}{A}]^2 + ...\},$$
$$= \frac{A_d}{A} \frac{R_s \Phi_0 \rho(1-f)}{1 - [\rho(1-f) + \frac{A_s R_s}{A}]}. \tag{3.31}$$

Using the sphere parameters defined in Eq. (3.15) we have

$$\Phi_{ds} = \frac{A_d}{A} \frac{R_s \Phi_0 \rho(1-f)}{1 - \rho(1-f) - \frac{A_s R_s}{A}} = R_s \Phi_0 \rho(1-f) \frac{\frac{1}{1-\rho(1-f)} \frac{A_d}{A}}{1 - \frac{1}{1-\rho(1-f)} \frac{A_s R_s}{A}} = \frac{R_s \Phi_0 \rho(1-f) b_1}{1 - b_2 R_s}. \tag{3.32}$$

Comparing this result to Eq. (3.18), we find that an extra factor ρ(1-f) is the consequence of the added baffle.

3.2.2.2.The Comparison Measurement I - With the Baffle Blocking the First Reflection

Using the same analysis and assuming that the baffle prevent the first reflection off the sphere wall from reaching the detector (Fig. 17), we can arrive at nearly identical results by replacing $\Phi'_1=\rho_0\Phi_0=R_S\Phi_0$ with $\Phi'_1=\rho_0\Phi_0=\rho\Phi_0$. This leads to a detector flux changed to:

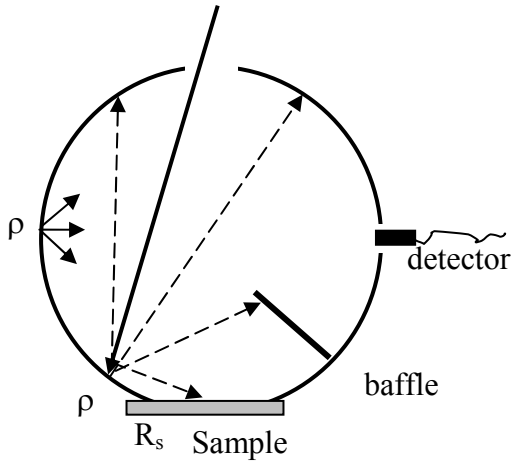

Fig. 17 Compare measurement with baffle blocking the first reflection.

$$\Phi_{dC} = \frac{\Phi_0 \rho^2 (1-f) b_1}{1 - b_2 R_s} = \frac{\rho}{R_s} \Phi_{ds} \,. \tag{3.33}$$

So the ratio of reflectance measurement Eq. (3.32) and comparison measurement Eq. (3.33) yields the diffuse reflectance of the sample:

$$R_S = \rho \frac{\Phi_{ds}}{\Phi_{dc}} \,. \tag{3.34}$$

3.2.2.3. The Comparison Measurement II – With the Baffle Not Blocking the First Reflection

Assuming that the baffle does not prevent the first reflection off the sphere wall from reaching the detector (Fig. 18), we find that

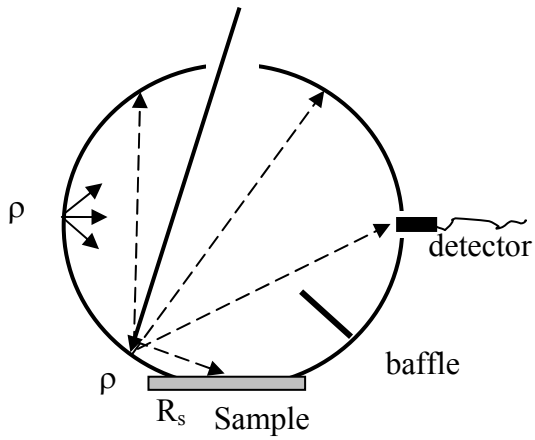

Fig. 18 Comparison measurement without block the first reflected light from sample.

$$\Phi_{dc1} = \frac{A_d}{A} \Phi_1 = \frac{A_d}{A} \rho \Phi_0 \,, \tag{3.35}$$

instead of zero. The other Φ_{dcn} terms remain the same with R_S replaced by ρ:

$$\Phi_{dc2} = \frac{A_d}{A}\rho(1-f)\cdot\Phi_1' = \frac{A_d}{A}\rho(1-f)\cdot\rho\Phi_0, \tag{3.36}$$

$$\Phi_{dc3} = \frac{A_d}{A}\rho(1-f)\cdot\Phi_2' = \frac{A_d}{A}\rho(1-f)\cdot[\rho(1-f)+\frac{A_S R_S}{A}]\cdot\rho\Phi_0, \tag{3.37}$$

$$\Phi_{dc4} = \frac{A_d}{A}\rho(1-f)\cdot\Phi_3' = \frac{A_d}{A}\rho(1-f)\cdot[\rho(1-f)+\frac{A_S R_S}{A}]^2\cdot\rho\Phi_0. \tag{3.38}$$

This leads to

$$\begin{aligned}\Phi_{dC} &= \Phi_{dC1} + \sum_{n=2}^{n\to\infty}\Phi_{dCn} = \frac{A_d}{A}\rho\Phi_0 + \frac{A_d}{A}\frac{\Phi_0\rho^2(1-f)}{1-[\rho(1-f)+\frac{A_s R_s}{A}]},\\ &= \frac{A_d}{A}\rho\Phi_0\frac{1-[\rho(1-f)+\frac{A_s R_s}{A}]+\rho(1-f)}{1-[\rho(1-f)+\frac{A_s R_s}{A}]},\\ &= \frac{A_d}{A}\frac{(1-\frac{A_s R_s}{A})\rho\Phi_0}{1-[\rho(1-f)+\frac{A_s R_s}{A}]},\end{aligned} \tag{3.39}$$

or

$$\Phi_{dC} = \frac{b_1\rho\Phi_0}{1-b_2 R_s}(1-\frac{A_s R_s}{A}). \tag{3.40}$$

Combining Eq. (3.40) with Eq. (3.32) $\Phi_{ds} = \frac{b_1\Phi_0\rho}{1-b_2 R_s}R_s(1-f)$ we find the diffuse reflectance of the sample given by:

$$R_s = \frac{A\Phi_{ds}}{A(1-f)\Phi_{dc} + A_s\Phi_{ds}}. \tag{3.41}$$

3.2.2.4.The Diffuse Transmittance Measurement

Assume that the collimated transmitted light escapes from the sphere through the port opening directly opposite to the entrance port, the diffuse transmitted component of the incident light is trapped inside the sphere with a flux given by $\Phi'_0=T_S\Phi_0$. None of this flux is received by the detector because of the baffle blocking the view of the sample from the detector, therefore

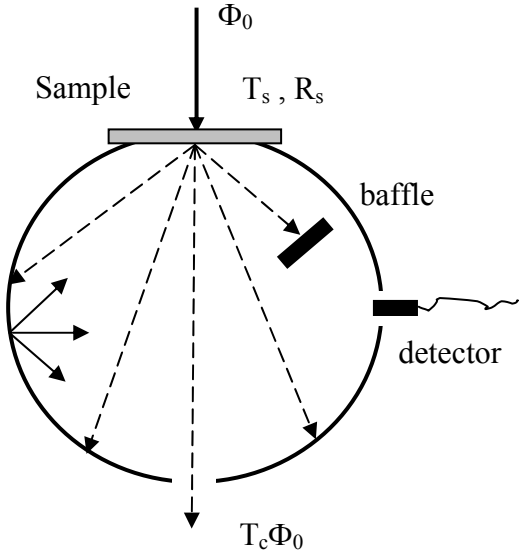

Fig. 19 Diffuse transmittance measurement with baffle

$$\Phi_{ds1} = 0\,. \tag{3.42}$$

After the first reflection off the inner sphere surface, the radiating flux comes from two parts due to Φ_0':

$$\Phi'_1 = [\rho(1-f) + \frac{R_S A_S}{A}]\cdot\Phi'_0 = [\rho(1-f) + \frac{R_S A_S}{A}]\cdot T_S\Phi_0\,, \tag{3.43}$$

but only the first term contributes to the detected flux because of the baffle:

$$\Phi_{ds2} = \frac{A_d}{A}\rho(1-f)\cdot\Phi'_0 = \frac{A_d}{A}\rho(1-f)\cdot T_S\Phi_0\,. \tag{3.44}$$

Similarly, the second reflection gives rise to the next round of radiating flux:

$$\begin{aligned}\Phi'_2 &= [\rho(1-f)+\frac{R_S A_S}{A}]\cdot\Phi'_1,\\ &= [\rho(1-f)+\frac{R_S A_S}{A}]\cdot[\rho(1-f)+\frac{R_S A_S}{A}]\cdot T_S\Phi_0,\\ &= [\rho(1-f)+\frac{R_S A_S}{A}]^2\cdot T_S\Phi_0.\end{aligned} \tag{3.45}$$

Again the term due to the sample (the second term in bracket) does not contribute to detected flux, so:

$$\Phi_{ds3} = \frac{A_d}{A}\rho(1-f)\cdot\Phi'_1 = \frac{A_d}{A}\rho(1-f)\cdot[\rho(1-f)+\frac{R_S A_S}{A}]\cdot T_S\Phi_0, \tag{3.46}$$

in turn we have

$$\Phi'_3 = [\rho(1-f)+\frac{R_S A_S}{A}]\cdot\Phi'_2 = [\rho(1-f)+\frac{R_S A_S}{A}]^3\cdot T_S\Phi_0, \tag{3.47}$$

and

$$\Phi_{ds4} = \frac{A_d}{A}\rho(1-f)\cdot\Phi'_2 = \frac{A_d}{A}\rho(1-f)\cdot[\rho(1-f)+\frac{R_S A_S}{A}]^2\cdot T_S\Phi_0, \tag{3.48}$$

$$\Phi_{dsn} = \frac{A_d}{A}\rho(1-f)\cdot\Phi'_{n-2} = \frac{A_d}{A}\rho(1-f)\cdot[\rho(1-f)+\frac{R_S A_S}{A}]^{n-2}\cdot T_S\Phi_0. \tag{3.49}$$

Adding all contributions for using a slow light detector, we find the power received by the detector as

$$\begin{aligned}\Phi_{dT} &= 0+\sum_{n=2}^{n=\infty}\Phi_{dsn} = \frac{A_d}{A}T_s\Phi_0\rho(1-f)\{1+[\rho(1-f)+\frac{A_s R_s}{A}]+[\rho(1-f)+\frac{A_s R_s}{A}]^2+....\},\\ &= \frac{A_d}{A}\frac{T_s\Phi_0\rho(1-f)}{1-[\rho(1-f)+\frac{A_s R_s}{A}]}.\end{aligned} \tag{3.50}$$

Using the sphere parameters in Eq. (3.15), we have

$$\Phi_{dT} = \frac{A_d}{A}\frac{T_s\Phi_0\rho(1-f)}{1-\rho(1-f)-\frac{A_sR_s}{A}} = T_s\Phi_0\rho(1-f)\frac{\frac{1}{1-\rho(1-f)}\frac{A_d}{A}}{1-\frac{1}{1-\rho(1-f)}\frac{A_sR_s}{A}} = \frac{T_s\Phi_0\rho(1-f)b_1}{1-b_2R_s}. \tag{3.51}$$

Comparing this result to Eq. (3.20), an extra factor ρ(1-f) is the consequence of the added baffle. However, we still obtain the same formula for diffuse transmittance by dividing Eq. (3.32) by Eq. (3.51):

$$T_S = \frac{R_S\ \Phi_{dT}}{\Phi_{dS}}. \tag{3.52}$$

3.3. Spatial Filtering Technique

Light interaction with turbid media like biological tissues is illustrated in Fig. 20. Before entering a sample, a small percentage (~ 4%) of the normally incident light beam is reflected from the sample surface due to the mismatch in refractive indice between the sample and holder. After penetrating into the tissue, the photons of the beam encounter multiple scattering before exiting from the tissue, if not absorbed. Absorbed light energy is converted to heat which increases the temperature of the tissue. In infrared region, scattering in most biological

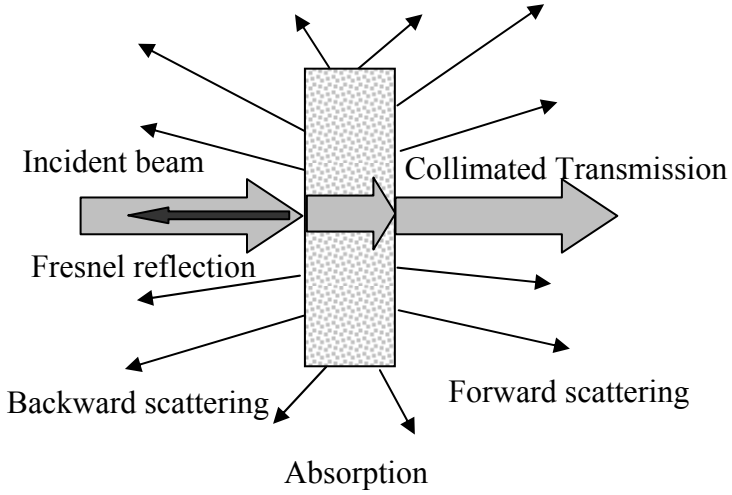

Fig. 20 Light interaction with tissue.

tissues is much stronger than absorption. Only a very small component of the incident light could travels through the sample without scattering as the collimated transmission. For samples with large optical thickness, $\tau = D\mu_t$, where D is the physical thickness of the sample on the order of 100μm, the collimated transmittance is usually around the order of 10^{-3} to 10^{-5}. Because of the multiple scattering, the scattered light out of the tissue is usually distributed isotropically, as indicated in Fig. 20. However, the collimated transmission beam propagates along its original trajectories and thus can be separated from the diffusely transmitted light by a spatial filtering setup using a combination of lenses and apertures, as shown in Fig. 21.

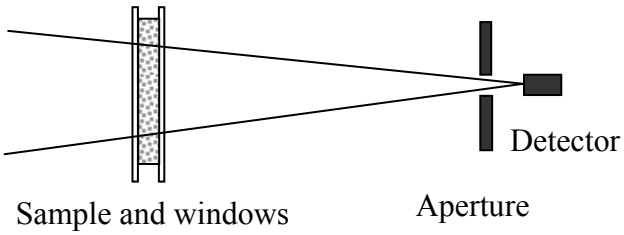

Fig. 21 Spatial filtering

The intensity of the collimated transmitted beam could be calculated from the Lambert-Beer's law expressed in Eq. (2.33). Considering a beam of radiance I_0 incidents on a slab tissue sample, as in Fig. 21 and Fig. 22. After the reflection loss at four interface, window-tissue interface at X_0 and X_1, and two window-air interfaces. the radiance of the collimated transmission beam becomes:

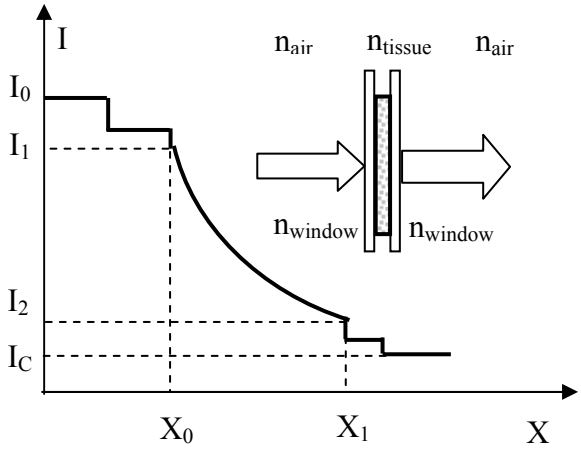

Fig. 22 Light pass through tissue between windows

$$I_C = I_2(1-R_3)(1-R_4) = I_0(1-R_1)(1-R_2)(1-R_3)(1-R_4)e^{-\mu_t D}, \quad (3.53)$$

and the collimated transmittance T_C is given by:

$$T_C = \frac{I_C}{I_0} = A \cdot e^{-\mu_t D}, \quad (3.54)$$

where $A=(1-R_1)(1-R_2)(1-R_3)(1-R_4)$ and R_i's are the reflection coefficient at each consecutive interfaces. The reflection coefficients are functions of the light wavelength and so A is constant for a given wavelength. A more detail analysis about Beer's law with consideration of reflected beam could be found in reference [Yoon 1987]. A plot of how the intensity of the beam shown in Fig. 21 changing with the path X is show in Fig. 22. Take the logarithm of both side of Eq (3.54), we have:

$$ln[T_C] = \ln[A] - \mu_t D. \quad (3.55)$$

It's easy to see that $\ln[T_C]$ varies as a linear function of the D, and the slope of the line provides the attenuation coefficient μ_t. Using the spatial filtering technique we can measure the T_C as a function of D of the tissue to obtain μ_t at each wavelength in the spectral region of interest.

3.4. Measurement of Scattered Light with CCD Camera

We have conducted preliminary measurements of distribution of scattered light by carcinoma cancer cells in cultures. For this purpose, a charge-couple-device (CCD) camera was used to obtain the 2-D distribution of the scattered light because of high data acquisition speed and low background noise. The heart of a CCD camera is a matrix of

light sensitive pure silicon cells, which is called image area gate (IAG), the area of each square cells is around 10×10 μm^2. Strips of dopant are deposited on the boundary of each square with voltage applied to form a potential well in each cell. While light is incident on the cells, electrons are freed from the crystal lattice and trapped in the potential well with a number proportional to the light intensity. By measuring the number of the freed electrons in each cell one can obtain the 2-D light distribution over an area which is usually about 5×5 mm^2. As shown in Fig. 23, electron packets in each potential well are pushed into an adjacent potential well after each clock pulse by altering the voltage on the strips. At the bottom of image area gate (IAG) there is a special row of potential wells called serial register gate (SRG). Upon triggering by a clock pulse train, one row of electron packets are moved into SRG and another clock pulse will push these packets into an amplifier output gate, which converts the charges to a series of voltage signals for image output.

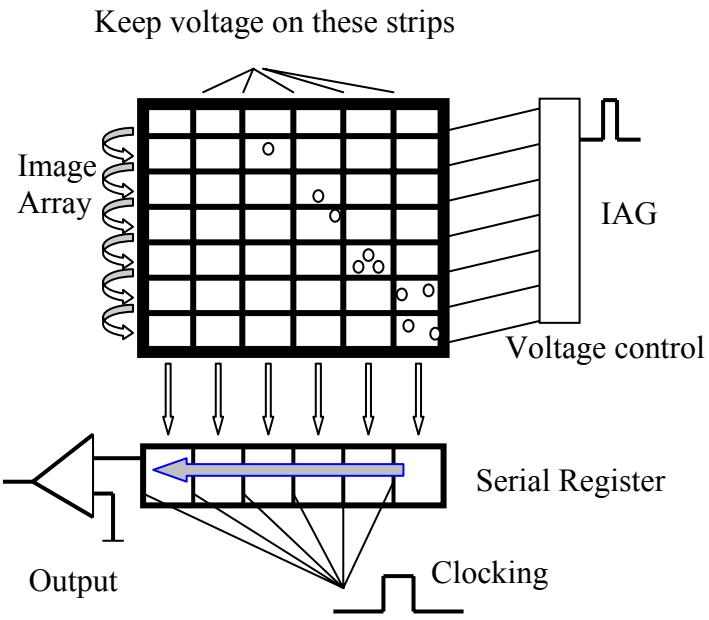

Fig. 23 Process of signal reading from CCD

A CCD camera (ST-7i, Santa Barbara Instrument Group) was used to study the light scattering from a monolayer of cultured MCF7 breast carcinoma cancer cells. The pixel matrix of the CCD is 756×510 with 9×9 μm^2 pixel size corresponding to an image area of 6.9×4.6 mm^2, The reading noise is 15 electrons with a well depth of 40,000 electrons. The experimental setup is show in Fig. 24 using a laser beam from a cw diode-pumped Nd:YAG laser at 1064nm wavelength. The laser beam is focused by a 400mm spherical lens to obtain a narrow and collimated beam centered at the cultured cells in the flask's bottom. The CCD camera and the flask are held in horizontal plane with the CCD beneath the flask to ensure the single layer of the cells. The CCD is controlled through a vendor-supplied software (CCDOPS) with an expose time set at 0.15 second and temperature at -10°C. The time need to read a full resolution image from the CCD camera through the parallel port is around 15 seconds using a Pentium PC.

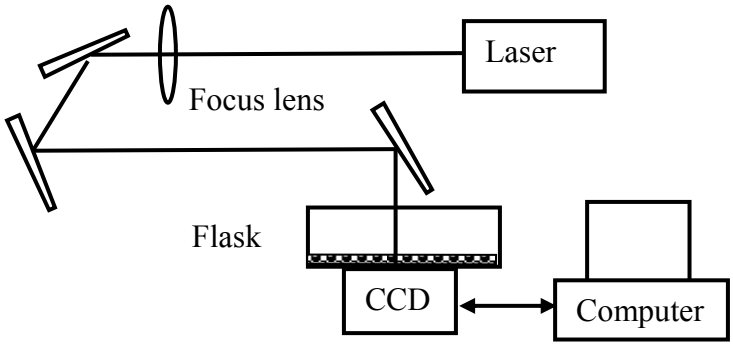

Fig. 24 Setup of measuring scattering from single layer cultured cells.

The image data acquired by the ST-7i CCD camera are of depth of 16 bits. Since regular image file formats such as BMP, GIF and JPEG are made of 8-bit pixels, the image cannot be saved in these formats. The CCDOPS software saves image files in a non-standard ST7 format with 16-bit pixels. We have developed a Visual C++ program

to convert the ST7 files into plain ASCII files with each pixel expressed in the form of decimal integers from 0 to 65535 for later data processing. The corresponding codes are contained in Appendix C.

4. Experimental Technique II

In this chapter we will describe sample preparation procedures and various experimental configurations for different measurements. Data processing and the inverse determination of the optical parameters from experimental results will also be discussed.

4.1. Sample Preparation

The optical parameters of porcine skin dermis were studied on different storage condition and postmortem time from 900 to 1500nm. Two procedures were used to prepare the skin dermis samples. In addition, cultured breast carcinoma cancer cells (MCF7) were used to conduct preliminary studies of light scattering by single cells at 1064nm.

4.1.1.Skin Tissue Structure

Skin is composed of two major layers: epidermis and dermis (Fig. 25). The epidermis consists of multiple surface layers that are keratinised. The dermis layer consists of the dense fibro-elastic connective tissues containing glands and hair [Anothony, *et al*, 1983]. Below the dermis is the subcutaneous tissue containing fat. There are also some sebaceous gland, nerve ending, hair bulbs and sweat gland distributed inside the skin dermis.

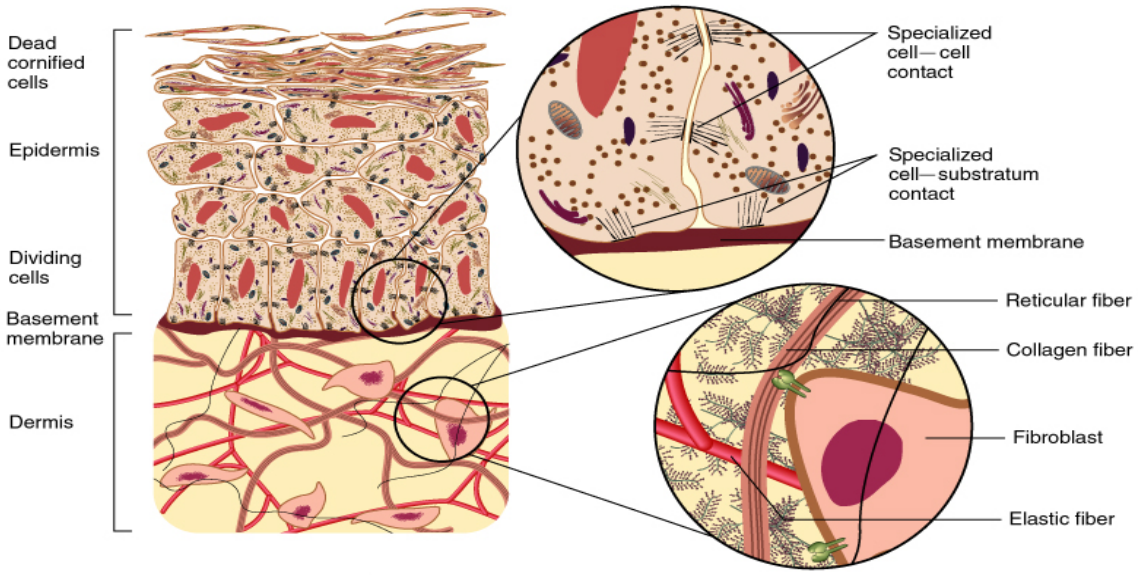

Fig. 25 The structure of skin tissue [adapted from Y. Tanguchi]

Skin can be classified according to its epidermis thickness. In average, the dermis is 3 mm thick, while the thickness of epidermis varies between 50 μm in the eyelids and 150 μm in the palms [Anderson *et al*, 1981]. The epidermis can be divided further into five sublayers from the skin surface to the inside: stratum corneum, stratum lucidum, stratum granulosum, stratum spinosum, and stratum

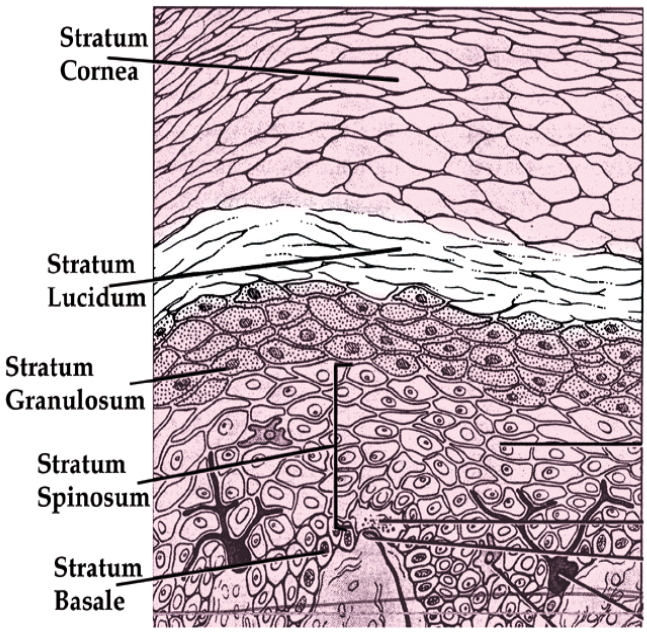

Fig. 26 The skin epidermis [Dong 2000]

germinativum or the stratum basale (Fig. 26). The principal cells of the epidermis are keratinocytes which gradually migrate from the deepest stratum to the surface exposed to the ambient environment and is sloughed off in a process called desquamation. The desquamation period from basal to superficial ranges from 25 to 50 days [Anothony, *et al*, 1983].

The skin dermis is 15~40 times thicker than the epidermis, depending on the anatomic site. A variety of cells are scattered in varying numbers throughout the mature

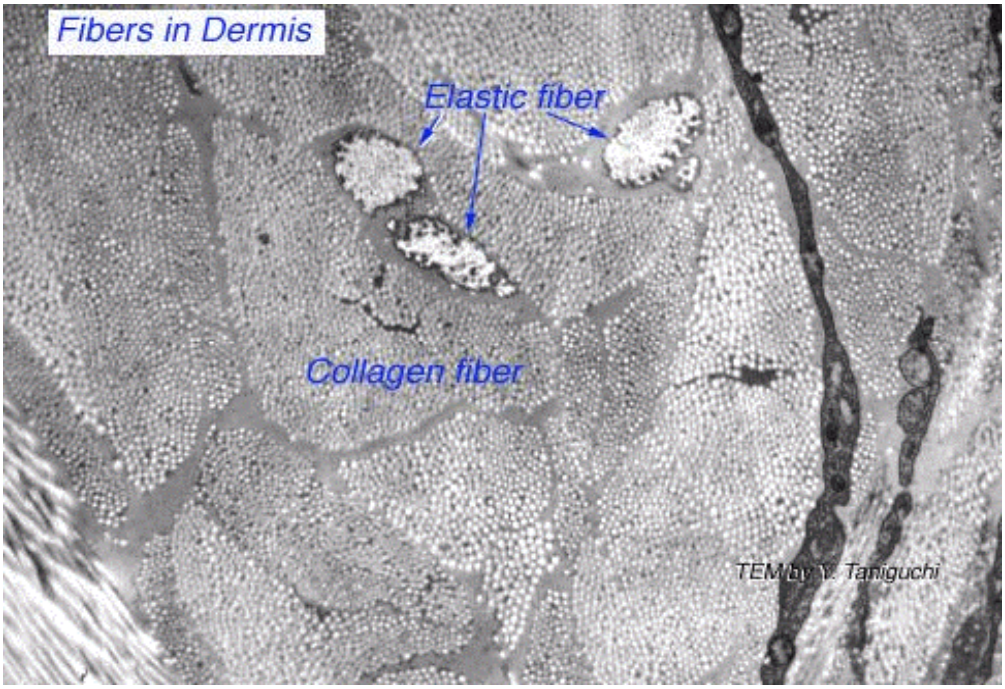

Fig. 27 Fibers in skin dermis [Adapted from Y. Tanguchi].

dermis. In descending order of concentration, these cells are fibroblasts, mast cells (ubiquitous secretory cells of the immune system), histiocytes, Langerhans cells, lymphocytes, and very rarely, eosinophils. The fully formed dermis may be divided into two well-circumscribed compartments: a thin layer immediately beneath the epidermis and around adnexa and a thick layer of reticular dermis extend most of dermis. Two

important structure of dermis are fibroblasts and fibers. Fibroblasts are the cells that generate all the collagen fibers. Fibers again could be divided into collagen and elastic fibers (Fig. 25 and Fig 27). Elastic fibers constitute about 3% of the dry weight of the dermis and impart to skin property of returning to its original shape following a depression. The diameter of the elastic fibers range from 1.0 to 3.0 μm, they could be strengthen to the twice of their length at rest. Collagen is the most abundant protein in the body, constituting about 70% of the dry weight of the dermis to serves as its major structural component and imparts most of tensile strength of the skin. Collagen fibers are composed of thinner microfibrils that, in turn, are formed by collagen molecules. There are at least 13 known types of connective tissue collagen, in normal human skin, the two major collagens are type I and type III. Type I collagen fibers, up to 15 μm wide, are arranged in a dense orthogonal network in dermis. In TEM type I collagen microfibrils are seen to have distinctive cross banding with a periodicity of 68 nm. In contrast, type III collagen is most loosely arranged in the thin layer of dermis beneath the epidermis. The histological characteristics of pig skin and human skin have been reported to be comparable, with similarities existing for epidermal thickness and composition, pelage density, dermal structure, lipid content and general morphology [Dick and Scott 1992]. Newborn pigs have much more supple skin, which is grossly more similar to human skin. Because of this similarities, skin from young pigs were used in our experiments as a model of human skin for ease in acquiring and handling.

4.1.2.Skin Sample Preparation

The skin tissue used in our experiments is porcine skin dermis. Fresh porcine skin patches of about $100\times100mm^2$ area were obtained from the back neck and shoulder area of 6-month-old white domestic pigs at the Department of Comparative Medicine, Brody School of Medicine at East Carolina University. Immediately after removal from animal, the skin tissue was kept under two conditions in a refrigerator: within crushed ice in an ice bucket or in Tyrode's physiological saline solution. The temperatures in both cases were measured to be between 2 to 4°C. For the measurement of diffuse transmittance T_d and reflectance R_d, the upper dermis was trimmed from the porcine skin into $20\times20mm^2$ squares. Using a specially designed microtome, the tissue square was sectioned to obtain samples with thickness D ranging from 0.48 to 1.34mm at 4°C in a refrigerated room. The sample was sandwiched between two sapphire optical windows of 25mm in diameter with a few saline solution drops on the sample to reduce the effect of index mismatch at the rough interface between the tissue sample and the windows. Care was taken to eliminate air bulbs between the sample and windows. The rim of the gap between the two sapphire windows was sealed with aseline grease to prevent tissue dehydration during the measurement. For measurements of collimated transmittance T_c, we used a cryostat microtome (Ames Lab-tek) to obtain dermis sections with D ranging from 30 to 250 μm at -18°C (Lembares *et al*, 1997) after the skin samples were stored within crushed ice for a period of time. The tissue sample was protected by OCT in order to keep the biological activity while being frozen at -18°C. Each frozen tissue sample was warmed up to room temperature in saline solution and measured within 0.5 hour after sectioning. Since the

skin dermis is composed mainly of water and collagen fibers and the tissue was frozen with coating of a special preservation compound OCT. We do not expect the tissue microstructure, and thus the optical properties, to significantly change as a result of freezing [Peters *et al* 1990]. Each section was visually examined before measurements to ensure that no holes existed in the sample and the thickness was satisfactorily uniform. A postmortem time was defined for each sample as the period from the animal death to the time of optical measurement or sectioning in the cryostat. All optical measurements were conducted at room temperature. Details procedures of tissue preparations are shown in Appendix A.

After the measurements of T_d and R_d with the integrating sphere, some tissue samples were randomly selected and fixed immediately for TEM examination [Cariveau 2000].

4.1.3.Preparation of Cultured Cells

The MCF7 breast cancer cells derived from mammary gland adenocarcinoma were purchased from American Tissue Culture Collection (ATCC #HTB-22). All the cell culture processes were done in the pathological department and tissue culture lab at Brody School of medicine at East Carolina University. Minium essential medium (MEM) with 10% Fetal Bovine Serium (FBS) and antibiotics (Appendix A) was use to grow the cells in 75cm^2 cell culture flask. The flasks were kept 37°C with 5% CO_2 concentration. Healthy cells form many small group and stick to the bottom of the flask in the log growing stage. After a monolayer is formed the cells connect to each other and cease to

grow. At this point the cells must be diluted to keep the cells from dying due to lack of space and nutrition. In the optical experiments $25cm^2$ flasks were used to fit into the optical setup. Cells were transferred to $25cm^2$ flasks before the experiment and incubated until they attached and formed monolayer. The recipe for making growth medium and other cell culture techniques are described in Appendix A.

4.2. Optical Setup and Instrument Control

A 30W tungsten lamp and a monochromator (CM110, CVI Laser) with a 600 grooves/mm ruled grating ablazed at 1200nm were used as a tunable light source from 900 to 1500nm in wavelength with a 2nm resolution. The light output was modulated at 18Hz by a chopper and passed through a long-pass filter to remove the second-order diffraction from the monochromator output. The light beam was collimated with a spherical lens of 150mm focal length before incident on the tissue sample. To measure the diffuse transmittance T_d and reflectance R_d, the scattered light signals were collected by an integrating sphere (IS-080-SF, Labsphere, Inc.) of 203mm diameter (2R) with the diameters of light entrance and exit ports reduced to 6.35mm with port reducers. The light signal inside the integrating sphere was picked up at the detection port by an InGaAs photodiode mounted flush with the inner surface of the sphere. The photodiode was assembled on a preamplifier of 10^{10}(V/A) transimpedance gain and output signal was sent to a lock-in amplifier (SR850, Stanford Research Systems) for detection at the modulated frequency. We used the comparison method discussed in Chapter 3 to determine T_d and R_d from three light measurements carried out in a sequence without

removing the sample. The first (P_T) was obtained with the sample port as the entrance for light, as shown in Fig. 28(a), the second (P_R) with the sample port as the exit by rotating the sphere 180° Fig. 28(b) and the third (P_C) with the sample port rotated 20° from the last position so that the incident light strikes on the sphere wall Fig. 28(c).

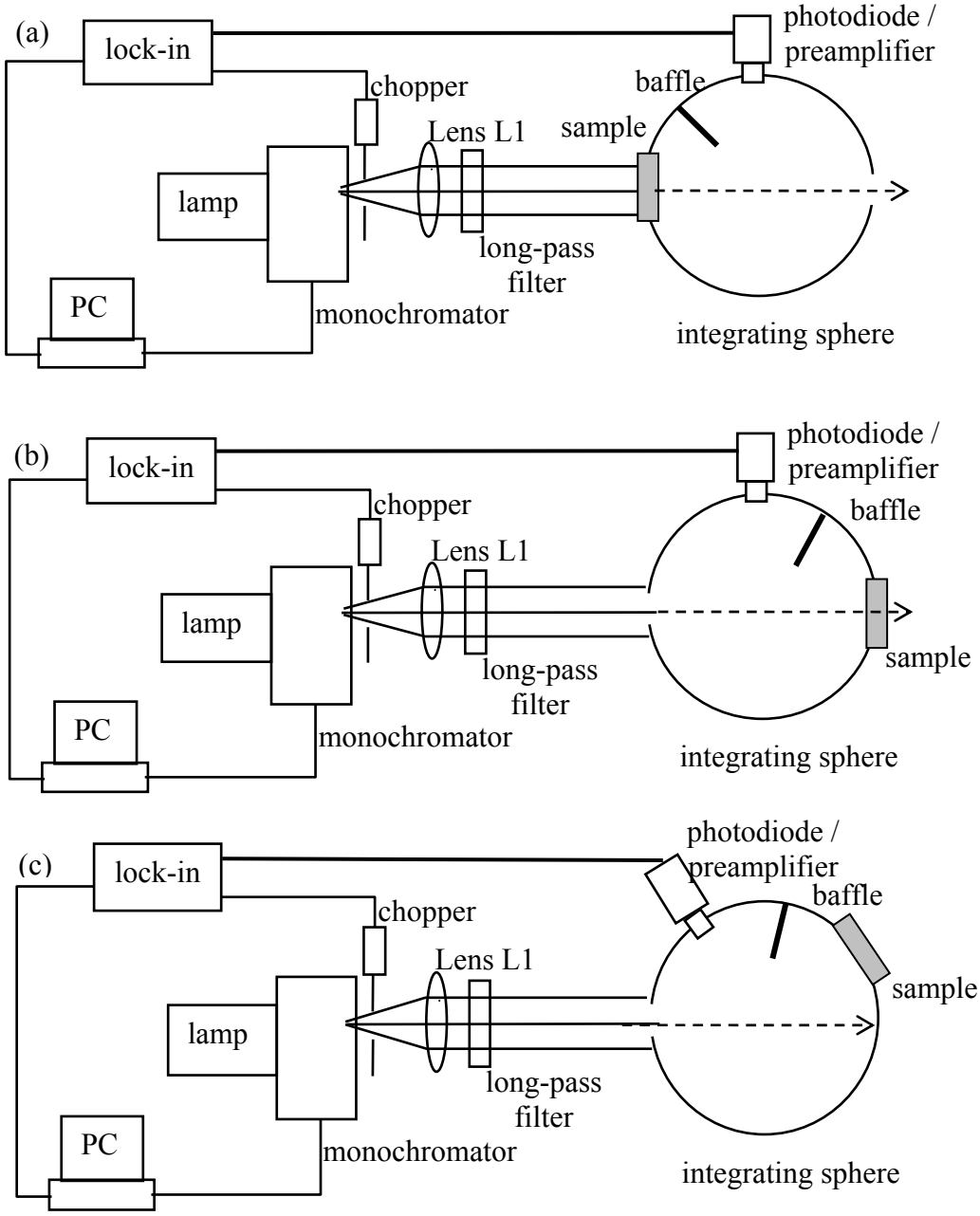

Fig. 28 The integrating sphere setup for experimental measurement of scattering.

A built-in small baffle between the sample port and the detector port, with the same diffuse reflective coating as the sphere wall, prevented the photodiode from receiving light directly from the sample for the P_T and P_R measurements. In the P_C measurement, though, the baffle did not block the first reflected light from the sphere wall reaching into the detector. Based on an analysis of light distribution inside the integrating sphere in chapter 3, we find that T_d and R_d of the sample are given by

$$R_d = \frac{AP_R \cos 20^0}{A(1-f)P_C + A_s P_R \cos 20^0}, \tag{4.1}$$

and

$$T_d = R_d \frac{P_T}{P_R}, \tag{4.2}$$

where $A=4\pi R^2$ is the total surface area of the sphere, f is the area ratio of the three ports to the sphere and $A_s = \pi(9.53)^2$ (mm^2) is the circular area of the sample exposed to the integrating sphere. The integrating sphere setup has been calibrated against two diffuse reflectance standards of 80% and 50% (SRS-80-020 and SRS-50-010, Labsphere, Inc) from 900 to 1500nm. Fig. 29 plots the measured reflectance of the 50% reflectance standard (circles) and the 80% reflectance standard (triangle) against the calibrated reflectance values supplied by the vendor. Based on these results, we estimated that the experimental errors in our integrating sphere measurements of diffuse reflectance and transmittance are about ±5%.

To measure the collimated transmittance T_c for determination of the attenuation coefficient $\mu_t = \mu_a + \mu_s$, the collimated light from the monochromator was focused with a

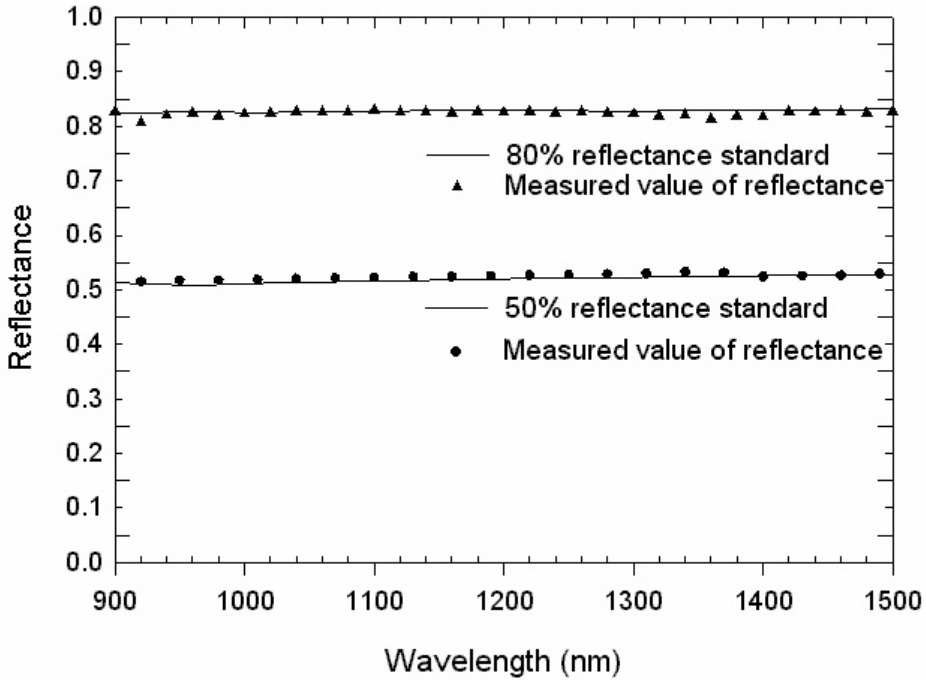

Fig. 29 Calibration of integrating sphere setup and data process methods with two reflectance standard of 50% and 80%. The solid lines are the calibrated values of reflectance by the vendor and the symbols are the measured values by the integrating sphere technique described in this section.

combination of a spherical lens of 400mm and a cylindrical lens of 75mm in focal length into a rectangular spot of about 4mm×0.5mm at the focus, as shown in Fig. 30. The tissue sample was placed in front of the cylindrical lens with an aperture of 6.4mm in diameter

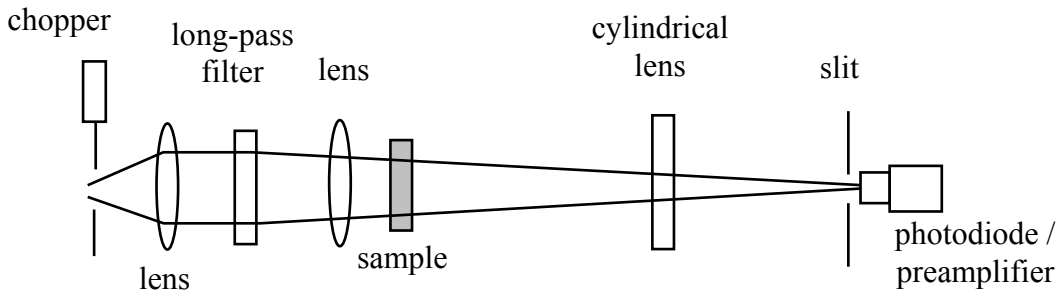

Fig. 30 Spatial filtering setup

fully illuminated. A 0.5mm slit was mounted in front of an identical InGaAs photodiode to spatially filter the transmitted light from the sample before reaching the photodiode. A preamplifier assembled with the photodiode was used to collect the light signal prior to the detection by the lock-in amplifier. With this setup and a 30s integration time of the lock-in, we can measure the collimated transmittance as low as 8×10^{-5} with the incoherent light source. There are two major sources of error in determining μ_t: the "leaking" of the scattered light through the slit of the spatial filter in the measurements of T_c for thick samples with thickness $D > 180\mu m$ and the thickness measurement for thin samples with $D < 100\mu m$. The average error in the T_c measurements was estimated to be about ±25% through the measurement of the light distribution in the focal plane by scanning the slit and photodiode assembly for samples of different thickness. The sample thickness D was measured by subtracting the thickness of the sample holder from that with the sample at room temperature using a micrometer of 3μm (0.0001 inch) resolution. The micrometer has a ratchet stop mechanism which enabled us to apply a consistent measuring pressure on the tissue between measurements. A personal computer was used to control the monochromator for wavelength scanning and the lock-in amplifier for data acquisition.

4.3. Data Processing and Inverse Calculation

With the methods discussed above, the integrating sphere technique was used to obtain the diffuse reflection and transmission with the three measurements on each

sample. Eq. (4.1) and Eq. (4.2) were used to calculate the diffuse reflectance R_d and transmittance T_d. Two measurements were performed on the thin dermis samples to obtain the collimated transmittance T_c using spatial filtering setup, one measuring the collimated transmitted light signal with the sample in the holder and another with only the holder. The ratio of the two measured transmittances was calculated to yield T_c.

Inverse calculations have been conducted through Monte Carlo simulations to determine the three optical parameters, μ_a, μ_s and g, from the three experimentally determined optical observables, T_c, T_d and R_d, from 920nm to 1520nm. The inverse calculation procedures were started by determining the attenuation coefficient $\mu_t=\mu_a+\mu_s$ at each wavelength from the collimated transmittance T_c of 36 thin dermis samples obtained by cryostat sectioning. These samples were separated into two groups to study the effect of postmortem time T. Assuming a Lambert-Beer's law for the collimated transmittance at a fixed wavelength, $T_C(D)=Ae^{-\mu tD}$ with A describing the loss and deflection of incident light at the interface of the tissue sample with glass window, the bulk attenuation coefficient μ_t can be calculated from the slope of the straight line fitted to $\log(T_c)$ versus D. An example of the fitting for two groups of samples is displayed in Fig. 31 at the wavelength of 980nm. After this procedure, the μ_t was used as an input parameter for the Monte Carlo simulations to determine the other two independent parameters, μ_s and g, from the T_d and R_d measured by the integrating sphere for each sample of different thickness at each wavelength.

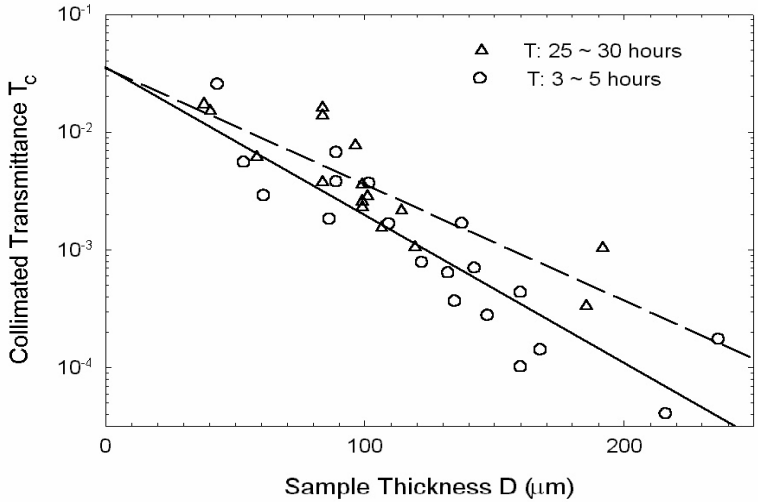

Fig. 31 Fitting of the collimated transmission and tissue thickness at wavelength 980nm. The triangles are the measured T_c of 17 samples stored on ice 25~30 hours and the circles are the measured T_c of 19 samples stored on ice 3~5 hours. Two straight lines are fitted to the data for calculating μ_t.

Using the Monte Carlo simulation method discussed in Chapter 3, we calculated the reflectances and transmittances of a collimated light beam incident on a tissue phantom with a configuration identical to the experimental at wavelength λ. The values of the three optical parameters, μ_a, μ_s and g, were selected prior to the simulation subject to the condition that $\mu_t = \mu_a + \mu_s$. The refractive index variation of the window material (sapphire) with the wavelength was used in the simulations while the refractive index was assumed as a constant, n = 1.41, for skin dermis [Tearney *et al* 1995] because of a lack of skin index data. In our Monte Carlo simulations, the photons were tracked individually inside the tissue phantom until absorbed or escaped from the tracked region ($20\times20mm^2$ with different sample thickness) in the tissue phantom. Since the tracked region is much larger than the illuminated region allowed by the holder aperture of 6.35mm diameter, the

portion of the incident photons escaped from the side of the sample was expected to be negligible in comparison to the experimental errors in T_d and R_d measurements for strongly forward scattering in the skin dermis. This was verified in the Monte Carlo simulations. We adopted the Henyey-Greenstein distribution function for the scattering phase function $p(\theta)$ characterized by an asymmetry factor g. Fig. 32 shows that the definition of the diffuse transmission and diffuse reflection are based on the geometry of the integrating sphere and the port sizes and positions which follow exactly the experimental configuration. The values of the calculated diffuse reflectance and transmittance, $(R_d)_{cal}$ and $(T_d)_{cal}$, were compared to the measured values, $(R_d)_{mea}$ and $(T_d)_{mea}$, and a squared error function $\delta^2(\mu_a, \mu_s, g)$ was obtained:

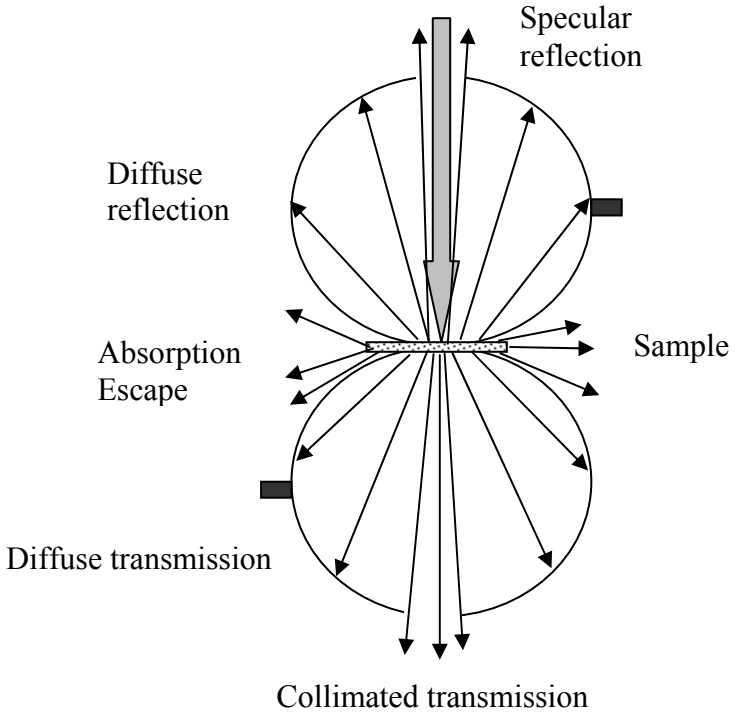

Fig. 32 Determination of the R_d T_d T_c R_c from the geometry of the integrating sphere.

$$\delta^2 = [\frac{(R_d)_{cal} - (R_d)_{mea}}{(R_d)_{mea}}]^2 + [\frac{(T_d)_{cal} - (T_d)_{mea}}{(T_d)_{mea}}]^2 . \qquad (4.3)$$

The simulation was repeated with a new set of μ_a, μ_s and g until $\delta^2(\mu_a, \mu_s, g) < 0.001$. With proper choice of the three parameters, it usually took two or three iterations to achieve $\delta^2(\mu_a, \mu_s, g) < 10^{-4}$. We found that the statistical fluctuation in the Monte Carlo simulation results of T_d and R_d becomes negligible when the total number of injected photons, N_0, exceeds 10^5 (Fig. 33) and therefore we chose $N=2.8\times10^5$ as the number of photons incident at the window-tissue interface for all the simulations. To ensure the uniqueness of the inversely determined optical parameters from the experimental observables, we further calculated the squared error function $\delta^2(\mu_a, \mu_s, g)$ against a large set of the two independent variables μ_s and g for selected samples. A typical example is shown in Fig. 34 which clearly indicates the convergence of the inverse procedure and confirms the expectation that the inverse calculation based on our Monte Carlo codes is well behaved.

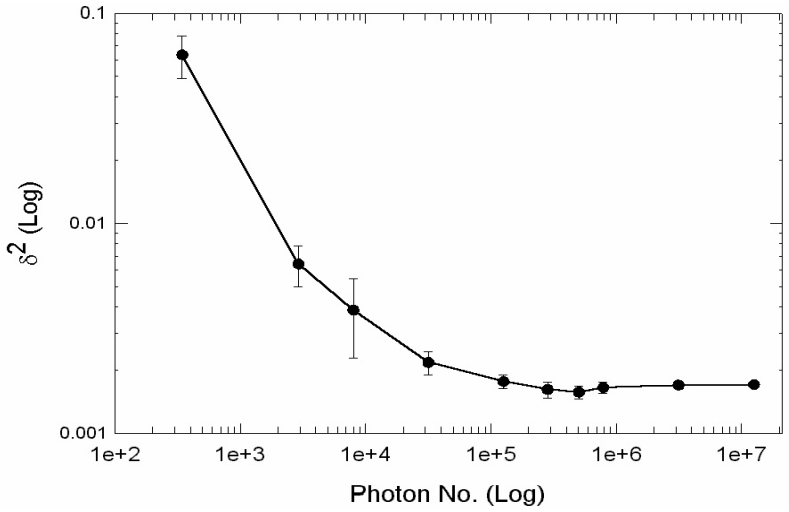

Fig. 33 The dependence of the squared error on the number of tracked photons averaged over five simulations. The simulated sample ID is 99090302 with D=0.93mm, λ=1400nm, μ_s=21.091mm^{-1}, μ_a=0.66mm^{-1}, g=0.90 and measured values of R_d=0.1504 and T_d=0.1268. The solid line is for guide of the eye.

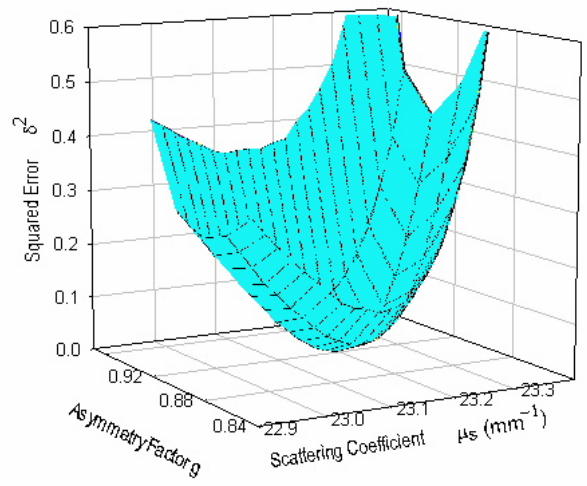

Fig. 34 The convergence of the inverse calculation. The sample ID is 99090302 at λ=1160nm, T=3hours, D=0.93mm, μ_s=23.278mm^{-1}, μ_a=0.1mm^{-1} and g=0.91, measured values of R_d=0.2902 and T_d=0.238.

5. Results and Discussions

Using the methods discussed in previous chapters, optical properties of porcine skin dermis were investigated through the reflectance and transmittance measurements. Based on the experimental data we inversely calculated the optical parameters of porcine skin dermis through Monte Carlo simulations which will be presented in the first section. Effects of storage condition and postmortem time on the optical properties of porcine skin dermis will be discussed in the second section. The third section presents preliminary results on the scattering of a laser beam at 1064nm through a monolayer of cultured carcinoma breast cancer cells (MCF7) and integrating sphere measurements of normal human breast tissue.

5.1. Porcine Dermis Tissue Measurements

The anatomical structure of porcine skin is very similar to that of the human skin and serves as a good model to study the properties of human skin tissue [Dick and Scott 1992]. We have investigated the optical properties of the porcine skin dermis for its making up the bulk of the skin.

The collimated transmittance T_c was measured from 58 thin samples obtained through cryostat sectioning in the SWIR region from 920 to 1520nm with 30nm step using the spatial filtering technique shown in Fig. 30. The time constant of lock-in amplifier was set at 3 second with the filter rolloff of 24dB/oct and optical chopper

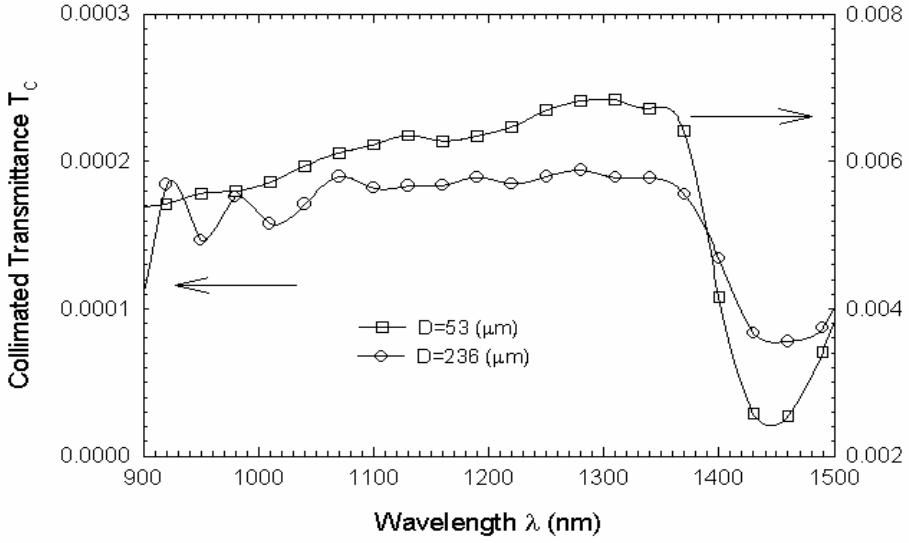

Fig. 35 Collimated transmittance as a function of wavelength measured from two samples 99112901 with D=53μm and 99112904 with D=236μm, the solid lines are for guide of eye.

frequency set at 18±1Hz. The collimated transmittances as a function of wavelength measured from two samples are plotted in Fig. 35. We determined the attenuation coefficient μ_t from the thickness dependence of T_c at different wavelengths. To study the effect of postmortem T on μ_t, the tissue samples were stored within crushed ice for T hours before frozen in the cryostat. The 58 thin dermis samples were separated into three groups: 19 samples with T between 3 and 5 hours, 17 samples between 25 and 30 hours and 22 samples around 170 hours (one week) (see Appendix B). At each wavelength the attenuation coefficient μ_t was obtained by fitting a straight line to the experimental data for each group, as shown by one example in Fig. 29. Three curves of μ_t as functions of wavelength λ for each of the three groups are plotted in Fig. 36 with the vertical bars calculated from the equation below:

$$\left|\frac{\delta\mu_t}{\mu_t}\right| = \sqrt{\frac{1}{N}\sum_{i=1}^{N}\left\{\left|\frac{\delta \ln(T_c)_i}{\mu_t D_i}\right|^2 + \left|\frac{\delta D}{D_i}\right|^2\right\}}, \tag{4.4}$$

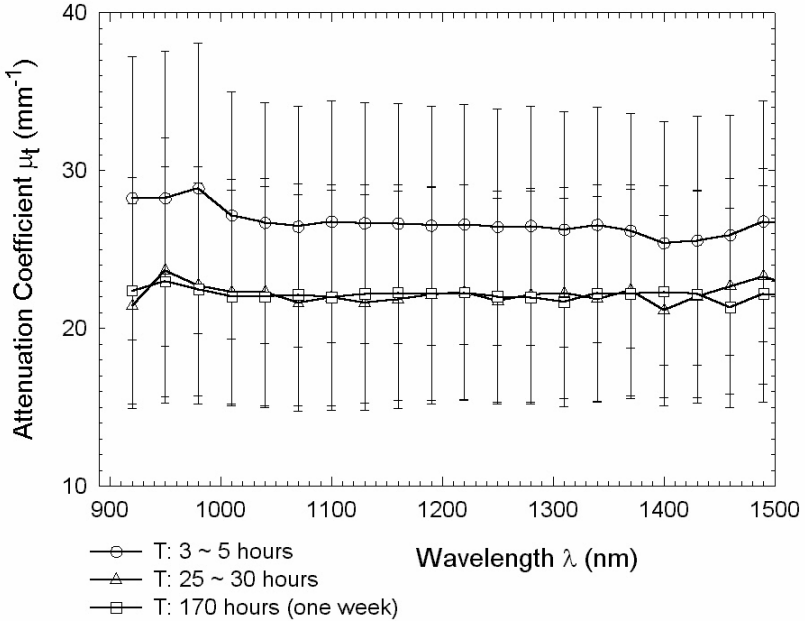

Fig. 36 The attenuation coefficients determined from different sample groups as a function of wavelength. The vertical bars represent the error calculated from Eq. (5.1) and the solid lines are for guide of eye.

where N is the number of samples in each group and $\delta\ln(T_c)_i$ is the relative error in the T_c measurement of the i^{th} sample. The term $\delta\ln(T_c)_i$ is obtained by calculating the deviation of the measured values of T_c of the i^{th} sample from the fitted value given by the respective straight line. The average error in thickness measurement, $\delta D/D_i$, were determined by repeating thickness measurements with dermis samples divided in three thickness groups: ±23% for samples with D < 100μm, ±16% for 100μm < D < 180μm and ±10% for 180μm < D < 270μm. Combing these calculations we determined the relative errors in the determination of μ_t for samples in both groups are about ±30%.

From these results, we observe an approximately 15% decrease in μ_t as the postmortem time T increases to larger than 20 hours for samples stored in the ice. Furthermore, we note that the decrease in μ_t is nearly wavelength-independent, suggesting the change is not a result of structural variation inside the dermis.

A total of 44 porcine dermis samples were obtained to measure T_d and R_d using the integrating sphere technique, the thickness of the sample ranged from 0.43 to 1.37mm. Among these, 22 samples were measured with postmortem time T between 3 and 5hours and another 22 samples were measured with T between 25 and 30hours. Most samples were stored on ice after the animal death with some samples stored in preserve solution to study the effect of the storage condition (see Appendix B). The measurements were conducted from 920nm to 1500nm with 30nm step and the lock-in amplifier and chopper parameters were set the same as the T_c measurements. The diffuse reflectance R_d and transmittance T_d as a function of wavelength from two sample stored 30 hours on ice is shown in Fig. 37, the thickness of these two samples are 1.34mm and 0.74mm, respectively. We note that the ratio of the absolute value of R_d and T_d depends on the sample thickness: T_d usually larger than R_d for thin samples and otherwise for thick samples. When the wavelength approaches to 1400~1520nm, T_d decreases steeply and becomes smaller than R_d regardless of the thickness of the sample. This implies a remarkable change of optical properties in this wavelength range, which is shown in more detail through the result of inverse calculations.

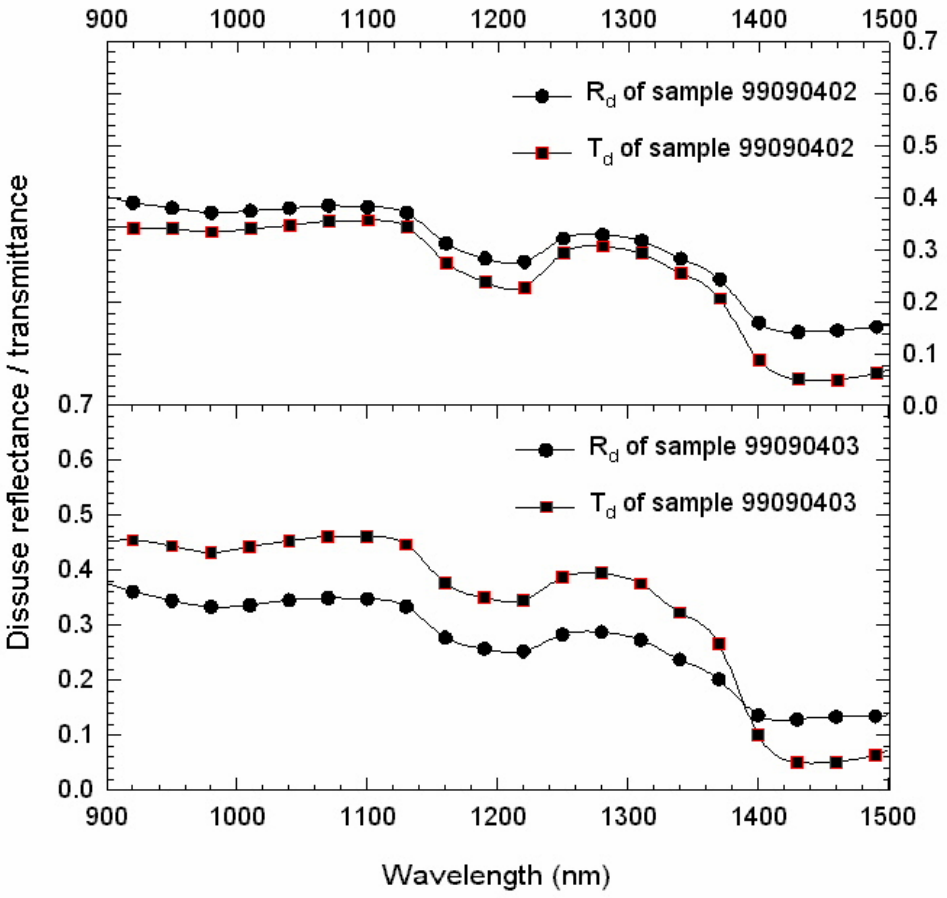

Fig. 37 Diffuse reflectance and transmittance of two porcine skin dermis samples: 99090402 with D=1.34 mm and 99090403 with D=0.74 mm. Both samples were stored on ice for 30 hours. The solid line are for guide of the eye.

Monte Carlo simulations have been performed for each sample to determine the value of μ_s, μ_a and g as a function of wavelength from the measured T_d and R_d. Because of lack of data about the refractive index n_t of the porcine skin dermis, we assumed that n_t=1.41 for all wavelengths. Different refractive indices of the sapphire windows in the sample holder were used according to wavelength. In order to speed up the Monte Carlo simulations, an experience-based algorithm was adopted in the codes to automatically adjust the three optical parameters μ_s, μ_a and g for minimizing δ^2, the squared error

function defined in Eq. (4.1). Since $\mu_s+\mu_a=\mu_t$, which had been determined previously from the T_c measurements, only two parameters are independent for the inverse calculation based on the measured values of T_d and R_d. As we have discussed in the previous paragraph, the absorption coefficient μ_a relates closely to the sum R_d+T_d and g relates to the ratio $\frac{R_d}{T_d}$. Therefore, increasing μ_a will cause R_d+T_d to decrease and increasing g will cause $\frac{R_d}{T_d}$ to decrease and vice versa. After initial simulation, the value of μ_a and g were adjusted in a direction for reducing $\delta^2(\mu_a, \mu_s, g)$ in the next simulation. The simulations were iterated until δ^2 reaches to 0.001 or less.

Different values of the attenuation coefficients μ_t were used in the simulations of the 44 samples according to their postmortem time. For samples with $T < 10$ hours, μ_t determined from the thin sample group with T between 3 and 5 hours were used in the simulations while for samples with $T > 20$ hours μ_t from the thin sample group with T between 25 to 30 hours were used. Typical results on the calculated and measured values of T_d and R_d from a sample with T = 2 hours and D = 930μm are plotted as a function of wavelength in Fig. 38 to demonstrate the excellent agreement between the calculated and measured values. The simulation carried out for this sample were ended when $\delta^2=2\times10^{-4}$.

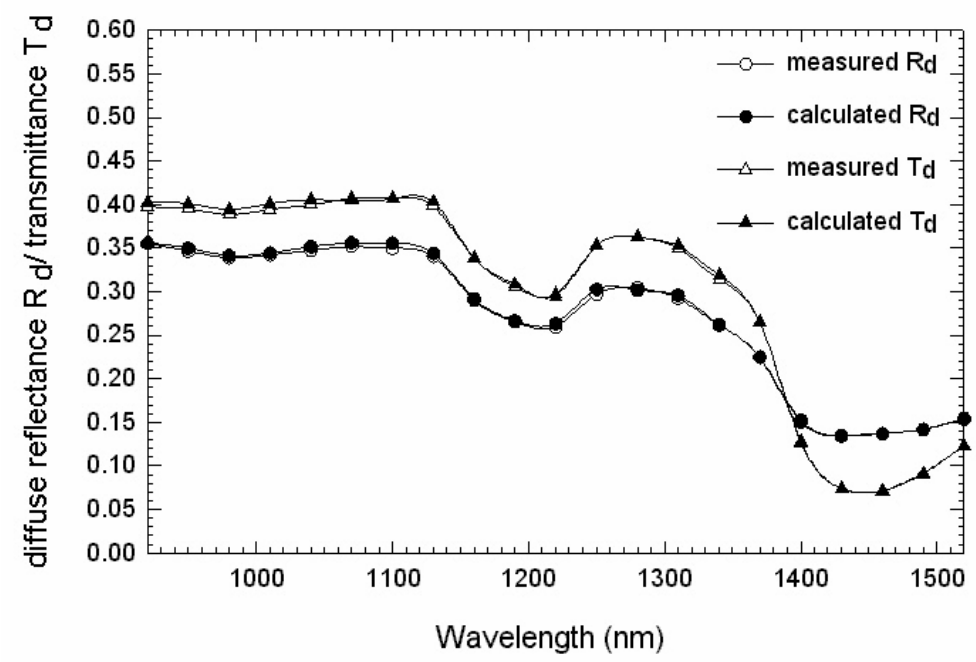

Fig. 38 The calculated and measured values of the R_d and T_d for sample 99090302 with D=0.93 mm, T= 2 hours. The solid lines are for guide of the eye.

In order to check the sensibility of the simulation on the determined value of the parameters, we shows the variations of $\delta^2(\mu_a, \mu_s, g)$ due to fractional changes in one of the three parameters, μ_a, μ_s and g, from their optimal values in Fig. 39 for two different samples. It becomes clear from Fig. 39 that the accuracy of the inverse determination of the optical parameters based on the Monte Carlo simulations is most sensitive to changes in the asymmetry factor g and least to changes in the absorption coefficient μ_a. In fact, a ±6% change in μ_a would still satisfy the tolerance requirement of $\delta^2 < 0.001$ for sample #1, revealing the large uncertainty in determining the absorption coefficient in a strong scattering medium of the skin dermis. By contrast, a mere ±0.4% change in the asymmetry factor g causes the squared error δ^2 for sample #1 to exceed the 0.001 because the choice of g strongly affects the simulated light distribution on two sides of the slab

sample. These results indicate that assuming g as a constant in the determination of the wavelength dependence of optical parameters of skin tissues [Simpson *et al* 1998] could add a significant source of error in calculating μ_a and μ_s. Comparing the same analysis applied to two different samples in Fig. 39, we note that the minimum values of the total

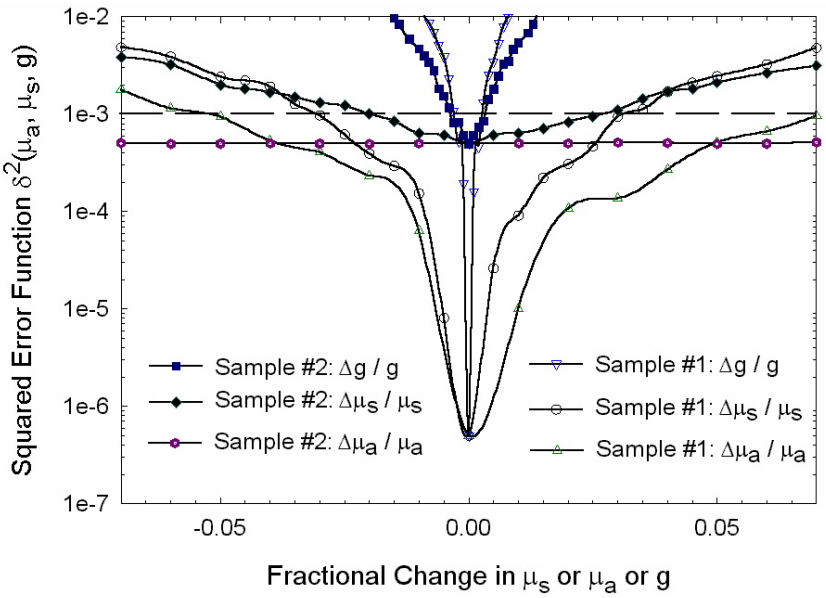

Fig. 39 The reliability test of the inverse simulation. The parameters for sample#1 (99090302) are T = 3hours, D = 0.93mm, λ = 1220nm, measured values of R_d=0.2596, T_d=0.2975 and the window index = 1.7518 and the minimum value of square error $\delta^2 = 5\times10^{-7}$ is obtained with μ_s=26.3639mm^{-1}, μ_a=0.221mm^{-1} and g=0.923. The parameters for sample#2 (20022303) are T = 3hours, D = 0.68mm, λ= 1070nm, measured values of R_d=0.3997, T_d=0.4535 and the window index = 1.7544 and the minimum value of square error $\delta^2 = 5\times10^{-4}$ is obtained with μ_s=26.4462 mm^{-1}, μ_a=0.0001mm^{-1} and g=0.8906. The dashed line indicates the threshold of δ^2 and solid lines are for guide of eye.

squared error, δ^2_{min}, differ by three orders of magnitude. The value of δ^2_{min} indicates the inconsistency between the values of $(T_d)_{mea}$ and $(R_d)_{mea}$ and the difference in δ^2_{min} can be attributed to the variation of the experimental errors among the measurements. For the

inverse calculations performed for the 44 samples at 21 wavelengths, we find all satisfy $\delta^2_{min} < 0.001$ or $\sqrt{\delta^2_{min}} < 3\%$, an independent evidence supporting the estimated errors of ±5% obtained from the measurements of T_d and R_d based on our calibration measurements with the reflectance standards.

Combining the results from 44 fresh porcine skin dermis samples, we obtained the average of the optical parameters as a function of the wavelength from 920 to 1520nm for each group of samples with different T, shown in Fig. 40. The error bars represent the standard deviation of the respective optical parameters among the samples within each group. From the wavelength dependence of the optical parameters of porcine skin dermis, shown in Fig. 40, one can clearly see that the response of skin dermis to SWIR light is dominated by scattering since μ_s is one to two orders of magnitude lager than μ_a. As expected, the asymmetry factor $g=\langle\cos\theta\rangle$ remains approximately a constant around 0.9 between 900 and 1400nm, indicating the strong forward nature of the light scattering by the dermis. The absorption coefficient μ_a displays a peak between 1400 and 1500 nm which can be associated with the light absorption by water [Hale and Querry 1973]. The similar increases of the absorption coefficient μ_a from 1310nm to 1430nm, a factor of 10 in the porcine dermis versus a factor of near 40 in water, suggests that the dermis absorption is mainly due to its water component. It also noted that the asymmetry factor g exhibits a significant decrease near 1430nm which is not an artifact of simulations but directly supported by the experimental observation of R_d becoming larger than T_d

between 1400 and 1500nm as displayed in Fig. 37. The correlation between μ_a and g in the porcine skin dermis is not well understood at this time.

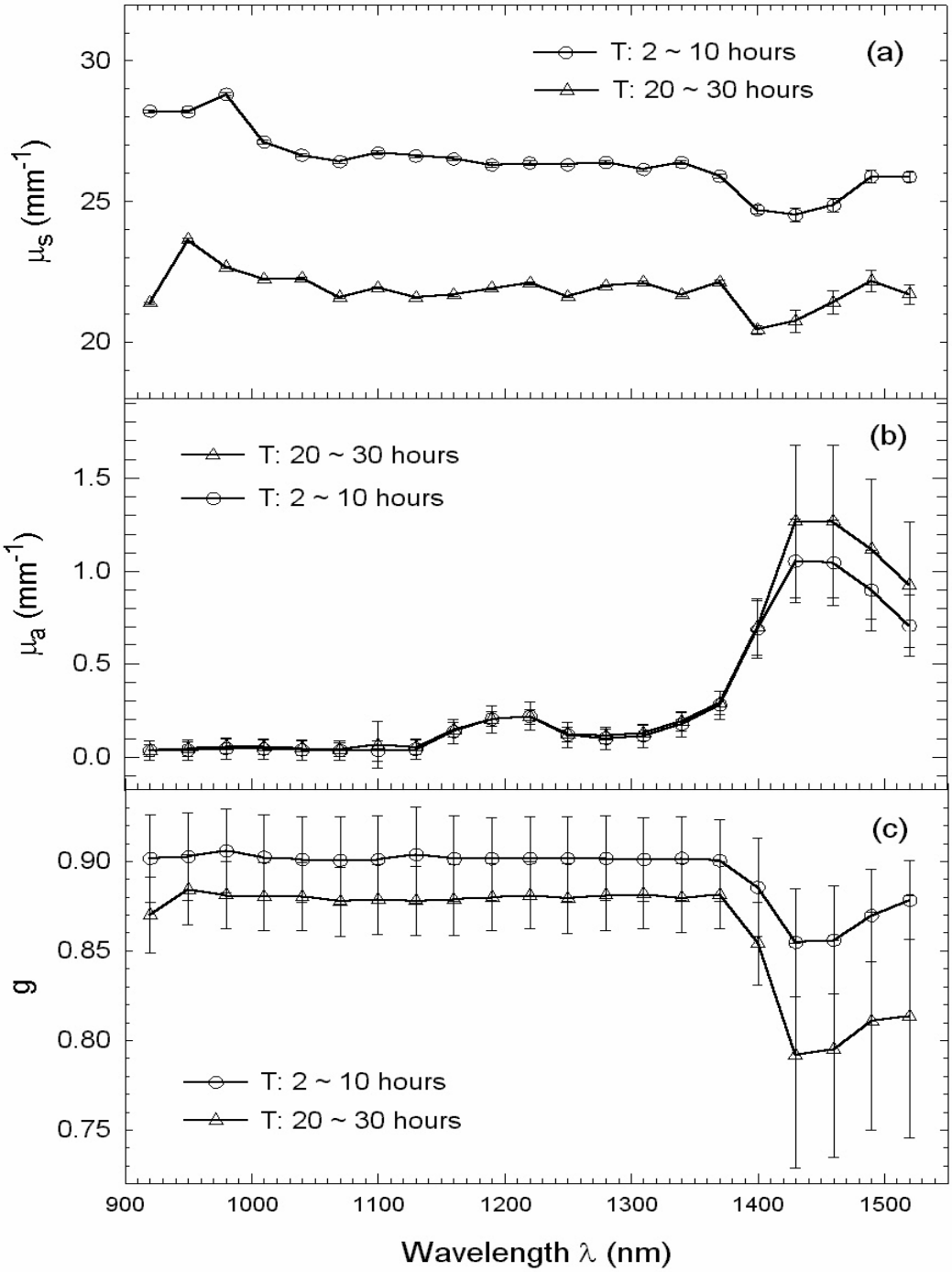

Fig. 40 The mean values of the optical parameters determined from 44 sample divided into two groups. The solid lines are for guide of eye and the error bars are the standard derivation of the parameters within each group.

5.2. Effect of Storage Condition and Time

To study the effect of storage condition and postmortem time T on the optical parameters, we selected 19 out of the 44 porcine dermis samples to be stored either within crushed ice or in Tyrode's solution with T ranging from 2 to 30hours (Appendix B). The three optical parameters, g, normalized μ_s and μ_a of the 19 samples are plotted in Fig. 41 as functions of the postmortem time T at three wavelengths of 980, 1370 and 1400nm. No significant changes in the three parameters can be identified in Fig. 41 among samples with different storage conditions. This suggests that the storage of the skin tissues within the crushed ice with T < 30 hours maintains the cellular structures intact in the skin dermis since the Tyrode's solution is a widely known physiological buffered saline (PBS) for tissue preservation.

To confirm this conclusion, we further examined the ultrastructure of skin dermis samples after the optical measurements through TEM [Cariveau 2000]. No observable cellular changes in cells and collagen fibers were noted in the dermis samples with T up to 30 hours. The TEM micrograph of one sample stored in Tyrode's solution with T=2 hours is shown in Fig. 42 and another TEM of sample stored on ice with T= 24hours is shown in Fig. 43. From the TEM studies, we observe no significant change in microscopic structures like collagen and nucleus. Based on these results, we concluded that skin samples stored within crushed ice within 30 hours postmortem are equivalent to those stored in Tyrode's solutions for *in vitro* optical measurements.

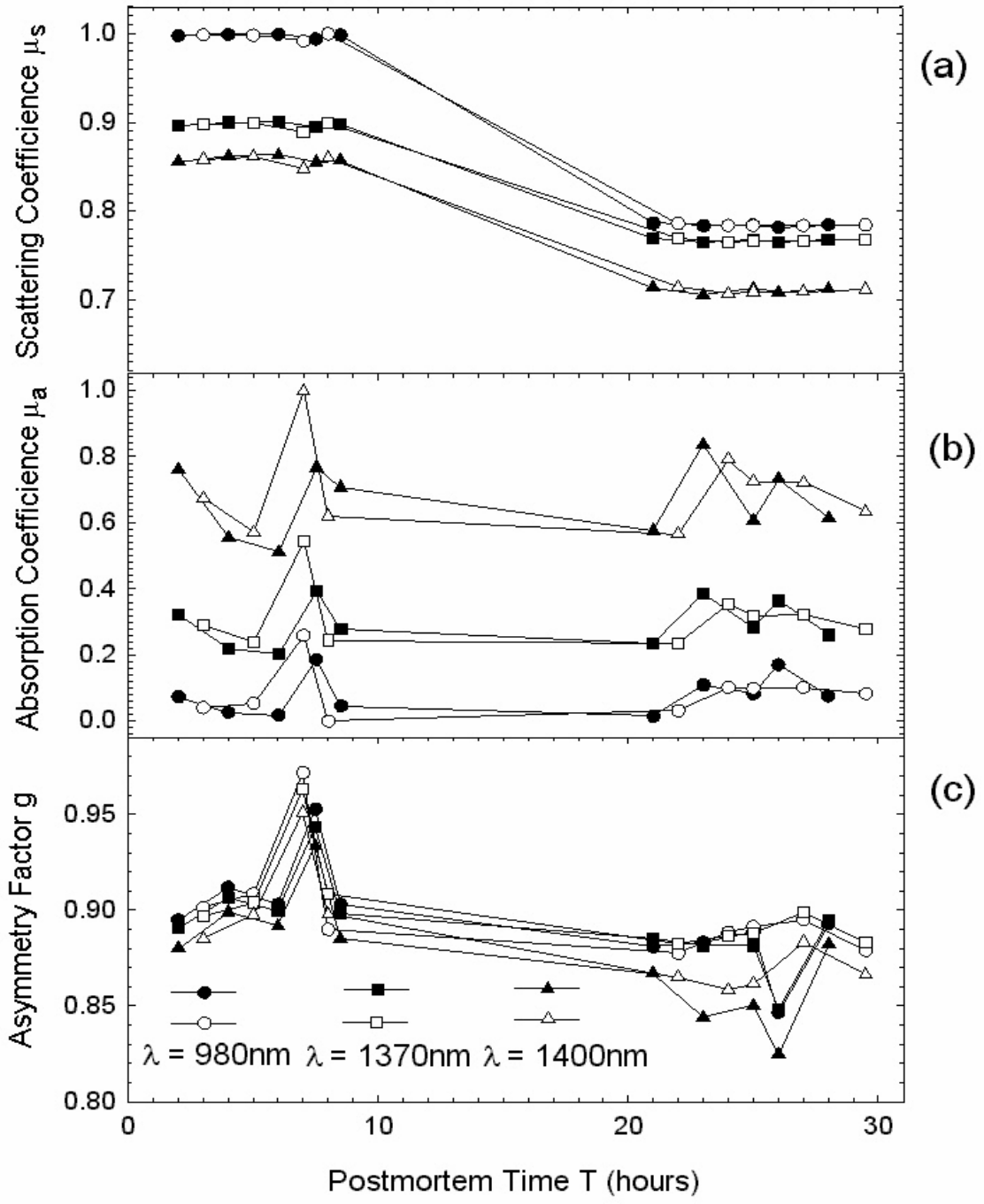

Fig. 41 The optical parameters inversely determined for 19 skin dermis samples with different postmortem time and storage conditions at three wavelengths. The solid symbols are for the samples stored within ice and the empty symbols are for samples in Tyrode's solution: (a) the scattering coefficients are normalized to μ_{s_max} = 28.9 (mm^{-1}); (b) the absorption coefficients are normalized to μ_{a_max} = 0.92 (mm^{-1}); (c) the asymmetry factor. The solid lines are for guide of the eye.

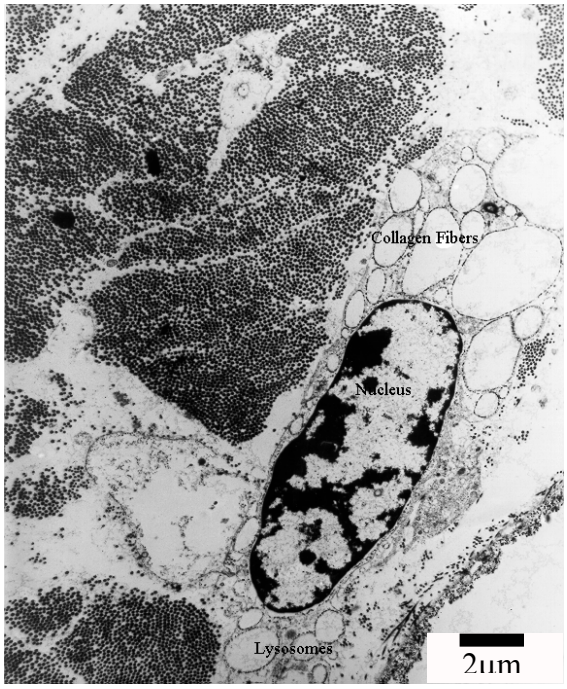

Fig. 42 TEM photo of porcine dermis stored in the tyrode's solution with T=2 hours

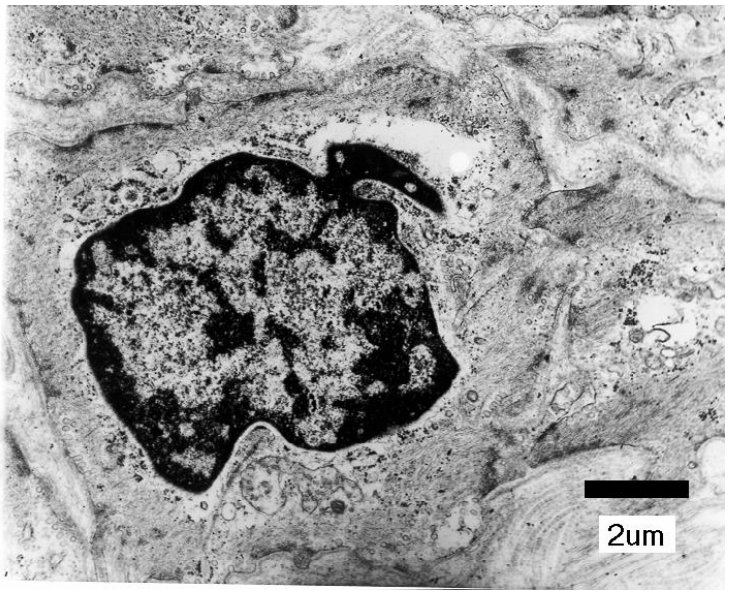

Fig. 43 TEM photo of dermis stored on ice with T=24 hours

The difference between the optical parameters of two dermis sample groups with different postmortem time T is unexpected. From Fig. 41, we note that the scattering coefficient μ_s displays an approximate 15% decrease as the postmortem time T increases from 2 hours to 30 hours while almost no relative changes exist in μ_a and g. It is obvious that the relative large difference in μ_s between samples in two groups is a consequence of using two different values of μ_t for the samples. While we observed no significant changes in cellular morphology and the collagen fibers in samples stored within crushed ice or in Tyrode's solution for T < 30 hours through TEM, we found that the tissue samples stored within ice developed wrinkles and signs of over-hydration as T approaches to 30 hours. Furthermore, the wavelength dependence of the parameters obtained from the two sample groups closely resembles each other. These facts indicate to us that the difference should be attributed to the change of the water content in the skin samples. This conclusion is further manifested by the near overlapping of the two curves of $\mu_a(\lambda)$ for $\lambda <$ 1370nm in Fig. 40 which separate only around the peak of water absorption band near 1430nm.

5.3. Breast Tissue and Cells

In addition to the porcine skin dermis, we also studied the scattering properties of normal breast tissue using the integration sphere techniques. The scattering of 1064nm laser beam through the cultured monolayer breast cancer cells were also studied by using CCD camera. These preliminary results are presented in this section.

5.3.1.Normal Human Breast Tissue

Fresh normal breast tissue samples were obtained from the breast surgery patients through the Department of Pathology, Brody School of Medicine, East Carolina University under an approved protocol (#98-1399E) by the UMCIRB of ECU. The diffuse reflectance R_d and diffuse transmittance T_d of the breast tissue were measured. Breast tissue is mostly made up of fat and is more flexible and transparent than the porcine skin dermis. Six breast tissue samples were measured from 900~1500nm with 20nm for each step. All the experiments were done within 24 hours after the surgery. Tissue preparation procedures were the same as the microtome methods used for preparing the dermis tissue. Thickness of sample ranges from 0.55~1.33mm. Results of diffuse reflectance and transmittance are shown in Fig. 44, we observe that diffuse transmittance of breast tissue is larger than diffuse reflectance. Diffuse reflectance almost have same value no matter the thickness and appear less sensitive to the wavelength than the porcine skin dermis. This implies that the diffuse reflection is mainly resulted from the superficial part of the sample at the entrance side. On the contrary, diffuse transmittance changes significantly with the thickness and thus suggests a strong forward scattering and the increase of absorption while the path of photon travel inside tissue increases with the thick tissues. The increase of absorption associated with water at 1200nm and 1400~1500nm still exist. Over all, the diffuse reflectance and transmittance as function of wavelength have similar shape as porcine skin dermis.

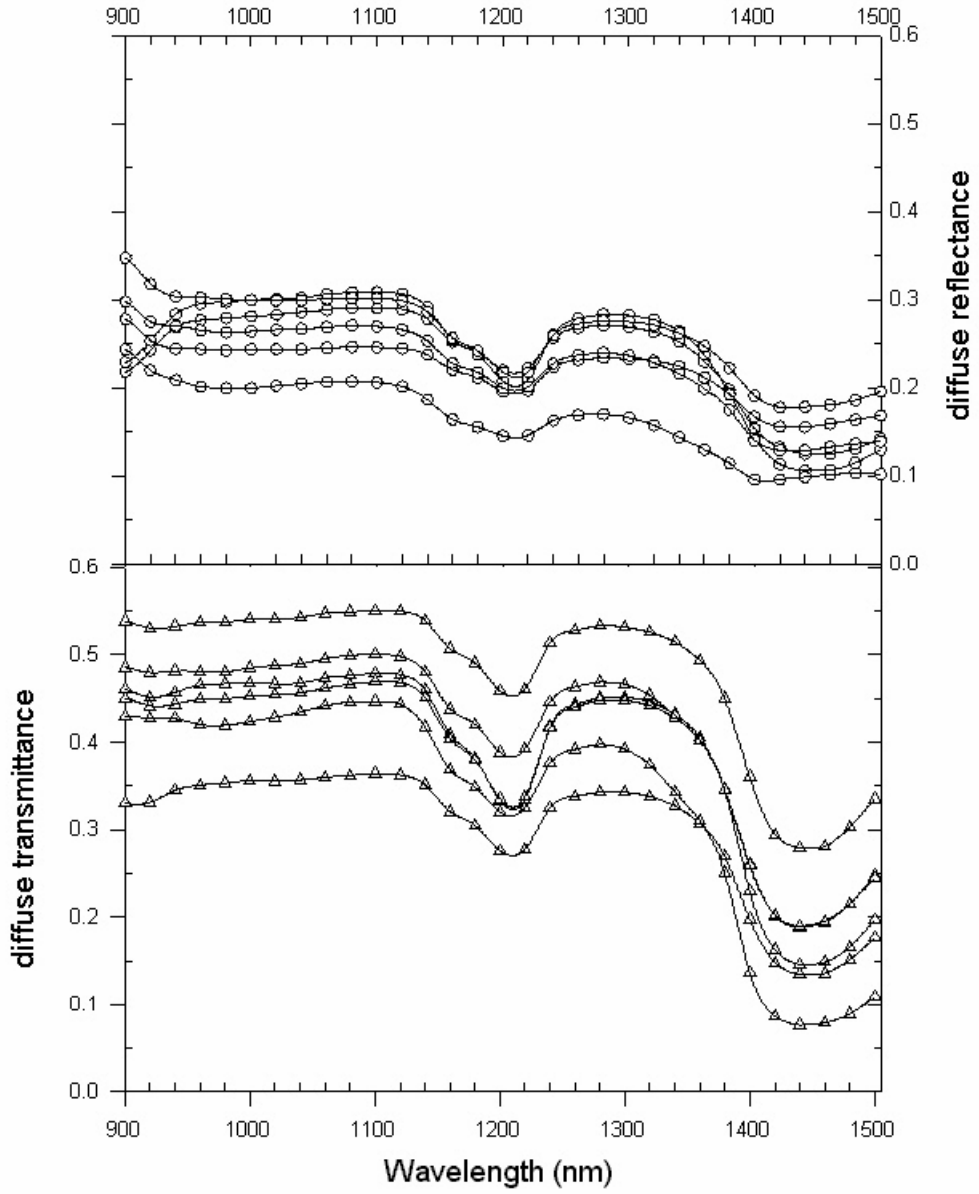

Fig. 44 Diffuse reflectance and transmittance of 6 normal breast tissue samples. The triangles are the diffuse transmittance and the circles are the diffuse reflectance, with the solid lines are for guide of the eye .

5.3.2.Light Scattering by Breast Cancer Cells

Scattering of a laser beam passing through a monolayer of cultured cell has been investigated with a carcinoma breast cancer cell line (MCF7). Cultured cells tend to form a monolayer at the bottom of the culture flask if nutrition is provided for the cells to grow. A monolayer of the MCF7 cells consists of cells tightly connected to each other with the healthy cells ranging 10~20μm in diameter with irregular shapes (Fig. 45).

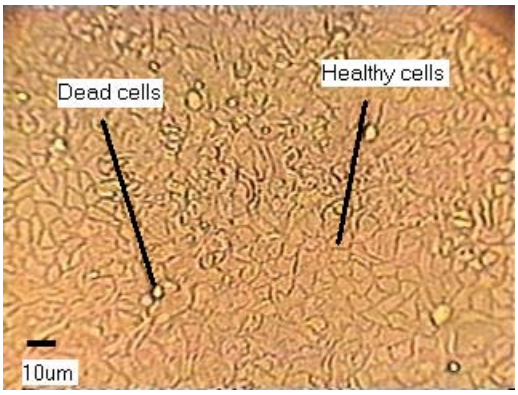

Fig. 45 The MCF7 cell monolayer.

The cytoplasm of the cells is nearly transparent to visible and SWIR light and the scattering of light by a single cell is due to the intercellular and intracellular organelles. A converging beam at 1064nm from a diode-pumped 300mW cw Nd:YAG laser was used to pass though the cell culture flask. The transmittance of the plastic flask at 1064nm was determined to be about 0.9 and the beam profile transmitted through the empty flask was found identical to the incident beam. The experimental setup was discussed in section 3.4 and shown in Fig. 23. The laser beam was focused on the monolayer of cells by a spherical lens of 400mm focal length to create a narrow and collimated beam waist at the sample. Three BK7 optical wedges were used to reduce the power of the beam incident at

the cell. The light transmitted through the flask holding the cells was taken by the ST7i CCD camera with each pixel of $9\times9\mu m^2$ in size and cooled at -10°C. The CCD and cell culture flask were kept in the horizontal direction with the CCD placed beneath the flask. To ensure the viability of cells during experiments, they were covered with phosphate buffer solution (PBS) or culture medium minium essential medium (MEM). Fig. 46 shows the results of the profile of the transmitted laser beam pass through the flask with MEM only (Fig. 46a), PBS only (Fig. 46b), monolayer MCF7 cells in MEM (Fig. 46c), monolayer MCF7 cells in PBS (Fig. 46d), dead MCF7 cells in MEM (Fig. 46e) and Hi-5 cells in Ex-cell-4000 medium (Fig. 46f). From Fig. 46a and 46b we can see that changing the culture medium MEM to PBS does not affect the beam profile because both are clear liquids. Therefore, the variations in the beam profiles displayed in Fig. 46c and 46d are due to the scattering by the monolayer of the cells. We can also observe that the collimated transmission is much stronger than the scattered portion in these cases and the scattering is strongly forward. For dead MCF7 cells, the monolayer no longer exists and the cells suspend in the medium with the diameters about 10μm. This may explain the stronger scattering shown in Fig. 46e. For comparison, we measured the light scattering by the Hi-5 cell, which is smaller than MCF7 cell with about 10 μm in diameter and close to spherical shape. Again, we observe that the scattering is strongly forward. Future studies based on the wave approach of light-cell interaction will be pursued to explain these results for understanding the microscopic mechanism of light scattering in biological tissues.

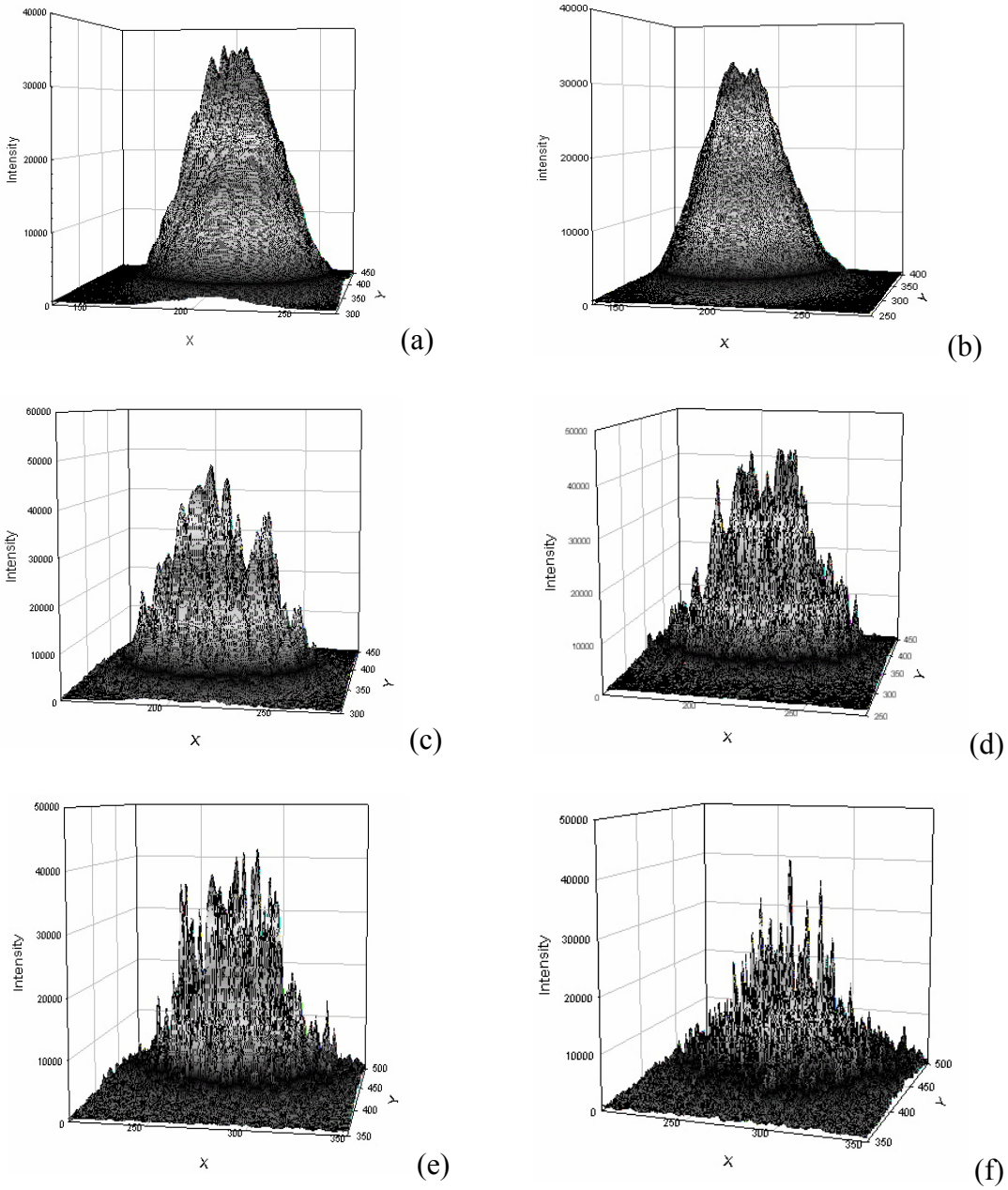

Fig. 46 The profile of a laser beam by cultured cells transmitted through a flask with (a) MEM only; (b) PBS only; (c) a monolayer of MCF7 cells in MEM; (d) a monolayer of MCF7 cells in PBS; (e) dead MCF7 cells in MEM; (f) Hi-5 cells in Ex-cell-4000 mediem.

6. Conclusion

The lack of the skin optical data in the important SWIR spectral region from 900 to 1500nm has motivated us to construct the current experimental setups and to perform our first measurements on the porcine skin dermis. In this spectral region the weak absorption band by water near 1400nm provides a unique opportunity to study the role of water in the optical response of the highly turbid media of skin tissues. The use of porcine skin tissues is based on the similarity between the tissue structures of porcine and human skin [Lavker *et al* 1991] and the relative ease in obtaining a large number of samples for our investigations of the postmortem effect.

We measured the collimated transmission T_c, diffuse transmittance T_d and diffuse reflectance R_d from porcine skin dermis samples in the spectral region from 900nm to 1500nm and inversely determined the scattering coefficient μ_s, the absorption coefficient μ_a and the asymmetry factor g. Based on these results, we investigated the effect of the tissue storage conditions and postmortem time on the optical response of the skin tissue to the SWIR light. We concluded that no significant changes occur in the cellular and collagen structures of the porcine skin dermis for samples stored within crushed ice with postmortem time up to 30 hours. The values of the scattering coefficient and asymmetry factor, however, were found to change as a result of sample hydration during the storage within crushed ice.

The theoretical framework of this study is provided by radiative transfer theory within which Monte Carlo simulations were used for accurately inverting the measured reflectance and transmittances to obtain the three optical parameters: μ_a, μ_s and g. To assess the validity of our method, we have analyzed the sensitivity of the parameter values on the experimental errors and inverse calculation procedures by calculating the squared error $\delta^2(\mu_a, \mu_s, g)$ as a function of individual variations in the optical parameters. We found that the inverse calculation is highly sensitive to small changes in the asymmetry factor g. Therefore, assuming g as a constant in the determination of the wavelength dependence of optical parameters of skin tissues [Simpson *et al* 1998] could add a significant source of error in determining μ_a and μ_s.

Preliminary studies on breast tissue show that the breast tissue is much more transparent than dermis tissue. The human breast tissues have similar dependence of diffuse reflectance and transmittance on wavelength, indicating the water component in the breast tissue dominates the absorption peak around 1400~1500nm. Light scattering by cultured cells at 1064nm exhibit a strongly forward characteristic with only a small portion of the photons contained in the beam experience single scattering by the cells.

We note two deficiencies in the current procedures of determining the optical parameters. First, the effect of surface roughness of the sectioned tissue samples has not been taken into account in the inverse calculations. This leads to overestimating the scattering coefficient because the deflection of the incident light at the two surfaces of the sample are treated as a part of bulk scattering. Second, we assumed the average refractive index of the tissue to be a constant, n =1.41, over the spectral region from 900 to

1500nm. The value of n has not been verified experimentally for skin dermis and, in any case, the assumption of n as a constant is not a good approximation in studying the light deflection due to the index mismatch at the tissue surfaces. Future investigations are needed to address these concerns.

References

Anderson R R and Parrish J A 1981 “The optics of human skin,” *J. Invest. Dermato*., **77**, *13-9*

Anderson R and Hu J 1981, “Optical Radiation Transfer in the Human Skin and Applications in *in vivo* remittance spectroscopy,” in *Bioengineering & the Skin*, ed. by Marks R and Payne P A, MTP Press, *253-265*

Anthony C and Thibodeau G 1983, *Anatomy & Physiology*, The C. V. Mosby Company, *76-85*

Baraga J J, Feld M S, Rava R P, 1992 "In situ optical histochemistry of human artery using near infrared Fourier transform Raman Spectroscopy", *Proc. Natl. Acad. Sci*., **89**, *3473-7*

Beek J F, Blokland P, Posthumus P, Aalders M, Pickering J W, Sterenborg H J C M and van Gemert M J C 1997, *In vitro* double-integrating-sphere optical properties of tissues between 630 and 1064nm, *Phys. Med. Biol.* **42**, *2255-2261*

Bohren F C and Huffman D R 1983, *Absorption and Scattering of Light by Small Particles*, John Wiley & Sons

Boyd R W 1983, *Radiometry and the Detection of Optical Radiation*, John Wiley & Sons

Chandrasekhar S 1960, *Radiative Transfer* Dover publication, New York

Cariveau M 2000, "The Interaction of Optical Radiation with Epithelial Tissue", MS Thesis, Department of Biology, East Carolina University, U.S.A.

Dong K, Song Z, Lu J Q, Hu X H 1999 “Monte Carlo Simulation of Converging Laser Beams Propagating in Skin Tissue Phantoms”, *Proceedings of SPIE*, **3590** , *4-10*

Dong K 1999, "Monte Carlo Simulation of Converging Laser Beams Propagating in the Skin Tissue Phantoms with Random Rough Surfaces", MS Thesis, Department of Physics, East Carolina University, USA

Firbank M, Hiraoka M, Essenpreis M and Delpy D T 1993, "Measurement of the optical properties of the skull in the wavelength range 650-950 nm", *Phys, Med. Biol.* **38**, *503-510*

Goebel D G 1967, Generalized Integrating-Sphere Theory, *Applied Optics*, **6**, *125-128*

Graaff R, Dassel A C M, Koelink M H, de Mul F F M, Aarnoudse J G, Zijlstra W G 1993 “Optical properties of human dermis *in vitro* and *in vivo*,” *Appl. Opt.*, **32**, *435-447*

Hale G and Querry M 1973 "Optical constants of water in the 200nm to 200 micrometer wavelength region", *Appl. Opt*., **12**, *555-63*

Hardy A C and Pineo O W 1931, *J. Opt. Soc. Am.* **21**, *502*

Ishimaru A 1978, *Wave Propagation and Scattering in Random Media----single scattering and transport theory*, Vol.1, Academic Press

Jacquez J A and Kuppenheim H F 1955, Theory of the Integrating Sphere, *J. Opt. Soc. Am.* **45**, *460-470*

Jackson D J 1975, *Classical Electrodynamics (Second Edition)*, John Wiley & Sons

Karrer E 1921, *Sci. Papers Bur. Standards*, No. 415, *203-225*

Keijzer M, Jacques S T, Prahl S A, Welch A J 1989 “Light distributions in artery tissue: Monte Carlo simulations for finite-diameter laser beams,” *Lasers Surg. Med.*, **9**, *148-54*

Kerker M 1969, "*The scattering of Light*", Academic Press, New York

Kortum G 1969, *Reflectance Spectroscopy*, Springer-Verlag

Lavker R M, Dong G, Zheng P S, Murphy G F 1991 "Hairless micropig skin. A novel model for studies of cutaneous biology", *Am. J. Pathology*, **138**, *687-97*

Lembares A, Hu X H, Kalmus G W 1997 “Absorption spectra of the cornea in the far ultraviolet region”, *Investigative Ophthalmology & Visual Science*, **38**, *1283-7*

Lu J Q, Hu X H, Song Z and Dong K 1999, Simulation of Light Scattering in Biological Tissues: the Coherent Component, *SPIE Proceeding*, **3601**, *474-481*

Mie G A 1908, *Physik* **25**, *377*

Miller O E and Sant A J 1958, Incomplete Integrating Sphere, *J. Opt. Soc. Am.* **48**, *828-831*

Moon P 1940, *J. Opt. Soc. Am*., **30**, *195*

Moschella S L and Hurley H J 1992, *Dermatology*, W. B. Saunders Company, *16-17*

O'Shea D C 1985, *Elements of Modern Optical Design* Wiley-Interscience Publication

Peters V G, Wyman D R, Patterson M S and Frank G L 1990, Optical properties of normal and diseased human breast tissues in the visible and near infrared, *Phys. Med. Biol.* **35**, *1317-1334*

Pickering J W, Moes C J M, Sterenborg H J C M, Prahl S A and van Gemert M J C 1992, Two integrating sphere with an intervening scattering sample, *J. Opt. Soc. Am. A*. **9**, *621-631*

Pickering J W, Prahl S A, van Wieringen N, Beek J F, Sterenborg H J C M and van Gemert M J C 1993, Double-integrating-sphere system for measuring the optical properties of tissue, *Applied Optics* **32**, *399-411*

Pickering J W, Moes C J M, Sterenborg H J C M, Prahl S A, van Gemert M J C 1992 "Two integrating sphere with an intervening scattering sample", *J. Opt. Soc. Am. A.*, **9**, *621-631*

Prahl S A, van Germert M J C, Welch A J 1993 An iterative adding-doubling algorithm for determining the optical properties of turbid media *Appl. Opt.* **32** *559-68*

Rayleigh J W 1881, *J. W.: Phil. Mag.*, **12**, *81*

Rayleigh J W 1899, *J. W.: Phil. Mag*., **47**, *375*

Rosa E B and Taylor A H 1922, *Sci. Papers Bur. Standards*, No.447, *281-325*

Simpson C R, kohl M, Essenpreis M and Cope M 1998, Near-infrared optical properties of ex vivo human skin and subcutaneous tissues measured using the Monte Carlo inversion technique, *Phys. Med. Biol.* **43**, *2465-2478*

Song Z, Dong K, Hu X H, Lu J Q 1999 "Monte Carlo simulation of converging laser beams propagating in biological tissues", *Appl. Opt*. , **37**, *2944-9*

Tearney G J, Brezinski M E, Southern J F, Bouma B E, Hee M R, Fujimoto J G 1995 "Determination of the refractive index of highly scattering human tissue by optical coherence tomography", *Opt. Lett*. **21** *2258-60*

Van Gemert M J C, Jacque S L, Sterenborg H J C M and Star W M 1989, Skin Optics, *IEEE Trans. Biomed. Eng*., **36**, *1146-1154*

Walsh T W T 1953, *Photometry*, Constable & Co. Ltd., London, second edition

Wilson B C and Adams G 1983 "A Monte Carlo model for the absorption and flux distributions of light in tissue," *Med. Phys*., **10**, *824-30*

Yoon G, Welch A J, Motamedi M, van Gemert M C J 1987, Development and application of three-dimensional light distribution model for laser irradiated tissue, *IEEE Journal of Quantum Electronics*, **QE-23(10)**, *1721-1733*

Y. Tanguchi, "*The Electronic Textbook of Dermatology*", http://www.telemedicine.org

Appendix A. Cell Culture and Tissue Preparation

A.1. Cell Culture

The human breast carcinoma cancer cell line MCF7 was derived from mammary gland adenocarcinoma. It was obtained from the American Tissue Culture Collection (ATCC # HTB-22).

A.1.1.Equipment and Medium

Cell culture was performed under a laminar flow cabinet, all the equipment and solutions were bought sterile or sterilized by autoclaving or sterile filtering techniques.

A.1.1.1.Media and Solutions

The media and solution needed are:

Minimum Essential Medium (1X) (MEM), liquid with Earle's salts and with L-glutamine, kept at 4° C.

Fetal Bovine Serum (FBS), kept in aliquot of 25ml at –80°C.

Trypsin-EDTA (1X), 0.05% Trypsin, 0.63mM EDTA.4Na stored in aliquot of 20ml at –80°C.

Gentamicin, 10mg/ml, stored at 4°C.

A.1.1.2.The Recipe of the Medium and PBS.

MEM medium: MEM medium was supplemented with 10% FBS and 5ml gentamicin.

Phosphate's Buffered Saline (PBS): 140 mM NaCl, 2.6 mM KCl, 8 mM KH_2PO_4 and 1.5 mM Na_2HPO_4.

Freezing medium: 90% FBS plus 10% DMSO (Dimethyl Sulfoxid).

A.1.2.Procedures

A.1.2.1.Thawing Method

Cells are stored in liquid nitrogen, they should be thawed as fast as possible. Thawed cells are transferred into 10ml MEM and centrifuged it 5 minutes at 1000xg. After centrifugation, pour off the supernatant and resuspend the cells in 10ml MEM. Cells are incubated in 75cm^2 flasks at 37°C, 5% CO_2.

A.1.2.2.Cell Culture

Dilution is needed when cells reach confluence, which is done with Trypsin-EDTA. Remove medium from the cells and wash the flasks one time with PBS. Then add 5-8ml of Trypsin-EDTA solution to the cells and observe the cells under the microscope until they start to round and loosen from the surface. This step might need a short incubation at 37°C. Transfer the cells to 5-10 ml Medium and centrifuge for 5 min at 1000 xg. The cells will then be washed with PBS or Medium and resuspended in Medium and divided into 5 new flasks.

A.1.2.3.Freezing Cells

For long-term storage, cells are frozen in liquid nitrogen. Follow the instructions described above. After the last wash resuspend the cells in freezing medium and divide them into freezing vials at a density of $5\sim10\times10^6$/ml. Store the cells at -80°C for about one week, the transfer them into liquid nitrogen.

A.2. Tissue Preparation

Fresh porcine skin patches of about $100\times100mm^2$ area were obtained from the back neck and shoulder area of 6-month-old white domestic pigs. Two different preparation procedures are used for different measurements.

A.2.1.Microtome Methods

For the measurement of diffuse transmittance T_d and reflectance R_d, the upper dermis was trimmed from the porcine skin into $20\times20mm^2$ squares. Using a specially designed microtome, the tissue square was sectioned to obtain samples with thickness D ranging from 0.48 to 1.34mm at 4°C in a refrigerated room. The steps are given below:

1. Shave off the hairs on the epidermis, cut the subcutaneous fat and trim the tissue into squares of size about $20\times20mm^2$.
2. In the 4°C refrigerated room, use a super glue to bond the tissue on the microtome stage and wait about 15~20 minutes for glue to cure.

3. Use a sharp knife to trim a dermis slab off the tissue and set the thickness of the sample by translating the microtome stage upward and make sure there is no fat or epidermis on the sample.
4. Sandwich the sample slab between two optical windows with a few saline solution drops on the sample and eliminate any air bulbs between the sample and windows. Seal the rim of the gap between the two sapphire windows with vaseline grease to prevent tissue dehydration during the measurement.

A.2.2.Cryostat Methods

A cryostat microtome (Ames Lab-tek) was used to obtain dermis sections with D ranging from 30 to 250 μm at -18°C with the following steps:

1. Shave off the hair and cut fat and muscles;
2. Cut the tissue into about $10\times10mm^2$ squares;
3. Put the tissue on the sample holder of cryostat, and protect the tissue with a tissue frozen medium OCT, this is to keep the biological activity while being frozen to -18°C.
4. Wait 15~20 minutes, cut the tissue into desired thickness in the cryostat and put the frozen tissue slab into saline solution to warmed up to the room temperature. The sample can be only cut as thick as 20μm by using the automatically control in the cryostat. To get the desired thickness 100μm <D<500μm, we could force the sample

to raise by rotating the black pad (on the bottom of the knife shelf) count clockwise. Extra force is needed well cut the thick sample.

5. Put the sample in the sample holder, visually examine the sample before measurements to ensure that no holes existed in the sample and the thickness was satisfactorily uniform. The measurement should be conducted within 0.5 hour after sectioning.

Appendix B. The ID Number and Parameters of Porcine Skin Dermis Samples.

Date	Sample ID No.	Thickness	R_d	T_d	T_c	Postmortem Time(hours)	Storage method	Sectioning †
99-06-16	99061601*	1.03142	Y	Y	N	2	in sol	m
99-06-16	9906161A*	0.88142	Y	Y	N	3	on ice	m
99-06-16	99061602*	1.01809	Y	Y	N	4	in sol	m
99-06-16	9906162A*	0.8780867	Y	Y	N	5	on ice	m
99-06-16	99061603*	1.0280867	Y	Y	N	6	in sol	m
99-06-16	9906163A*	1.05142	Y	Y	N	7	on ice	m
99-06-16	99061604*	1.078087	Y	Y	N	7.5	in sol	m
99-06-16	9906164A*	1.154753	Y	Y	N	8	on ice	m
99-06-16	99061605*	0.95142	Y	Y	N	8.5	in sol	m
99-06-16	9906165A*	0.86142	Y	Y	N	9	on ice	m
99-06-17	99061606*	0.9680867	Y	Y	N	21	in sol	m
99-06-17	9906166A*	0.984753	Y	Y	N	22	on ice	m
99-06-17	99061607*	0.7380867	Y	Y	N	23	in sol	m
99-06-17	9906167A*	0.9080867	Y	Y	N	24	on ice	m
99-06-17	99061608*	1.07142	Y	Y	N	25	in sol	m
99-06-17	9906168A*	0.8580867	Y	Y	N	25.5	on ice	m
99-06-17	99061609*	0.744753	Y	Y	N	26	in sol	m
99-06-17	9906169A*	0.7680867	Y	Y	N	27.8	on ice	m
99-06-17	99061610*	1.1	Y	Y	N	28	in sol	m
99-06-17	99061610A*	0.80142	Y	Y	N	29.5	on ice	m
99-09-03	99090301	1.0033	Y	Y	N	3	on ice	m
99-09-03	99090302	0.92964	Y	Y	N	3	on ice	m
99-09-04	99090401	0.99822	Y	Y	N	30	on ice	m
99-09-04	99090402	1.33858	Y	Y	N	31	on ice	m
99-09-04	99090403	0.7366	Y	Y	N	32	on ice	m
99-11-23	99112301	0.056	N	N	Y	3	on ice	c
99-11-23	99112302	0.061	N	N	Y	3	on ice	c
99-11-23	99112303	0.147	N	N	Y	3	on ice	c
99-11-23	99112304	0.122	N	N	Y	3	on ice	c
99-11-23	99112305	0.16	N	N	Y	3	on ice	c

99-11-23	99112306	0.216	N	N	Y	3	on ice	c
99-11-29	99112901	0.05334	N	N	Y	3	on ice	c
99-11-29	99112902	0.0889	N	N	Y	3	on ice	c
99-11-29	99112903	0.1016	N	N	Y	3	on ice	c
99-11-29	99112904	0.23622	N	N	Y	3	on ice	c
99-11-29	99112905	0.1374	N	N	Y	3	on ice	c
99-12-20	99122001	0.05842	N	N	Y	30	on ice	c
99-12-20	99122002	0.0381	N	N	Y	30	on ice	c
99-12-20	99122003	0.04064	N	N	Y	30	on ice	c
99-12-20	99122004	0.09906	N	N	Y	30	on ice	c
99-12-20	99122005	0.08382	N	N	Y	30	on ice	c
99-12-20	99122006	0.10668	N	N	Y	30	on ice	c
99-12-20	99122007	0.11938	N	N	Y	30	on ice	c
99-12-20	99122008	0.18542	N	N	Y	30	on ice	c
99-12-23	99122301	0.05588	N	N	Y	1 WEEK	on ice	c
99-12-23	99122302	0.06858	N	N	Y	1 WEEK	on ice	c
99-12-23	99122303	0.08128	N	N	Y	1 WEEK	on ice	c
99-12-23	99122304	0.09398	N	N	Y	1 WEEK	on ice	c
99-12-23	99122305	0.11684	N	N	Y	1 WEEK	on ice	c
99-12-23	99122306	0.1143	N	N	Y	1 WEEK	on ice	c
99-12-23	99122307	0.18542	N	N	Y	1 WEEK	on ice	c
00-01-13	20011301	0.61214	Y	Y	N	3	on ice	m
00-01-13	20011302	0.7747	Y	Y	N	3	on ice	m
00-01-13	20011303	0.82042	Y	Y	N	3	on ice	m
00-01-13	20011304	0.48	Y	Y	N	3	on ice	m
00-01-13	20011305	0.64516	Y	Y	N	3	on ice	m
00-01-13	20011306	0.6477	Y	Y	N	3	on ice	m
00-01-14	20011401	0.68834	Y	Y	N	30	on ice	m
00-01-14	20011402	0.55372	Y	Y	N	30	on ice	m
00-01-14	20011403	0.73406	Y	Y	N	30	on ice	m
00-01-14	20011404	0.62992	Y	Y	N	30	on ice	m
00-01-20	20012001	0.07366	N	N	Y	1 WEEK	on ice	c
00-01-20	20012002	0.10922	N	N	Y	1 WEEK	on ice	c
00-01-21	20012003	0.1016	N	N	Y	1 WEEK	on ice	c
00-01-21	20012004	0.24384	N	N	Y	1 WEEK	on ice	c
00-01-21	20012005	0.14224	N	N	Y	1 WEEK	on ice	c
00-01-21	20012006	0.04064	N	N	Y	1 WEEK	on ice	c
00-01-21	20012007	0.1143	N	N	Y	1 WEEK	on ice	c
00-02-17	20021701	0.11176	N	N	Y	3	on ice	c

00-02-17	20021702	0.08894	N	N	Y	3	on ice	c
00-02-17	20021703	0.04318	N	N	Y	3	on ice	c
00-02-17	20021704	0.132	N	N	Y	3	on ice	c
00-02-17	20021705	0.08636	N	N	Y	3	on ice	c
00-02-17	20021706	0.10923	N	N	Y	3	on ice	c
00-02-17	20021707	0.14227	N	N	Y	3	on ice	c
00-02-17	20021708	0.13462	N	N	Y	3	on ice	c
00-02-17	20021709	0.16761	N	N	Y	3	on ice	c
00-02-17	20021710	0.16	N	N	Y	3	on ice	c
00-02-18	20021801	0.09906	N	N	Y	30	on ice	c
00-02-18	20021802	0.19192	N	N	Y	30	on ice	c
00-02-18	20021803	0.25654	N	N	Y	30	on ice	c
00-02-18	20021804	0.08382	N	N	Y	30	on ice	c
00-02-18	20021805	0.10116	N	N	Y	30	on ice	c
00-02-18	20021806	0.09652	N	N	Y	30	on ice	c
00-02-18	20021807	0.1143	N	N	Y	30	on ice	c
00-02-18	20021808	0.09906	N	N	Y	30	on ice	c
00-02-18	20021809	0.08382	N	N	Y	30	on ice	c
00-02-24	20022401	0.09398	N	N	Y	1 WEEK	on ice	c
00-02-24	20022402	0.08382	N	N	Y	1 WEEK	on ice	c
00-02-24	20022403	0.0635	N	N	Y	1 WEEK	on ice	c
00-02-24	20022404	0.04572	N	N	Y	1 WEEK	on ice	c
00-02-24	20022405	0.06939	N	N	Y	1 WEEK	on ice	c
00-02-24	20022406	0.1016	N	N	Y	1 WEEK	on ice	c
00-02-24	20022407	0.12192	N	N	Y	1 WEEK	on ice	c
00-02-24	20022408	0.14478	N	N	Y	1 WEEK	on ice	c
00-02-24	20022301	0.68834	Y	Y	N	3	on ice	m
00-02-24	20022302	0.67864	Y	Y	N	3	on ice	m
00-02-24	20022303	0.67818	Y	Y	N	3	on ice	m
00-02-24	20022304	0.7747	Y	Y	N	3	on ice	m
00-02-24	20022305	0.8382	Y	Y	N	3	on ice	m
00-02-25	20022501	0.6223	Y	Y	N	30	on ice	m
00-02-25	20022502	1.15824	Y	Y	N	30	on ice	m
00-02-25	20022503	1.0795	Y	Y	N	30	on ice	m
00-02-25	20022504	0.92202	Y	Y	N	30	on ice	m
00-02-25	20022505	0.92964	Y	Y	N	30	on ice	m

Note: On ice means the sample is on the crushed ice and stored in 4°C
In solution means the sample stored in Tyrode's solution and stored in 4°C

* These sample were used to study the effect of storage condition.

† Sectioning methods:

m: above freezing temperature.

c: sectioned at -18 ° C.

Appendix C. Monte Carlo Codes

The Monte Carlo simulation codes including the windows can be divided into four modules with the following flow chart:

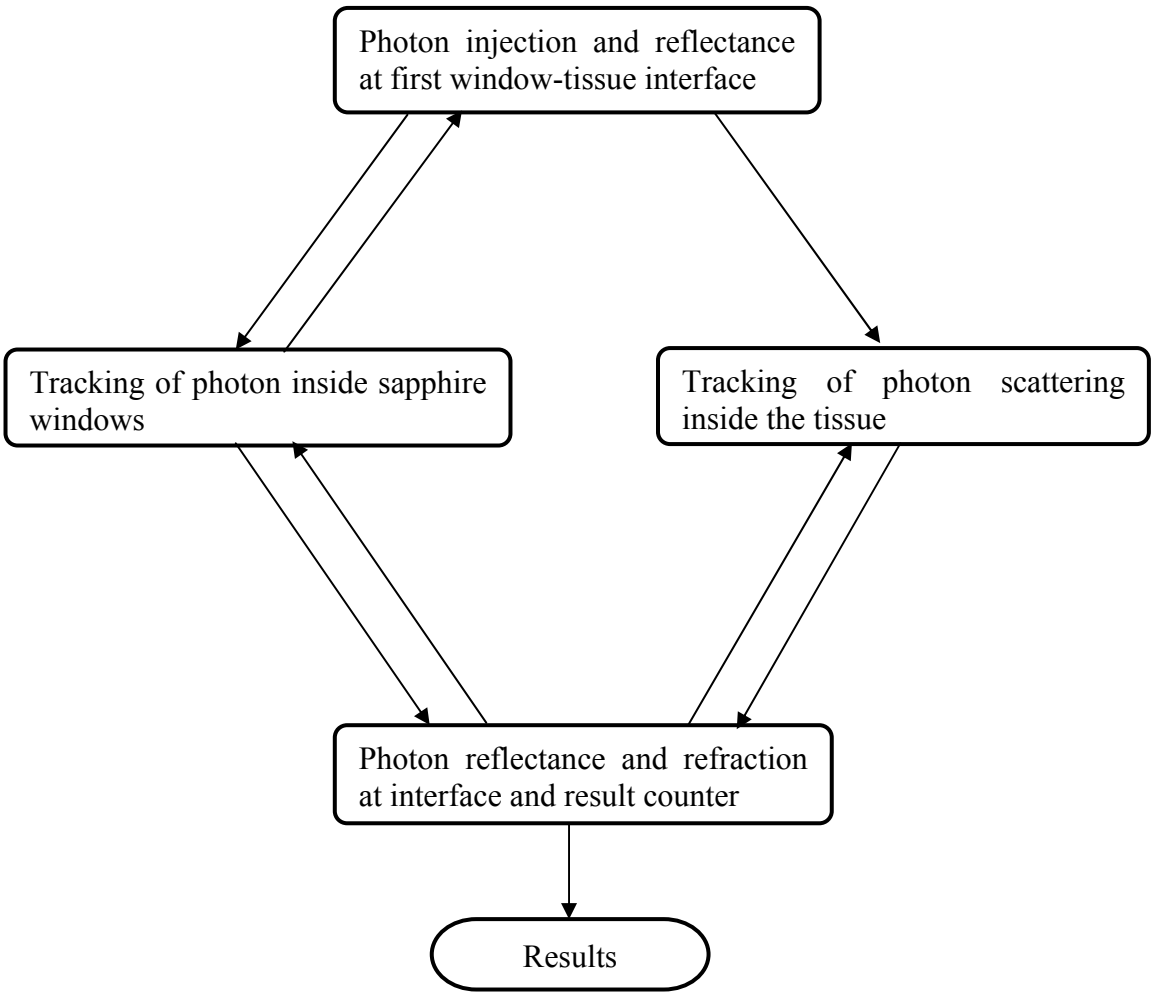

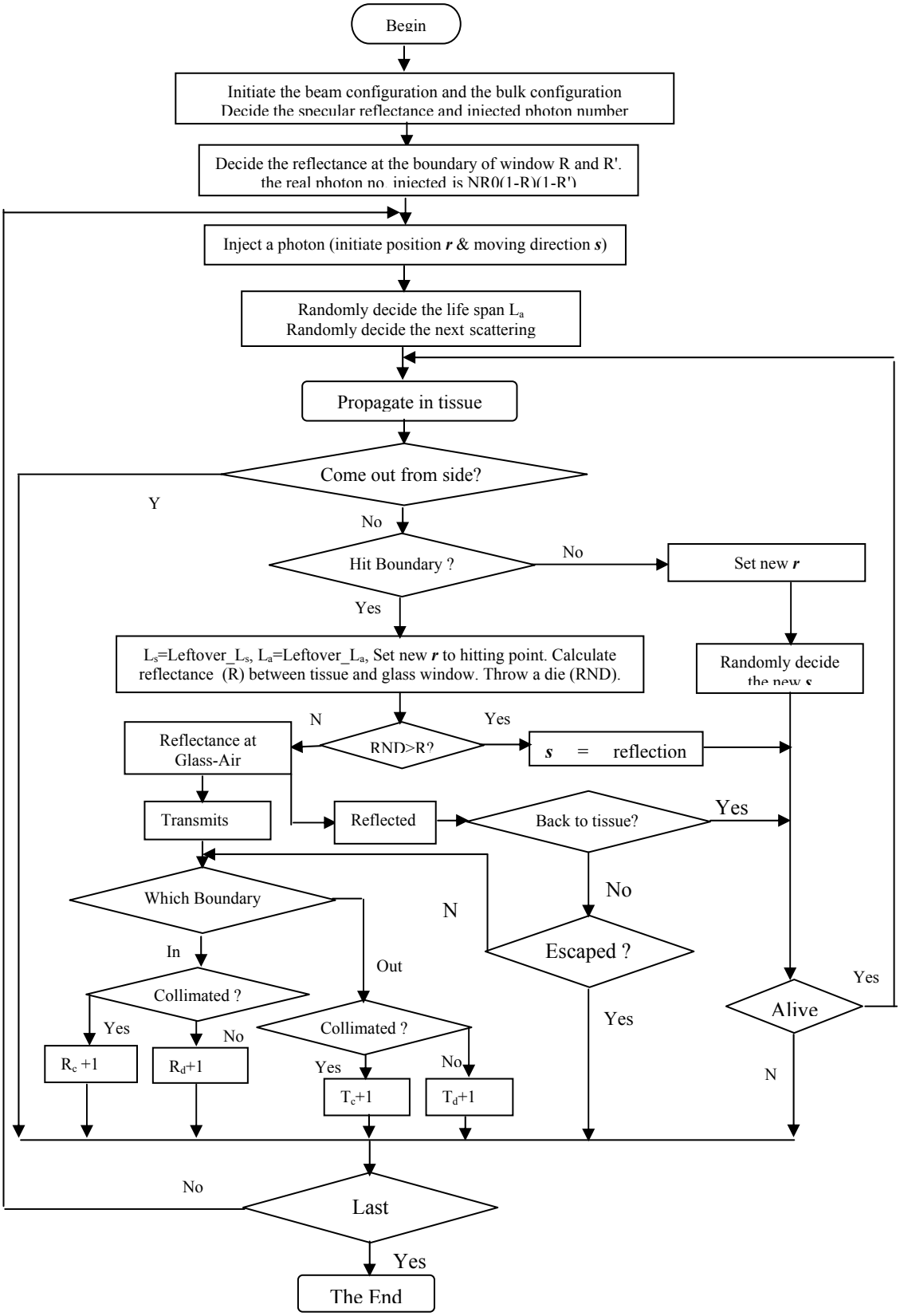
Begin
Initiate the beam configuration and the bulk configuration
Decide the specular reflectance and injected photon number
Decide the reflectance at the boundary of window R and R'.
the real photon no. injected is NR0(1-R)(1-R')
Inject a photon (initiate position r & moving direction s)
Randomly decide the life span La
Randomly decide the next scattering
Propagate in tissue
Come out from side?
Y
No
Hit Boundary ?
No
Set new r
Yes
Ls=Leftover_Ls, La=Leftover_La, Set new r to hitting point. Calculate reflectance (R) between tissue and glass window. Throw a die (RND).
Randomly decide the new s
N
Yes
Reflectance at Glass-Air
RND>R?
s = reflection
Transmits
Reflected
Back to tissue?
Yes
Which Boundary
No
N
In
Out
Escaped ?
Collimated ?
Yes
Alive
Yes
Collimated ?
Yes
No
Rc +1
Rd+1
Yes
No
N
Tc+1
Td+1
No
Last
Yes
The End

The MAIN portion of the codes is listed below:

```
      !*****************************************************************************************************
*******
      ! This program is to simulate the propagation of the photon in slab tissue and give out the
diffuse
      ! ref and trans the effect of the sapphire window is considered and the configuration is
more like
      ! the experimental setup.
      !*****************************************************************************************************
********

      !********----------   main   ----------**********

      !----------   define the parameter and variable   ---------

          Implicit real(a-h, o-z)
          external Ran2

      !----  Beam and sample profile -----------------

          parameter(Ibeam=2)          !1:gauss beam; 2:top-hat beam
          parameter(Isampletype=1)    !1:slab; 2:semi
          parameter(SmplDpsR=1.)      !(sample size)/(Deposit Size): >=1
          parameter(NX=1, NY=nx, NZ=1)
          parameter(Maxscatt=1500, maxIr=140)
          parameter(NR0=100,MAxNN=3.141592654*NR0*(NR0+1))

      !---- variable used in the calculation   ----------

          INTEGER DEPOSIT(NX,NZ)
          INTEGER DPS_XY(NX,NY)
          integer Ph_nsct(Maxscatt),Dps_nsct(Maxscatt)
          integer Snp_nsct(Maxscatt)
          integer mnscatt,mnshot

          real X(Maxscatt),Y(Maxscatt),Z(Maxscatt)
          real PHI(Maxscatt),PSI(Maxscatt)
          real Xinc(2*NR0+1),Yinc(2*NR0+1)
          real ax1(maxIr),ay1(maxIr)

          common/const/Pi,zero_p,one_m
          common/medium/Aindex,g,winDEX
          common/cphs/phs1,phs2,phs3,phs4
          common/snap/DTp,deltaD,Lshot,nshot,nishot
          common/deposit/fnx,fny,fnz,nxhp,nyhp,nzhp,Xdps,Ydps,Zdps,
         +DpsRs,Zbegin,Zend
          common/ref/ref_norm,Iout,intref
          common/beam/R0,aI0,tows,ovf,fr0,Zpls_w,xpls_w
          common/dir/phi_im1,psi_im1,sinphi,cosphi,sinpsi,cospsi
          common/coord/X_im1,Y_im1,Z_im1
```

```
c---in-line function to calculate the trans distance of photon---

      Dfn(dZ)=dZ/(abs(cosphi)+1.0e-20)

c---Problem is that "cosphi" may equal 0  ------------------------


      PI=4.*atan(1.)

      write(*,*)'maxNN=', maxNN


!----  to input the parameter from the user ----------------

       In_param=1             !Input parameters on screen? 1:yes; 0:no

!--- we can change and modify the program to read the data from file.

11          write(*,*)'Please enter the following parameters'

            write(*,*)'1.  g, muS, muA'
            write(*,*)'2.  index of refraction(n) of tissue'
            write(*,*)'3.  thickness of the sample ='
            write(*,*)'_____'
                  read(*,*)g, amuS, amuA, ainDEX, z0
            write(*,*)'-----------------------------------'
            write(*,*)'4.  please input the index of window'
            read(*,*)winDEX
            write(*,*)'-----------------------------------'
            write(*,*)'***********************************'
12                write(*,*)'You entered g=',g
            write(*,*)'you entered muS=', amuS
            write(*,*)'you entered muA=', amuA
            write(*,*)'you entered tissue index =',ainDEX
            write(*,*)'tissue thickness =',z0
            write(*,*)'window index =',winDEX
            write(*,*)'***********************************'

! ---- To check if the input is right ------------------

            write(*,*)'correct: enter 1; incorrect: enter 0; to end: enter 3'

                  read(*,*)N_enter

             if(N_enter.eq.1)then
                  goto 77
                   else if(N_enter.eq.0)then
                              goto 11
                   else if(N_enter.eq.3)then
```

```
                    goto 11111
                end if

                write(*,*)'Wrong key ,Please try again!'
                    goto 12

!-----------------------------------------------------------

77    if(Isampletype.eq.1)then                    !slab sample

!------------------------------------  If no input parameters
          If(In_param.eq.0)then
                    g=0.48
                    albedo=0.9666
                    amuT=1.014
                    amuS=amuT*albedo
                    amuA=amuT-amuS
                    ainDEX=1.33
                    z0=17.01  !sample thickness: 0.3 ~ 1.0 mm
                end if
!------------------------------------ then use the default values above

                x0=0.75*25.4       ! the square of tissue 0.75" X 0.75"
                y0=X0

                cnAngle=0.5*0.001*pi/180.

                w=0.5*.25*25.4     ! w=4.86 the radius of beam
                N_interface=4

!-----define the "F"  focus length for two different kind of beam ----

                if(Ibeam.eq.2)then          !top hat beam
                        F=w/tan(cnAngle)
                else if (Ibeam.eq.1)then
                        F=w/sin(cnAngle) !GaussBeamCorrection1
                end if

!-----define the "dF" the change of F by medium for two different kind of interface----

                If (N_interface.eq.2)then !consider two interfaces

                 dF=sqrt(1.-sin(cnAngle)*sin(cnAngle)/aindex/aindex)

                 dF=0.5*(2.-(1.+cos(cnAngle)/dF)/aindex)*Z0

                else if (N_interface.eq.1)then  !consider one interface
                 dF=sqrt(1.-aindex*aindex*sin(cnAngle)*sin(cnAngle))

                 dF=0.5*(2.-(1.+dF/cos(cnAngle))/aindex)*(F-Z0)

           else if (N_interface.eq.4)then
```

```
                        dF=0.0      ! for collimated beam dF = 0.0

                        end if


!-------------------- Define "Zdps" --------------------------
                        if(Ibeam.eq.2)then          !top hat beam
                                Zdps=F+dF       !2 refrct
                                aI0=maxNN
!top hat beam: aI0 is the total # of photons

!-------------------
          else if (Ibeam.eq.1)then
                                Zdps=0.5*(1.+cos(cnAngle))*F+dF
!GaussBeamCorrection1--replace above
!-------------------
                        end if

!---------------------------------------------------------------
                        dZdps=0.5*6.4*5
                        dXdps=0.75*25.4         !diameter of the sample hole
                        Zbegin=Zdps-0.5*dZdps
                        Zend=8*25.4             !diameter of the integral sphere
                        Zsample=Z0
                        deltaD=30.*0.001/3.2
    end if
!------------ END of if 77 ahead----------------------------------

!------------ The parameters of the glass window ----------------------------------

      win_T=1.94            ! thickness = 1.94 mm
      win_Dia=1.2*25.4      ! diameter = 1.2 inch

!------------ Calculate the reflectance at the boundary of air-glass window Ra_w ---
!------------ The reflectance on the input air-glass interface can be consider as constance --
----
!------------ which we can disregard at the the simulation progress and correct at the end  -
-----
!------------ of the simulation and add in out put of the program ----------------------------

      Ra_w=((winDEX-1.0)/(winDEX+1.0))**2
      write(*,*)Ra_w

!------------ Give out the initial values about the sample and beam.---

          Xsample=SmplDpsR*x0
          Ysample=SmplDpsR*y0
          SmpRs=0.25*Xsample*Xsample
          Xbeam=0.
          Ybeam=0.
          Xdps=Xbeam
          Ydps=Ybeam
```

```
          hz0=0.5*z0

!---------- Run the initial subroutine to give the incident photon's
!---------- information as for distribution and angle etc. ---------

          call Initl_sys(Ibeam,cnAngle,F,maxNN,NR0,nx,ny,nz,dXdps,dZdps)


!-----  "idum" is the random function seed -----------

          idum=-375027620

!----  SET THE DEPOSIT AND DPS_XY INITIAL VALUE ALL BE 0 ----

          DO I=1,NY,1
        DO J=1,NX,1
                  DEPOSIT(J,I)=0
                  DPS_XY(J,I)=0
        ENDDO
      ENDDO

c--- Jpht0=position # & Itotal0=# of photons in previous run
!--- here we just setup it to be 0 for the beginning of the new run  ----

          Jpht0=0
          Itotal0=0

          DO I=1,Maxscatt
             X(I)=0.
             Y(I)=0.0
             Z(I)=0.0
             PHI(I)=0.0
             PSI(I)=0.0

             Ph_nsct(i)=0
             Dps_nsct(i)=0
             Snp_nsct(i)=0
      ENDDO



c***440 & 120*** Loop each photon on the number of photons

c-------------------------------------------------------

c---  set the initial value of the statistic result to be 0

          iRdf=0
          iTdf=0
          IescR=0
          IescT=0

     Iwrite=0
```

```
      MNscatt=0
      MNshot=0
      DL_MN=0.
      DT_MN=0.

      intref=0
      Iout=0
      Itrans=0
      Idead=0
      Maxs=1
      Itotal=0
      Incident=0



           NN=0

c- ("Ixinc", "Iyinc") marks different grid in the 2NR0+1*2NR0+1 square.

      DO 1440 Iyinc=1,2*NR0+1

                  Yinc_nn=NR0-(Iyinc-1)
                  NNx=0

           DO 2440 Ixinc=1,2*NR0+1

                  Xinc_nn=NR0-(Ixinc-1)
                  rsq=Xinc_nn*Xinc_nn+Yinc_nn*Yinc_nn

!---     r^2=x^2 + y^2, if r < NR0^2 mean photon is in the circle
!---     and give out the point position in mm use fro*grid number. -------

                  if ( rsq.LE.(NR0**2) ) then
                    NNx=NNx+1
                    Xinc(NNx)=fr0*Xinc_nn
                    Yinc(NNx)=fr0*Yinc_nn
           end if

2440       end do

           NN=NN+NNx     ! counter for total photon number.

!          write(*,*)'starting loop 440 Iyinc Ixinc =',Iyinc,Ixinc

      DO 440 Inc_x=1,NNx

           x1=Xinc(Inc_x)
           y1=Yinc(Inc_x)

!          call Gauss_beam(idum,x1,y1,ax1,ay1,Ir,aIr)       ! for gauss beam only

           Ir=1                !
           ax1(1)=x1           !       For top-hat beam with TopWt=1
```

```
            ay1(1)=y1          !

        !--- this subroutine initials the information of the injected photon of each loop ------
        !--- it also decides the reflectance and refraction at the Glass-Tissue interface -----
        ! ********************************************************************

            call Tophat_beam(idum,x1,y1,Ir,aIr)

        ! ********************************************************************
        !--- Ir=1 pass into tissue, Ir=0 reflected back ------------

        !--- If Ir=1 we should go on propagating in tissue, but if Ir=0 we should reconsider ------
        !--- the reflectance at the  glass-air interface this is the following few lines ---------


          JFK=Ir

          Do while(JFK.eq.0)              ! reflected back to glass-air interface

            CALL refrct(0.0,winDEX,1.0,Rphii)
            temp_ran=Ran2(idum)
            ref_res=Rphii-temp_ran

            if( ref_res.ge.0.0) then    ! reflected back to glass-tissue boundary
              Ir=1
              CALL  Tophat_beam(idum,x1,y1,Ir,aIr)          ! recalculate at the glass-tissue
boundary
              JFK=Ir
            else                  ! refracted out to air and escaped from sphere hole.
              Ir=0
              JFK=1
            end if

          end do



            Itotal=Itotal+Ir                    !total # of photons entering the tissue
            Incident=Incident+Nint(aIr)                 !total  #  of  photons  incident  to  the
tissue

            do 120 Igauss=1,Ir

                x1=ax1(igauss)
                y1=ay1(igauss)

                call Initl_coord1(idum,Ibeam,F,x1,y1,Z(1),phi(1),psi(1))

                X(1)=x1
                Y(1)=y1

                TEMP=Ran2(idum)
```

```
                    DL=-ALOG(1.-TEMP)/amuA  !random decided the life length of the
current photon
                    maxshot=Int(DL/deltad)  !SnapShot use

                    DT=0.
                    Lshot=0

        !---- photon propagation inside the tissue , loop on each scattering till dead or out of
tissue --

              DO 60 Iscatt=2,Maxscatt          !loop on the scattering

                        InG_Flag=2     !0,in air.  1,in glass. 2,in tissue.
                    X_im1=X(iscatt-1)
                        Y_im1=Y(iscatt-1)
                        Z_im1=Z(iscatt-1)
                        phi_im1=phi(iscatt-1)
                        psi_im1=PSI(Iscatt-1)
                        sinphi=sin(phi_im1)
                        cosphi=cos(phi_im1)
                        sinpsi=sin(psi_im1)
                        cospsi=cos(psi_im1)

                        Ndps=0
                        Nsnap=0

                        DTp=DT
                        TEMP=ran2(idum)
                        D=-ALOG(1.-TEMP)/amuS       ! random decided the scatt.
length of
                        DT = DT + D           ! record of how long has the photon travel.

                        IF ( DT.gt.DL )then
                              DT=DL
                              D=DT-DTp
                        end if

                        nshot=int(DT/deltaD)
                        nishot=nshot
                        Ref_int=0.
                        Zi=Z_im1+D*cosphi          ! the new coordinate
                        Yi=Y_im1+D*sinphi*sinpsi    ! of the photon after
                        Xi=X_im1+D*sinphi*cospsi    ! the scattering.



        !***The next a few lines is for slab-sample only
        !---To check if the photon get to the boundry of the tissue and if it
        !---pass out of the tissue ----------------------------------------
        !--- if(zi<0) come out,   elseif(zi>thickness) come out     ----------


                        zout=abs(Zi-hz0)-hz0                                  !For
```

```
                    IF(zout.gt.0.)THEN                    ! >0 photon come to surface

                        RANS=ran2(idum)                                    !
                        nishot=int((DT-zout/abs(cosphi))/deltaD) !

                        call reflct(Rans,Zout,Zi,ref_int)     !check the surface reflect

      !---- reflect give out the value of ref_int, if(ref_int>0)then reflectance elseif(ref_int<0)
transmittance
      !---- if(ref_int=0)then photon stay in side the tissue, change the direction as internal
reflection ------

                        phi(iscatt-1)=phi_im1                    !

                    END IF


      !######## Photon really trans into glass windows, the next block is for photon in glass
######

                    If(Ref_int.ne.0)then      !photon got out into glass window

                      sign_zi=sign(1.,zi)
                    InG_Flag=1     ! 1 inside glass, 0 in air,2 in tissue.

      !---Z_im1 is the z coordinate of the photon before this scattering.  ----------
      !--- here dZ give out the distance of the point to the surface which photon will trans thou. -
---
      !--- if(zi>0) dZ=(z0-z_im1), if(zi<0) dZ=z_im1.          ----------

                    dZ=int(1.+sign_zi)*0.5*(Z0-Z_im1)+int(1.-sign_zi)*0.5*(-Z_im1)

                        D=Dfn(dZ)

      !--- new position of photon zi<0 refl out z_im1=0, zi>0 trans z_im1=z0  --------

                        Z_im1=int(1.+sign_zi)*0.5*Z0

                        X_im1=X_im1+D*sinphi*cos(psi_im1)
                        Y_im1=Y_im1+D*sinphi*sin(psi_im1)

                    R_im1s=X_im1*X_im1+Y_im1*Y_im1
      !--- if the R_imls>0.75/2 photon already come out of the side of the sample it should
dead. ------
                    if(R_imls.gt.DpsRs) goto 40

      !--- the above X Y Z is the point on the interface through which the photon will go out. -----
--

                        phi_im1=asin(aindex*sinphi/winDEX)          !refraction angle in
glass.
```

```
                                                    !the angle psi_im1 which is in X-Y plane not
change.
                        theta_i=phi_im1                          !theta_i will be used to calculated
refraction.

                        if(Z_im1.eq.0)then          ! change phi_im1 to the angle with respected to Z
axil.
                          phi_im1=PI-phi_im1
                        else
                          phi_im1=phi_im1
                        end if


                    DO while(InG_Flag.eq.1)     ! Flag to mark photon is in glass. end at line 544


        !-------------  FROM TISSUE_GLASS SIDE TO GLASS_AIR SIDE -------------
                    cosphi=cos(phi_im1)      !Calculated begin from tissue-glass interface.
                      sinphi=sin(phi_im1)      !phi_im1 is the angle in glass side.

        !--- once the photon get into the glass , it will travel to the glass-air interface without
scattering ---
        !--- so the distance in z direction it moves is window thickness "win_T". ----------------------
--------
        !--- the next few line give out the coordinate of the photon when it come to the glass-air
interface -----

        !%%%%% PHOTON MOVE FROM TISSUE_GLASS TO GLASS_AIR INTERFACE
%%%%
                        dZ=win_T
                        D=Dfn(dZ)
                        X_im1=X_im1+D*sinphi*cos(psi_im1)
                        Y_im1=Y_im1+D*sinphi*sin(psi_im1)

                        if(Z_im1.eq.0)then
                           Z_im1=-win_T
                        else
                           Z_im1=z0+win_T
                        end if

                                R_im1s=X_im1*X_im1+Y_im1*Y_im1

        !--- R-im1s give out the radius which photon comes out. if it > 1.2 inch sample area. it will
dead.

                        win_R2=win_Dia*win_Dia*0.25

                                if(R_im1s.gt.win_R2) goto 40


        !-----------   Check the refraction and reflectance at the glass-air boundary. ----------------------
-------
                        CALL refrct(theta_i,winDEX,1.0,R_g_a)
```

```
                    Rans=Ran2(idum)

                    ref_g_a=R_g_a-Rans

      !---------------------  Check if it inter-ref or refraction out .----------------------------------------
                    if(ref_g_a.lt.0.0) then       !--- coming out calculated refraction angle.

      !$$$$$ Photon come out of glass into the air. check Rd Td Rc Tc $$$$

      phi_iml=asin(winDEX*sinphi/1.0)       !the refraction angle in air. psi still not
       change.

                      if(Z_im1.lt.0) then
                        phi_im1=PI-phi_im1
                      else
                        phi_im1=phi_im1
                      end if                          !modified the phi_im1 to and angle with Z axil.
                      InG_Flag=0

      !-------------------------------------------------------------------------------------------------------

                    else          ! photon still in glass, internal reflection.
                      phi_im1=PI-phi_im1   !reflection change the angle phi_im1 with Z axil
and psi not
      change.

      !%%%% PHOTON MOVE FROM GLASS_AIR TO GLASS_TISSUE INTERFACE
%%%%%

                      dZ=win_T
                      D=Dfn(dZ)
                      X_im1=X_im1+D*sin(phi_im1)*cos(psi_im1)
                      Y_im1=Y_im1+D*sin(phi_im1)*sin(psi_im1)

                      R_im1s=X_im1*X_im1+Y_im1*Y_im1
                        if(R_im1s.gt.win_R2) goto 40      !check if photon move out of glass
form side.

                      if(Z_im1.lt.0.0) then
                        Z_im1=0.0
                        theta_i=phi_im1
                      else
                        Z_im1=z0+win_T
                        theta_i=PI-phi_im1
                      end if                    ! get the z coordinate of the point on glass-tissue
interface.

      !------------- Check the refraction and reflectance at glass-tissue boundary. ----------------
------
                      CALL refrct(theta_i,ainDEX,winDEX,R_g_t)
                      Rans=Ran2(idum)
                      ref_g_t=R_g_t-Rans
```

```
!% After reflect at glass-tissue interface still in glass, so keep going,change phi_im1. %

                    if(ref_g_t.gt.0.0) then
                       phi_im1=PI-phi_im1
                       InG_Flag=1

!$$$$$$$$$$$$$  Photon reenter the tissue and going on scattering. $$$$$$$$$$$

                    else
                       InG_Flag=2
                       ref_int=0
                       Xi=X_im1
                       Yi=Y_im1
                       Zi=Z_im1
                    end if


                  end if
!-----------------------------------------------------------------------------------------------------------

544          End do   !the block of the photon move inside glass window.

!######## The end of the block, which simulated the move of photon inside glass window.
!******** if flag show photon in air so check teh collimated and diffuse , trans or refl. **********


                   if(InG_Flag.eq.0) then


                       sinphi=Sin(phi_im1)
                       cosphi=Cos(phi_im1)
                       dZ=Zend       !the diameter of integrating sphere
                          D2=Dfn(dZ)
                          X2=X_im1+D2*sinphi*cos(psi_im1)
                          Y2=Y_im1+D2*sinphi*sin(psi_im1)
                          R2s=X2*X2+Y2*Y2
                          Iesc=0

                       OutR=X_im1*X_im1+Y_im1*Y_im1

                       if(OutR.gt.DpsRs)then
                          goto 40  !photon come out point larger than 0.75 inch tissue hole.
                       end if


                     if(R2s.le.w*w) Iesc=1      ! Photon escape from the hole of integrating sphere.
```

```
                        if((Z_im1.lt.0.)) then        !Z_im1<0; out-up ref, Z_im1>0: out-
down trans
                            iRdf=iRdf+1-Iesc     !Rd
                            IescR=IescR+Iesc     !Rc
                            goto 40                    ! diffuse reflected
                        else if(Z_im1.gt.0.) then          !
                            iTdf=iTdf+1-Iesc     !Td
                            IescT=IescT+Iesc     !Tc
                            goto 41                  ! diffuse transmitted
                        end if
                    end if                          !

                end if
        !########## END OF THE IF CHECK THE IF PHOTON COME INTO GLASS FROM
TISSUE ###

        !---------- Ref_int=0 mean photon still scattering in tissue. ----------
------


                    if(nshot.eq.maxShot) then
                        idead=idead+1              !check if the photon is dead.
                        goto 40
                    end if

        c***Calculated at the end pt. of the current scatt.

                    IF ((Xi*Xi+Yi*Yi).GT.SmpRs) goto 40   ! the photon come out from the
side of
        tissue.

                    Z(Iscatt)=Zi
                    X(Iscatt)=Xi
                    Y(Iscatt)=Yi

                    call scatt_dir(idum,Phi(Iscatt),Psi(Iscatt))

        60      end do


        41      Itrans=Itrans+1

        !------  call slab_dep(Z0,nx,nz,deposit,Ndps,Nsnap,DPS_XY)
        !------  Dps_nsct(iscatt-1)=Dps_nsct(iscatt-1)+Ndps
        !------  Snp_nsct(iscatt-1)=Snp_nsct(iscatt-1)+Nsnap


        40      Ph_nsct(iscatt-1)=Ph_nsct(iscatt-1)+1
                mnscatt=mnscatt+iscatt-1
                mnshot=mnshot+nshot
                DL_MN=DL_MN + DL
                DT_MN=DT_mn + DT
```

```
            if((iscatt-1).gt.maxs) maxs=iscatt-1

      120   end do

      440   end do

      1440  end do

      c------ calculation complished, output the result to screen and file.-----

            Incident=Incident/(1-Ra_w)        !add the photon been reflected at the input being
reflected
      by first air-window interface.

      !----- Write to screen -----------------------------------------------

            if(In_param.eq.1)then

                  write(*,*)'mu_s, mu_a, g, index = ',amus, amua, g, aindex
                  write(*,*)'NR0,NN,Itotal,Incident =',nr0,NN,Itotal,Incident
                  write(*,*)'mnscatt =',mnscatt/Itotal
            write(*,*)'Max. # of scatt.=',Maxs
                  write(*,*)'# of Itrans, Idead,IntRef=',Itrans,idead,intref
                  write(*,*)''
                  write(*,*)'Results for Integral Sphere simulated result'
                  write(*,*)'**************************************************'
                  write(*,*)'# of refl., trans.; ref., trans. through hole', iRdf,iTdf,IescR,IescT
            write(*,*)''
                  write(*,*)'Measured reflectivity and tramsmission = ', 1.0*iRdf/Incident,
1.0*iTdf/Incident

                  write(*,*)'**************************************************'
            end if

      !----- Write to the file ---------------------------------------------

          open(13, file='xzd101g.dat')

              call Write_Deposit(Deposit,Nx,Nz,x0,y0,z0,R0,w,
         +SmplDpsR,Xsample,Ysample,Zsample,Isampletype,Ibeam,Itotal0,Jpht0,
         +amus,amua,g,aindex,F,deltad,NR0,maxNN,NN,Itotal,Incident,Jpht,
         +mnscatt,mnshot,DL_mn,DT_mn,Iout,Itrans,intref,Idead,Maxs,Maxscatt,
         +Zdps,dZdps,dXdps,zpls_w,xpls_w,iRdf,iTdf,IescR,IescT )

          close(13)

      !-----  CLOSE the program ---------------------------------------------

      2     format(I5,I7)
      3111  format(3I10)
      11111 STOP

          END
```

Appendix D. The codes to convert SBIG CCD file into ASCII file

```
FILE *image_File;
int i,j,rdim,cdim,dim2;
double d_image;
double d_phase;
char mm;
unsigned char hh;
unsigned char ll;
cdim=765;rdim=510;
Z.cDim=765;Z.rDim=510;
dim2=765*510;

if ( (image_File=fopen(fileName,"rb") ) == NULL )
        printf("\n Can't open %s", fileName);       // open the file

        for(i=0;i<2048;i++)
        {
           fscanf(image_File,"%c",&mm); // to read the 2K (2048 byte File head)
        }

Z.Array=new  double [dim2];
Z.Phase=new double [dim2];

if(!Z.Array && !Z.Phase)
{
        printf("\n Insufficient Memory: InitImage"); exit(0);
                fclose(image_File);
}

for(i=0; i<rdim; i++)
        {
                for(j=0; j<cdim; j++)
                {
                        fscanf(image_File,"%c",&ll);
                        fscanf(image_File,"%c",&hh);
                        *(Z.Array+i*cdim+j)=int(hh)*256+int(ll);
                }
}

fclose(image_File);
```

First few lines define the size of the data array as 765×510. In the ST7 file, data is stored sequentially, so it should be opened as binary file "fopen(fileName,"rb")" to ensure

no losing of the data while read it. There is a 2064 byte (2K) head in ST7 giving out information about the image, we use a "for" loop jump through it. The 16-bits pixels are saved as two bytes with lower significant byte stored before higher significant byte, two unsigned integer (1 byte in size) is defined as "ll" and "hh" stand for the lower and higher byte respectively. Each time the program read twice from the file for one pixel, with the first read is "ll" and second one is "hh", and then calculate the value of the correspond pixel (i, j) through "256*hh+ll" and store in array "Z.array". After reading, the value of the pixel are saved as a standard ASCII file using following program:

```
if ( (image_File=fopen(fileName,"w") ) == NULL )
        printf("\n Can't open %s", fileName);    // open the file

    for(i=Nmin; i<Nmax; i++)
    {
        for(j=Mmin; j<Mmax; j++)
        {
            fprintf(image_File,"%d%d%E\n",i,j,*(Z.Array+i*Z.cDim+j));
        }
    }
```